Development of high rate capability GEM detectors for CBM experiment at GSI

By

Chandrasekhar Ghosh

Enrolment No: PHYS04201904013

Variable Energy Cyclotron Centre, Kolkata

A thesis submitted to the
Board of Studies in Physical Sciences

In partial fulfillment of requirements

for the Degree of

DOCTOR OF PHILOSOPHY

of

HOMI BHABHA NATIONAL INSTITUTE

January, 2026

Homi Bhabha National Institute

Recommendation of the Viva Voce Board

As members of the Viva Voce Board, we certify that we have read the dissertation prepared by **Chandrasekhar Ghosh** entitled **"Development of high rate capability GEM detectors for CBM experiment at GSI"** and recommend that it may be accepted as fulfilling the thesis requirement for the award of Degree of Doctor of Philosophy.

..... (In person) **Date:** 20/05/26
Chairman- Dr. Arup Bandyopadhyay

..... (In person) **Date:** 20/05/26
Guide- Dr. Anand Kumar Dubey

..... (In person) **Date:** 20/5/26
Member 1- Dr. Kaushik Banerjee

..... (In person) **Date:** 20/5/2026
Member 2- Dr. Sarmishtha Bhattacharyya

..... (In person) **Date:** 20/5/26
Member 3- Dr. Nayana Majumdar

..... (In person) **Date:** 20/5/26
External examiner- Gobinda Majumdar

Final approval and acceptance of this thesis is contingent upon the candidate's submission of the final copies of the thesis to HBNI.
I hereby certify that I have read this thesis prepared under my direction and recommend that it may be accepted as fulfilling the thesis requirement.

Date: 20.05.26

Place: VECC, Kolkata

/ 20/05/26
Signature
Guide

CERTIFICATION ON ACADEMIC INTEGRITY

Undertaking by the Student

1. I **Chandrasekhar Ghosh**, HBNI Enrolment No. **PHYS04201904013** hereby undertake that the Thesis, titled " **Development of high rate capability GEM detectors for CBM experiment at GSI"** is prepared by me and is the original work undertaken by me.

2. I also hereby undertake that this document has been duly checked through a plagiarism detection tool and the document is found to be plagiarism free as per the guidelines of the Institute/ UGC.

3. I am aware and undertake that if plagiarism is detected in my thesis at any stage in the future, suitable penalty will be imposed as per the guidelines of the Institute/ UGC.

Chandrasekhar 20/05/2026
Signature of the Student with date

Endorsed by the Thesis Supervisor:

I certify that the thesis written by the researcher is plagiarism free as mentioned above by the student.

Dubey / 20.05.26

Signature of the Thesis Supervisor with Date and Name: Dr. Anand Kumar Dubey
Designation: Scientific Officer-G
Department/ Centre: Department of Atomic Energy
Name of the CI/ OCC: Variable Energy Cyclotron Centre

STATEMENT BY AUTHOR

This dissertation has been submitted in partial fulfillment of requirements for an advanced degree at Homi Bhabha National Institute (HBNI) and is deposited in the Library to be made available to borrowers under rules of the HBNI.

Brief quotation from this dissertation are allowable without special permission, provided that accurate acknowledgement of source is made. Requests for permission for extended quotation from or reproduction of this manuscript in whole or in part may be granted by the Competent Authority of HBNI when in his or her judgement the proposed use of the material is in the interests of scholarship. In all other instances, however, permission must be obtained from the author.

Chandrasekhar Ghosh

DECLARATION

I, hereby declare that the investigation presented in the thesis has been carried out by me. The work is original and has not been submitted earlier as a whole or in part for a degree/diploma at this or any other Institution/University.

Chandrasekhar Ghosh

Homi Bhabha National Institute

Certificate from the Guide on Publications

1. **Name of the Student: Chandrasekhar Ghosh**
2. **Name of the Constituent Institution: Variable Energy Cyclotron Centre**
3. **Enrolment No. and Date: PHYS04201904013 and August 01, 2019**
4. **Title of the Thesis: Development of high rate capability GEM detectors for CBM experiment at GSI.**
5. **Board of Studies: Physical Sciences**

1. The following are the publications resulted from the work reported in the thesis:

S. No.	Journal Publication(s)	Student's Contribution
1.	First prototype of MuCh second station GEM module: design, fabrication and testing for CBM experiment at GSI, Germany. Chandrasekhar Ghosh *et al* 2025 *JINST* **20** P09005 https://doi.org/10.1088/1748 0221/20/09/P09005	Design, Simulation, Fabrication, testing and manuscript preparation.
2.	Performance study and gas system development for large size GEM modules in the CBM MuCh detector system. Chandrasekhar Ghosh et al 2025 JINST 20 P10036 https://doi.org/10.1088/1748 0221/20/10/P10036	Design, Development, testing and manuscript preparation.

2. It is further certified that the part of the work included in this thesis will not be included again in any other thesis.

3. It is also certified that the co-authors of the above papers have no objection for including the indicated parts of the work in the present thesis.

Signature of the Guide

Date: 10/11/2025

To
HBNI Office

List of Publication arising from the thesis

In Journal

1. "**First prototype of MuCh second station GEM module: design, fabrication and testing for CBM experiment at GSI, Germany**"
   Chandrasekhar Ghosh, Abhishek Kumar Sharma, Shruti Gudla, Jogender Saini, Anand Kumar Dubey, and Arup Bandyopadhyay,
   2025 JINST 20 P09005.
   https://doi.org/10.1088/1748-0221/20/09/P09005

2. "**Performance study and gas system development for large size GEM modules in the CBM MuCh detector system**"
   Chandrasekhar Ghosh, Shruti Gudla, Jogender Saini, Anand Kumar Dubey, and Arup Bandyopadhyay,
   2025 JINST 20 P10036.
   https://doi.org/10.1088/1748-0221/20/10/P10036

In Conferences/Symposia :

1. "**Design, Fabrication and Testing of real size MuCh second station GEM module prototype for CBM experiment at GSI, Germany**"
   Chandrasekhar Ghosh, Shruti Gudla, Jogender Saini, Anand Kumar Dubey, and Arup Bandyopadhyay,
   Journal of Subatomic Particles and Cosmology, **2025**, 100262.
   https://doi.org/10.1016/j.jspc.2025.100262

2. " **Design and Development of Various Cooling Arrangements for Muon Chamber Detector Electronics.**"

Ghosh, C., Dubey, A.K., Kumar, J., Kumar, A., Chattopadhyay, S. (2021)
XXIII DAE High Energy Physics Symposium. DAEBRNS HEPS 2018 2018. Springer Proceedings in Physics, vol 261. Springer, Singapore.
https://doi.org/10.1007/978-981-33-4408-2_105

3. "**Testing of 10 cm x 10 cm Triple GEM Detector Using MUCH-XYTER v2.0 Electronics.**"
Ghosh, C., Sikder, G., Kumar, A., Saini, J., Dubey, A.K., Chattopadhyay, S. (2021).
XXIII DAE High Energy Physics Symposium. DAEBRNS HEPS 2018 2018. Springer Proceedings in Physics, vol 261. Springer, Singapore.
https://doi.org/10.1007/978-981-33-4408-2_176

4. "**Fabrication and testing of the upgraded GEM module for the station 1 of MuCh system of CBM experiment at FAIR, Germany**"
C. Ghosh, J. Saini, A. Agarwal, A. K. Dubey, and S. Chattopadhyay
Proceedings of the DAE Symposium on Nuclear Physics, **2022**, Vol.66, 1144.
https://www.sympnp.org/proceedings/66/G35.pdf

5. "**Installation and commissioning of pre-production series MuCh-GEM modules in mini-CBM, June 2024 beamtime at GSI, Germany**"
Chandrasekhar Ghosh, Anand Kumar Dubey, Jogender Saini, Apar Agrawal, Pawan Kumar Sharma, Vikas Singhal, Vinod Singh Negi,Christian Sturm, David Emschermann, and Arup Bandyopadhyay
Proceedings of the DAE Symposium on Nuclear Physics, **2024**, Vol.68, 1091.
https://www.sympnp.org/proceedings/68/G19.pdf

Other publications (in refereed journals)

1. "**Test and characterisation of STS/MuCh-XYTER and integration with multiple detectors of CBM-MuCh detector systems**"

J. Saini, **C. Ghosh**, A.K. Dubey, Z. Ahammed, M. Mondal, R. Ganai, G. Sikder, V. Negi, S. Chattopadhyay and A. Chakrabarti

2023 JINST 18 P01009

https://doi.org/10.1088/1748-0221/18/01/P01009

2. "**Commissioning and testing of pre-series triple GEM prototypes for CBM-MuCh in the mCBM experiment at the SIS18 facility of GSI**"

   A. Kumar, A. Agarwal, S. Chatterjee, S. Chattopadhyay, A.K. Dubey, **C. Ghosh**, E. Nandy, V. Negi, S.K. Prasad, J. Saini, V. Singhal, O. Singh, G. Sikder, J. de Cuveland, I. Deppner, D. Emschermann, V. Friese, J. FrÃijhauf, M. GumiÅĎski, N. Herrmann, D. Hutter, M. Kis, J. Lehnert, P.-A. Loizeau, C.J. Schmidt, C. Sturm, F. Uhlig and W. ZaboÅĆotny

   2021 JINST 16 P09002

   https://doi.org/10.1088/1748-0221/16/09/P09002

3. "**Testing a large size triple GEM detector for the first station of the CBM-Muon Chambers with a high-intensity gamma source at GIF++ under large-area illumination**"

   Apar Agarwal, Souvik Chattopadhay, Pawan Kumar Sharma, Anand Kumar Dubey, Jogender Saini, Vikas Singhal, Vinod Negi, Ekata Nandy, **Chandrasekhar Ghosh**, David Emschermann, Zubayer Ahammed and Subhasis Chattopadhyay

   2025 JINST 20 P04022

   https://doi.org/10.1088/1748-0221/20/04/P04022

4. "**Development of a water-based cooling system for the Muon Chamber detector system of the CBM experiment**"

   Sumit Kumar Kundu, Saikat Biswas, Subhasis Chattopadhyay, Supriya Das, Anand Kumar Dubey, **Chandrasekhar Ghosh**, Ajit Kumar, Ankhi Roy, Jogender Saini,Susnata Seth, Sidharth Kumar Prasad.

   Methods in Physics Research Section A: Volume 1050, 2023, 168143

   https://doi.org/10.1016/j.nima.2023.168143

Dedicated to my 'Parents',

Smt. Rekha Ghosh and Shri Sukumar Ghosh

and my Uncle,

Shri Mritunjoy Ghosh

ACKNOWLEDGMENTS

I would like to express my sincere and profound gratitude to my Ph.D. thesis supervisor, Dr. Anand Kumar Dubey, for his invaluable guidance, constant support, encouragement, and genuine interest throughout the entire duration of my Ph.D. programme. I feel privileged to have had the opportunity to work under his supervision. His continuous motivation and encouragement to think critically and work independently have significantly shaped my academic and professional development. This thesis would not have been possible without his unwavering support and guidance.

I would also like to extend my sincere thanks to the members of my Ph.D. advisory committee Dr. Arup Bandyopadhyay, Dr. Kaushik Banerjee, Dr. Sarmishtha Bhattacharyya, and Dr. Nayana Majumdar for their valuable suggestions, constructive comments, and insightful discussions, which greatly contributed to the improvement of this work.

I would like to express my sincere gratitude to Dr. Arup Bandyopadhyay, former Head of EHEPAG, VECC, for his valuable help in carefully reviewing and correcting the proofs of several research papers. His guidance and suggestions were instrumental in improving the clarity and quality of my work.

I am extremely thankful and grateful to Jogender Saini for his continuous encouragement and wholehearted support throughout the course of this thesis work. I have learned many important aspects from him, including data analysis techniques, effective graphical representation, and the practical intricacies of experimental work. He provided invaluable support in the areas of DAQ, electronics, and detector high-voltage and low-voltage systems, which greatly contributed to the successful completion of this work.

I would also like to sincerely thank Dr. Vikas Singhal for his support in understanding the data formats used in this study. He played a crucial role in unpacking the large volume of mCBM data from the raw format to the rootified format and also assisted significantly in online data monitoring and analysis during beamtime.

I would like to express my sincere gratitude to Dr. Christian Sturm, Dr. David Emschermann, and Dr. Pierre-Alain Loizeau at GSI, Germany, for their constant support and assistance during the mCBM beamtime campaigns. They provided invaluable help in the design and construction of mechanical structures for detector mounting, detector installation, DAQ setup, and data taking. In particular, Dr. Christian Sturm consistently motivated and guided me toward maintaining high standards in the analysis and interpretation of mCBM data.

I am extremely grateful to Dr. Sumit Som, Director, VECC, for granting me permission to travel abroad to GSI, Germany, to participate in the mCBM beamtime campaigns and for enabling the successful acquisition of meaningful data using our detector system.

I would also like to express my special thanks to Shri Jayant Kumar and Shri Ganesh Das of EHEPAG for their constant support and assistance in detector fabrication and the development of related infrastructure.

Finally, I would like to express my heartfelt gratitude to my wife, Mrs. Payel Ghosh, and my daughter, Ms. Subhangi Ghosh, for their constant support, patience, and care throughout this work. Their understanding and encouragement allowed me to remain focused on my research and successfully complete this academic journey

I sincerely apologize for any inadvertent omissions and extend my gratitude to all those who have contributed to this work.

Chandrasekhar Ghosh

SUMMARY

The Compressed Baryonic Matter (CBM) experiment at the Facility for Antiproton and Ion Research (FAIR) is designed to explore strongly interacting matter at high net baryon densities using nucleus-nucleus collisions at unprecedented interaction rates, reaching up to 10 MHz in a free-streaming data acquisition paradigm. Meeting the stringent requirements of high rate capability, radiation tolerance, and long-term operational stability demands detector technologies that combine fast response, fine granularity, and robust performance under sustained irradiation. For the Muon Chamber (MuCh) subsystem of CBM, large-area triple Gas Electron Multiplier (GEM) detectors have been adopted as the baseline tracking technology for the innermost stations.

This thesis presents a comprehensive study on the design, fabrication, characterization, quality assurance, and system-level validation of large area triple-GEM detectors developed for the CBM-MuCh system. The work begins with the mechanical and electrical design of full scale trapezoidal GEM modules for MuCh stations, emphasizing detector robustness, gas tightness, high-voltage stability, and seamless integration of front-end electronics. Novel fabrication solutions, including multilayer readout PCB joining techniques and segmented high-voltage distribution schemes, were developed and validated to ensure uniform performance over meter-scale detector areas.

Extensive bench level characterization using radioactive sources and cosmic muons established the fundamental detector performance. Gain measurements using ^{55}Fe X-rays demonstrated stable and reproducible amplification behavior, while efficiency studies confirmed detection efficiencies approaching 98% with time resolutions at the level of tens of nanoseconds. These studies verified the intrinsic suitability of the developed GEM modules for high-rate tracking applications.

A major contribution of this thesis lies in the development and optimization of detector services, particularly the gas delivery system and thermal management infrastructure, which are critical for long term operation at high particle fluxes. A precisely calibrated mass flow controller based gas mixing system was developed to deliver stable Ar:CO_2 mixtures with controlled flow rates. Systematic gas studies revealed a strong dependence of detector gain on flow rate, oxygen contamination, and relative humidity, with optimal and stable performance achieved beyond a threshold flow where oxygen levels fall below 160 ppb. Based on these results, a parallel gas distribution architecture was proposed for the CBM-MuCh system, ensuring uniform gas quality across all detector modules and enabling real time flow monitoring and leak diagnostics.

Thermal studies demonstrated the limitations of air based cooling under sustained high rate operation and led to the development of a water cooled aluminum plate solution capable of maintaining front end electronics temperatures below 25°C with excellent spatial uniformity. The combined gas and cooling solutions form an essential part of the detector system, directly contributing to stable gain, reduced noise, and reproducible long term operation.

The detector performance was further validated under realistic conditions during multiple mini-CBM (mCBM) beam campaigns at the SIS18 facility of GSI. Two full size MuCh GEM modules were operated in a high intensity heavy ion beam environment and analyzed within the free streaming DAQ framework. Detailed studies of digi rates, noise behavior, timing synchronization, spatial correlations, and rate capability were performed. The detectors exhibited linear response up to particle fluxes of several hundred kHz/cm^2, stable timing alignment with other CBM subsystems, and strong spatial correlations between MuCh stations, confirming correct alignment and common acceptance. Methods for hit reconstruction and time based event building were developed and successfully applied, demonstrating the readiness of the MuCh GEM system for integration into the full CBM experiment.

Finally, production oriented quality assurance procedures, including high flux X-ray testing using controlled laboratory setups at VECC and GSI, were performed. These tests enabled

early identification of non uniformities, verification of rate capability, and validation of detector stability prior to beam deployment, providing a QA framework for large scale series production.

In conclusion, this thesis establishes that large area triple GEM detectors, together with optimized gas and cooling infrastructures and rigorous production QA protocols, constitute a reliable and well validated solution for high rate tracking in the CBM-MuCh system. The results presented here provide a strong technical foundation for large scale detector deployment and support the successful realization of forthcoming FAIR physics runs.

Contents

List of Figures

List of Tables

Chapter 1

Introduction to CBM Experiment at FAIR

High energy heavy ion collisions provide a controlled environment to study strongly interacting matter under extreme conditions of temperature and density. By varying the beam energy and the size of the colliding system, one can scan the Quantum Chromodynamics (QCD) phase diagram and probe the transition from hadronic matter to a deconfined medium of quarks and gluons [1]. Over the last three decades, a coherent picture has emerged at high temperature and low net baryon density ($\mu_B \approx 0$), largely through the RHIC and LHC programs: the produced medium behaves as an almost perfect fluid with remarkably small shear viscosity to entropy density ratio, and exhibits strong parton energy loss, collective flow, and quarkonia modification [2] [3]. In contrast, the regime of moderate temperature and high μ_B remains much less explored, despite its direct relevance to the equation of state at supra nuclear densities, the inner dynamics of compact stars, and the thermodynamics of the early hadronic epoch. The Facility for Antiproton and Ion Research (FAIR) at GSI, with the Compressed Baryonic Matter (CBM) experiment as a flagship, addresses this gap [4] [5]. CBM is designed to operate at interaction rates up to 10 MHz in continuous, triggerless mode, enabling precision measurements

of rare probes in an environment of high track multiplicities and large radiation loads [6]. This chapter outlines the physics landscape that motivates the CBM program, summarizes the evolution of detector technologies toward high rate operation, and introduces the Muon Chamber (MuCh) system in which this thesis is situated. The later chapters of the thesis provide the technical development, characterization, and system level validation of large area triple GEM detectors for MuCh, together with gas and cooling infrastructure tailored to sustained high rate running.

1.1 The QCD Phase Diagram and Key Observables

QCD predicts a rich phase structure as a function of temperature (T) and baryon chemical potential (μ_B). Lattice QCD calculations indicate a smooth crossover at $\mu_B \approx 0$, while various effective models anticipate a first order phase boundary at higher μ_B, possibly ending in a critical point [7]. Heavy ion experiments access this phase diagram (as shown in Figure 1.1) by tuning the center of mass energy per nucleon pair, $\sqrt{s_{NN}}$, and by selecting projectile target combinations. Thermodynamic trajectories at top RHIC [8] and LHC [9] energies start at high T and low μ_B, whereas fixed target programs at lower energies (e.g., at SPS and FAIR/SIS100) probe higher μ_B at moderate T [10]. Penetrating probes provide sensitivity to the space time evolution and the in medium spectral properties of the fireball. Dileptons (e^+e^-, $\mu^+\mu^-$) from Low mass vector mesons (ρ, ω, ϕ) are particularly informative about chiral symmetry restoration and broadened spectral functions; intermediate mass dileptons encode thermal radiation; and quarkonia (e.g., J/ψ) [11] are sensitive to deconfinement via color screening. Hadrons with strange and multi strange content, as well as collective flow coefficients, further constrain the equation of state. Achieving statistically significant measurements for these rare channels at FAIR energies require sustained, high rate data taking and robust online reconstruction.

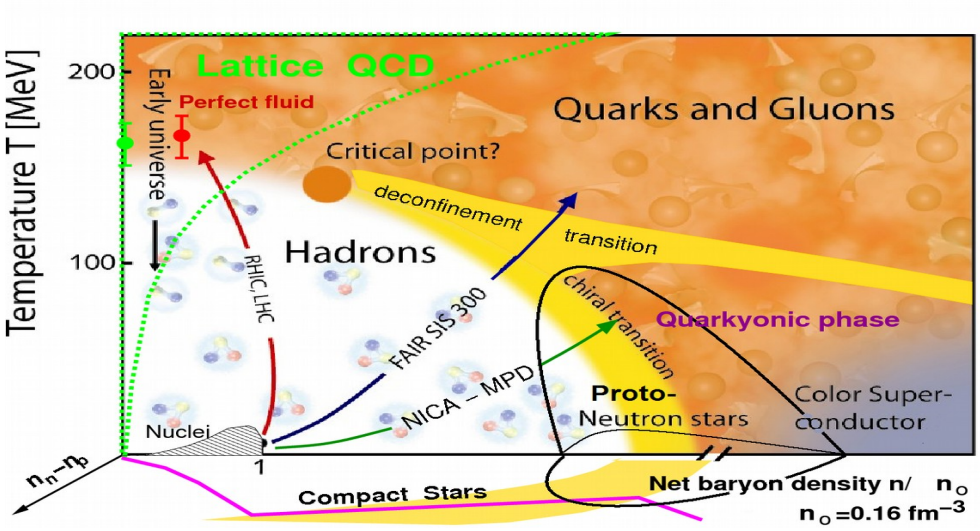

Figure 1.1: QCD matter phase diagram. Figure taken from Ref. [7].

1.2 Historical Evolution Heavy Ion Experiments: AGS → SPS → RHIC → LHC → FAIR

The exploration of hot and dense QCD matter progressed through a sequence of accelerator complexes and detector concepts. Early efforts at the AGS (BNL) and SPS (CERN) pioneered fixed target programs that delivered first evidence for collective flow [12] and in medium vector meson modifications. SPS era experiments, in particular, suggested excess low mass dileptons over hadronic cocktail expectations, consistent with broadening of the ρ spectral function in matter. RHIC then established the strongly coupled quark gluon plasma (sQGP): anisotropic flow scaling, jet quenching, and heavy flavor energy loss pointed to a nearly perfect fluid with strong coupling at the partonic level. At the LHC, these phenomena persist at higher temperatures and multiplicities, enabling differential studies of jet substructure and quarkonia sequential suppression. At lower $\sqrt{s}$, fixed target experiments have targeted the high μ_B region with enhanced sensitivity to the nucleon density driven dynamics of the medium. FAIR extends this strategy decisively with beams from SIS100 (proton: 2 to 29 AGeV; heavy ions: 2 to14 AGeV), providing access to several times the nuclear saturation density. The CBM experiment

is optimized for this environment: it emphasizes rare probe statistics, free streaming readout, and robust real time computing to keep pace with interaction rates far beyond the traditional triggered model.

1.3 The CBM experiment at FAIR: Concept and Architecture

CBM is a fixed target experiment optimized for rare probe measurements at high interaction rates. It's detector suite includes a Micro Vertex Detector (MVD), a Silicon Tracking System (STS), a Ring Imaging Cherenkov detector (RICH), a Transition Radiation Detector (TRD), Time of Flight (TOF) walls, and the Muon Chamber (MuCh) [14], arranged downstream of segmented absorber system [6]. The overarching concept is a fast, radiation tolerant apparatus that streams data continuously to a high performance computing farm. Precise time stamping in front end electronics, low latency transport, and event building based on time space correlations replace traditional level 1/level 2 trigger logic. This paradigm allows CBM to reach and sustain interaction rates of order 10 MHz, a prerequisite for collecting adequate statistics in the most background challenged channels. The MuCh system is central to the di-muon physics program. MuCh employs alternating absorber layers and tracking stations to separate muons from hadronic background and to reconstruct di-muon invariant masses. Stations 1 and 2 confront the highest local hit densities, so the detectors must combine high granularity, fast response, and excellent stability under sustained irradiation. The choice of triple GEM technology for these stations follows extensive R&D and beam tests within the collaboration and in allied programs.

1.4 Micro Pattern Gas Detectors and GEM Technology

Micro Pattern Gaseous Detectors (MPGDs) were developed to surpass rate and stability limits inherent to wire based technologies. The Gas Electron Multiplier (GEM), introduced by F. Sauli [13], consists of a thin polyimide foil of 50 μm clad with copper coating of 5 μm on both side and perforated with a dense, regular array of microscopic holes. A potential difference of 500 Volts across the foil creates intense electric fields of 100 kV/cm inside the holes; electrons drift into the holes and undergo avalanche multiplication. Cascading multiple GEM foils (typically three) yields high effective gain while keeping the per foil voltage low enough to suppress discharges and photon feedback. For large area tracking in high flux environments, GEM detectors provide several key advantages: (i) their intrinsic segmentation and distributed amplification significantly reduce space charge effects; (ii) gain uniformity is ensured through segmented foils and well defined high voltage distribution; (iii) discharge probability is minimized by the multi stage amplification structure; and (iv) their mechanically lightweight and radiation tolerant designs integrate well with the absorber constrained geometries of the MuCh stations. Bench tests and mini CBM beam campaigns demonstrate detection efficiencies exceeding 95%, time resolutions at the level of 30 nanoseconds, and stable gain at rates upto 400 kHz/cm^2, consistent with MuCh requirements.

1.5 Rate, Pileup, and Online Reconstruction in a Free Streaming Experiment

Operating at interaction rates approaching 10 MHz necessitates a fundamental redefinition of the interface between the experimental subsystems and the computing infrastructure. In the free streaming paradigm, front end electronics continuously digitize, time stamp, and transmit detector signals; downstream, a data acquisition network and event processing farm perform

time slice building, clustering, and track segment finding in near real time [15]. For MuCh, the pattern recognition must cope with absorber induced multiple scattering and a broad momentum spectrum, while maintaining high efficiency for dimuons from ω and J/ψ. Achieving this performance requires: (a) high granularity readout with minimal dead time; (b) excellent time alignment across subsystems; (c) stable detector gain; and (d) thermal and power management compatible with long runs. The detector technologies, electronics, and services must therefore be engineered as a coherent system. This thesis contributes to that integration by developing and validating full size triple GEM modules for Station 2, together with a calibrated gas mixing and distribution system and a scalable cooling solution for the front end electronics.

1.6 The MuCh System and Detector Requirements for Stations 1 and 2

MuCh comprises multiple tracking stations interleaved with absorbers. Close to the beam pipe, local hit densities are the highest; rate capability and granularity are thus the dominant constraints for stations 1 and 2. Detector segmentation must follow the radial decrease of flux to keep occupancy and channel counts manageable. Uniformity of response across large surfaces requires robust high voltage segmentation, gas distribution without gradients, and thermally stable readout electronics. Within this context, triple GEM modules were designed with progressive pad sizes, foil segmentation, and optimized field configurations. Their readout integrates self triggered front end ASICs compatible with continuous DAQ. The gas system must deliver reproducible mixtures at stable flow with oxygen and humidity control; the cooling system must keep electronics temperatures below 25°C to minimize noise and drift. These system level requirements are derived from mini CBM beam tests [16] and from detailed simulations documented by the collaboration.

1.7 Large Area Triple GEM Modules for MuCh Station 2

The MuCh second station of CBM comprises 60 trapezoidal triple GEM detector modules arranged in three concentric layers, covering a polar angular acceptance from 5.6°to 26.8°. Each module measures approximately one meter along its long edge, making it one of the largest GEM detectors fabricated for high rate operation [17]. To accommodate fabrication limitations in the Indian PCB industry while maintaining gas tightness, the readout board was realized as two multilayer sub boards joined using a precision prepeg based technique. The joint corridor is kept track free, with a dead zone limited to about 0.2 mm after surface milling, ensuring both mechanical integrity and leak tightness. The readout board, designed at VECC, is an eight layer PCB containing 1,824 pads distributed across 19 columns and 96 rows. The pad sizes vary radially, increasing from 4 x 4 mm^2 near the beam pipe to 21 x 21 mm^2 at the outer radius, matching the expected particle flux gradient. Each pad connects to the front end electronics through multilayer tracks, and 15 Front End Boards (FEBs), each housing a STS/MuCh XYTER v2.1 ASIC, are required to readout a single module. High voltage distribution employs an opto coupler based biasing network that allows individual control of the 72 segmented GEM foils, enabling remote isolation of faulty segments without interrupting overall operation. Module assembly was carried out in a class 1000 cleanroom using three single mask GEM foils procured from CERN and stretched with the NS-2 technique, which avoids gluing and minimizes mechanical stress. A 3-2-2-2 mm gap configuration was maintained using precision spacers. All foils underwent pre-assembly quality assurance at 500 V to verify low leakage current ($<$5 nA per segment) and absence of shorts. Post assembly, the modules were conditioned under a continuous Ar:CO_2 (70:30) flow to ensure leak integrity and stable operation. Performance characterization using ^{55}Fe X-rays and cosmic rays established an exponential dependence of detector gain on summed GEM voltage, a detection efficiency approaching 98% in a simple three fold cosmic telescope, and a time resolution of about 18 ns. Gain uniformity measurements across the active area showed variations within 43%, attributed mainly to charge

sharing among fine pads. These results confirm the mechanical precision, electrical stability, and robustness of the indigenously fabricated modules, validating their readiness for integration into the CBM MuCh second station. Subsequent tests in the mini CBM setup further demonstrated stable performance under high rate beam conditions and successful alignment within the integrated detector environment.

1.8 Services: Gas Delivery and Thermal Management

The long term stability and performance of large area GEM detectors depend critically on the reliability of the associated service infrastructure particularly the gas delivery and cooling systems. A precisely calibrated mass flow controller (MFC) based gas mixing and distribution system has been developed to ensure reproducible and uniform supply of ultra high purity Ar:CO_2 mixtures. Each MFC is independently calibrated against a standard flow meter for several mixture ratios (60:40, 70:30, 80:20, and 90:10), allowing accurate control over both composition and flow rate. Systematic measurements performed on full size MuCh second station GEM modules demonstrate that, for a 70:30 Ar:CO_2 mixture, the effective detector gain increases with flow rate up to approximately 8 L/h and then saturates [18]. At this point, the oxygen contamination falls below 160 ppb and the relative humidity drops below 50%, providing the most stable and reproducible operating conditions. Based on these results, a parallel gas distribution architecture has been proposed for the CBM MuCh system, in which each module receives gas through an independent supply line. This configuration eliminates interdependence inherent to daisy chain connections and ensures consistent gain across modules irrespective of local leak conditions or line resistance. Each input and output channel is instrumented with calibrated flow sensors, providing per module diagnostics and online leak detection capability. Thermal management of the front end electronics is equally critical under high rate operation. To address this, water cooled aluminum plates are designed and tested using resistive heater

loads equivalent to the dissipation of the full front end board array. Extended operation demonstrated excellent temperature uniformity and stability, with surface temperatures maintained below 25 °C even under continuous load conditions. The water based solution provides sufficient thermal headroom to accommodate long term beam operation while minimizing temperature induced gain variations. These service developments comprising the calibrated gas handling, parallel distribution network, and water cooled thermal management, will be integrated with the mechanical and readout structures of the GEM modules to ensure stable, low noise, and long duration data acquisition in the CBM MuCh environment.

1.9 Chapter Summary and Thesis Roadmap

This introduction set the stage for the CBM physics program at high μ_B, the historical trajectory of heavy ion experiments, and the detector and computing paradigm required for sustained operation at 10 MHz interaction rate. It reviews earlier heavy ion programs (AGS $\rightarrow$ SPS $\rightarrow$ RHIC $\rightarrow$ LHC) leading to FAIR's high rate (10 MHz) approach. The MuCh system, central to the dimuon detection program, places stringent requirements on detector granularity, rate capability, and operational stability requirements effectively addressed through the use of large area triple GEM technology. The remainder of the thesis is organized as follows. **Chapter 2** details the design, fabrication, and bench characterization of real size station-2 modules, with emphasis on readout architecture, high voltage segmentation, and clean assembly. **Chapter 3** presents mini CBM beam results relevant to rate handling, timing, and alignment within the integrated setup. **Chapter 4** documents the development and calibration of the gas system, including mixture stability and distribution architecture. **Chapter 5** addresses cooling solutions and their validation under sustained load. **Chapter 6** describes the production oriented X-ray QA methodology and acceptance criteria. The thesis closes with a summary of achievements and an outlook toward series production and integration into the CBM cave.

Bibliography

[1] ALICE Collaboration, "The ALICE experiment: a journey through QCD," Eur. Phys. J. C (2024) 84:813. doi:10.1140/epjc/s10052-024-12935-y

[2] K. Fukushima and T. Hatsuda, Rept. Prog. Phys. 74 (2011) 014001 doi:10.1088/0034-4885/74/1/014001

[3] STAR Collaboration, "Experimental and theoretical challenges in the search for the quark gluon plasma: The STAR Collaboration's critical assessment of the evidence from RHIC collisions" Nuclear Physics A, Volume 757, Issues 1-2, 8 August 2005, Pages 102-183 doi:https://doi.org/10.1016/j.nuclphysa.2005.03.085

[4] The Cbm Experiment. doi:https://www.cbm.gsi.de/

[5] The Fair Experiment. doi:https://fair-center.eu/.

[6] Subhasis Chattopadhyay et al., editors. Technical Design Report for the CBM : Muon Chambers (MuCh). GSI, 2015. doi:https://repository.gsi.de/record/161297/files/much-tdr-final-for-gsi-report.pdf

[7] Ablyazimov, T. et. al. Challenges in QCD matter physics The scientific programme of the Compressed Baryonic Matter experiment at FAIR. Eur. Phys. J. A 53, 60 (2017). doi:https://doi.org/10.1140/epja/i2017-12248-y

[8] STAR Collaboration, "Elliptic flow of heavy-flavor decay electrons in Au+Au collisions at $\sqrt{s_{NN}}$ = 27 and 54.4 GeV at RHIC" Physics Letters B, Volume 844, 10 September 2023, 138071 doi:https://doi.org/10.1016/j.physletb.2023.138071

[9] Berndt Muller et. al. "First Results from Pb+Pb Collisions at the LHC" Vol. 62 (2012), pp. 361-386 doi:https://doi.org/10.1146/annurev-nucl-102711-094910

[10] Chattopadhyay, S. Physics of strongly interacting matter at high net-baryon density. Eur. Phys. J. Spec. Top. 230, 689-696 (2021). doi:https://doi.org/10.1140/epjs/s11734-021-00024-0

[11] T. Matsui, H. Satz, "J/ψ suppression by quark-gluon plasma formation" Physics Letters B, Volume 178, Issue 4, 1986, Pages 416-422, doi:https://doi.org/10.1016/0370-2693(86)91404-8

[12] Ulrich Heinz and Raimond Snellings, "Collective Flow and Viscosity in Relativistic Heavy-Ion Collisions" Vol. 63 (2013), pp. 123-151 doi:10.1146/annurev-nucl-102212-170540

[13] Fabio Sauli, "The gas electron multiplier (GEM): Operating principles and applications" Nuclear Instruments and Methods in Physics Research A 805 (2016) 2âĂŞ24 doi:http://dx.doi.org/10.1016/j.nima.2015.07.060

[14] A.K. Dubey et al. GEM detector development for CBM experiment at FAIR. Nucl. Instrum. Meth.A, 718:418 - 420, 2013. doi:https://doi.org/10.1016/j.nima.2012.10.043

[15] V. Singhal et al 2021 JINST 16 P08043, "Development and implementation of a time-based signal generation scheme for the muon chamber simulation of the CBM experiment at FAIR" doi:10.1088/1748-0221/16/08/P08043

[16] A. Kumar et al., Commissioning and testing of pre-series triple GEM prototypes for CBM-MuCh in the mCBM experiment at the SIS18 facility of GSI, 2021 JINST 16 P09002 [arXiv:2108.05646]. doi:https://doi.org/10.1088/1748-0221/16/09/P09002

[17] Chandrasekhar Ghosh et al 2025 JINST 20 P09005, "First prototype of MuCh second station GEM module: design, fabrication and testing for CBM experiment at GSI, Germany" doi:https://doi.org/10.1088/1748-0221/20/09/P09005

[18] Chandrasekhar Ghosh et al 2025 JINST 20 P10036, "Performance study and gas system development for large-size GEM modules in the CBM-MuCh detector system" doi:https://doi.org/10.1088/1748-0221/20/10/P10036

Chapter 2

Design, fabrication and testing of MuCh second station real size module for CBM experiment

2.1 Introduction

The International Facility for Antiproton and Ion Research (FAIR) in Darmstadt, Germany, provides unique research opportunities in the field of hadronic and leptonic physics. The upcoming Compressed Baryonic Matter (CBM) experiment at FAIR is designed to investigate the dense nuclear matter in nucleus-nucleus collisions with an interaction rate up to 10 MHz. The identification of rare probes like low mass vector mesons (LMVM), multi-strange hyperons, charmonia etc, requires a very high interaction rate and efficient background suppression. CBM will initially use proton beam from SIS100 synchrotron with an energy of 2-29 AGeV and heavy ion beam with an energy of 2-14 AGeV. Finally it will be using beam from SIS300 synchrotron with an energy upto 90 AGeV for proton and upto 45 AGeV for heavy ions [1]. CBM will consist

of four circular stations of Muon Chambers (MuCh) sandwiched between absorber layers and each station will consist of three circular layers of gaseous tracking detectors. As a part of the collaboration, MuCh group needs to fabricate and install all the four stations of MuCh. The maximum particle incidence rate at second station is expected to reach upto 90 KHz/cm^2. For central collision those incidence rates are expected to be higher by a factor of four. As the first two stations of MuCh will be exposed to very high particle rates and therefore to handle such high rates, detectors based on Gas Electron Multiplier (GEM) technology [3] [4] [5] [6] will be used for building MuCh. As this is a fixed target experiment, all the detector stations will be positioned in forward rapidity region and the MuCh second station will cover an acceptance of 5.6^0 to 26.8^0. This will consist of three circular layers of GEM modules with each layer consisting of twenty such trapezoidal modules, i.e sixty trapezoidal GEM modules will be required to populate the entire second station of MuCh. Detailed descriptions of 1st and 2nd station modules are provided in Table 1. Mixture of Argon and CO_2 gas in proportion of 70:30 will be used as the sensitive medium of the detector. All details about the first station chamber of MuCh has been reported in [2] and in this present article we will report about the design, fabrication and lab test results of the MuCh second station GEM module in detail.

MuCh Station number	Number of layers	Total number of GEM modules	Total no of readout pads	Total number of FEBs	Active area dimension of each module (cm)	Pad granularity (mm)	Detector acceptance
1	3	48	107088	864	Length ∼80 Inner ∼7.5 Outer ∼40	Min ∼3.2 Max ∼17	Min ∼5.6^o Max ∼27.2^o
2	3	60	109440	900	Length ∼100.5 Inner ∼7.9 Outer ∼41.5	Min ∼4.5 Max ∼21.5	Min ∼5.6^o Max ∼26.8^o

Table 2.1: Specifications of first two stations of MuCh modules.

2.2 Design and Fabrication of the detector

The detector module is made of one drift PCB, one readout PCB and three GEM foils, with a gap configuration of 3-2-2-2 mm respectively [3]. The readout PCB for the module has been designed at VECC using Proteus-8 software. This is a eight layer PCB consisting of 1824 readout pads distributed among 19 columns and 96 rows. As the incident particle rate will be higher in the inner zone near the beam pipe and will gradually decrease outward radially from beam pipe, the pads are designed accordingly with progressive geometry. The innermost annular ring pad size is around 4 mm x 4 mm and this size increases progressively up to around 21 mm x 21 mm for the outermost ring. Each readout pad has been connected by copper track through the multiple layers of PCB up to the Front End Board (FEB) input channel connector. One FEB consists of one STS/MUCH-XYTER v2.1 ASIC [5], which can acquire data from 128 readout pads. A total of 15 FEBs will be required to read out one complete module. As the trapezoidal readout PCB length is about a meter, due to fabrication constraint of such a large size multi layer PCB by Indian Industry, a PCB joining technique has been adopted. The drift PCB length is 1164 mm and width is 468 mm.

The Gerber layout of the readout PCB is shown in Figure 2.2a and this shows how the readout pads are connected to the FEB connectors through multiple layers (different colors) of the PCB. The Gerber layout of drift PCB is shown in Figure 2.1a and this PCB consists of the high voltage (HV) distribution circuit at the outer end as shown in Figure 2.1b. The second station module has been assembled at VECC clean room using three GEM foils, readout PCB, drift PCB and other necessary components. The fabrication procedure is shown in Figure 2.2b. The prototype module after fabrication is shown in Figure 4.1b and this shows the drift PCB has 18 through holes on top, covered with Kapton foil. Those holes are kept for the passage of X-rays from ^{55}Fe source for measuring the gain of the module. The gain has been measured across the entire active area.

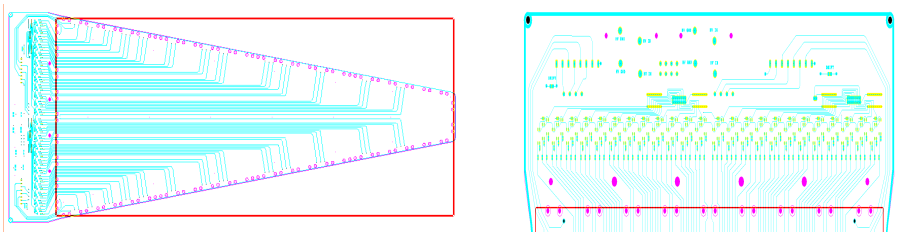

(a) (b)

Figure 2.1: (a) Gerber layout of 2nd station drift PCB. (b) High voltage section layout

The HV is applied through a ceramic resistor divider chain and the output voltages are passed through an opto coupler (OC) circuit [7]. Each GEM foil has 24 segments and three layers of such foils are placed inside this module, so the module consists of total 72 GEM segments. All those 72 segments are powered using 72 opto couplers. During operation if any particular GEM segment goes bad then the voltage to that particular segment can be switched off by controlling the opto coupler using slow control over ethernet. Thus the detector will remain operational, even if any GEM segment goes bad. On the drift PCB, 72 dip switches are also provided to switch on or off any segment manually.

The drift PCB consists of a ground plane on the top for EMI shielding. The necessary high voltage (HV) distribution circuit is placed in the outer region of the drift PCB. HV is fed through one SHV connector and it is channeled into two voltage divider ceramic resistances for distribution among the three GEM foils.

The real size trapezoidal shape, single-mask GEM foils are procured from CERN. Those foils are stretched using 'NS-2' technique [6], which does not involve any gluing operation. The entire GEM foil is segmented into 24 segments which takes care of large capacitance of such large size foils. Before fabrication, each segment of all three foils has been tested with 550 V, with a criterion of no short and low leakage current of less than 5 nA. All the measurements are done at 23^0 C ambient temperature and 50% relative humidity inside a clean room of class 1000 at VECC. After all those necessary Quality Assurance (QA) the three GEM foils along with

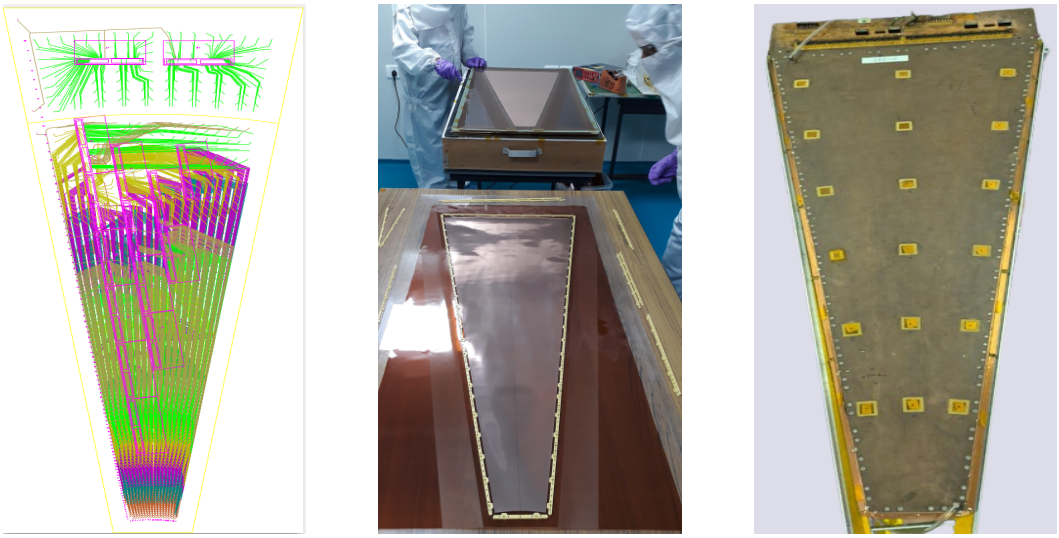

(a) (b) (c)

Figure 2.2: (a) Gerber layout of 2nd station readout PCB. (b) Fabrication procedure in VECC clean room. (c) Prototype Module

necessary spacers and screws are placed within the drift and readout PCB at a gap of 3-2-2-2 mm, where these numbers represent the consecutive gaps in mm between different layers [4].

After fabrication, the module was put under Ar : CO_2 (70:30) gas flow for several days and investigated for any possible leaks with a leak detector.

2.3 Joining technique of the multilayer readout PCB

The PCB manufacturing was entrusted to a vendor in India having the capability of making the multilayered PCB up to 800 mm and if supporting boundaries do not contain any active circuitry, then they can reach up to 900 mm of length. The station-2 PCBs are of even bigger size so it couldn't be produced in a single go. Therefore, considering the processing sizes available with industries, a new concept of joining PCBs has been adopted. There were a few prerequisites for joining PCB design which are as follows: (a) The design should be made such

that there should be no tracks passing through the joining region. (b) two tracks connecting 2 separate readout pads should not cross each other in same layer- there should be a minimum distance of 8 thou between 2 tracks. (c) long tracks are not kept parallel to each other, as it can lead to cross talk. (d) the dead area along the joining line is minimized to 0.2 mm which is only 0.05mm higher than the other regions of the PCB.

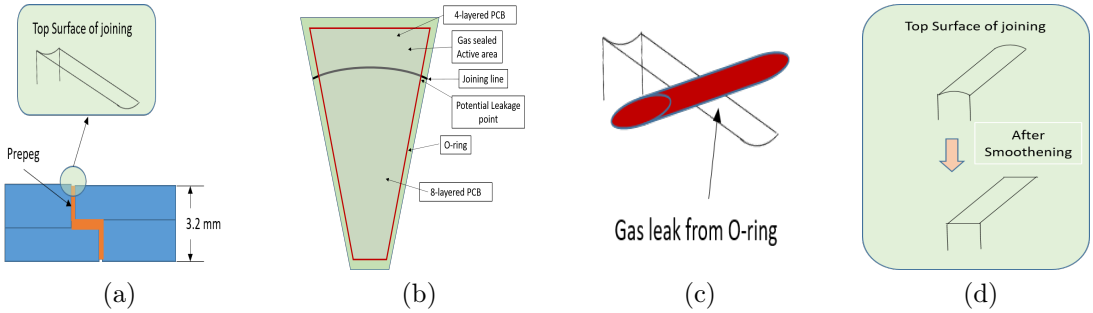

(a) (b) (c) (d)

Figure 2.3: (a) Joining profile. (b) Schematic of PCB. (c) Gas leak region. (d) Smoothening of surface.

The Gerber design consists of two PCBs, one of 8-layered and the other of 4-layered and both are joined by the prepeg of thickness 0.4 mm as shown in Figure 2.3a. These two PCBs along with the prepeg are put in the hot press with the limited region. In the first version of joining, the surface finish was missing and there was a dip in the joining region. In this version, the prepeg used in joining of the PCB was not enough and the dip created due to lack of prepeg on the surface. Figure 2.3b shows the PCB and the red line shows the O-ring, which is essential for gas tightness. A gap can be seen between the red O-ring and the dip in the PCB in Figure 2.3c. This resulted in gas leak at the joining region which creates a serious performance issue of the GEM detector and was initially cured by filling glue in the gaps and sealing them. Later in the corrected version, this issue is rectified by over filling of prepeg in the gap and later on smoothening of the surface by milling as shown in Figure 2.3d. After fabrication of PCB, the GEM detector was assembled at VECC and no gas leak was found.

2.4 CBM Rate Simulation

This section presents the results of simulation studies conducted for the second station of the Muon Chamber (MuCh) Detector system, designed for the CBM experiment. The SIS-100 accelerator ring at FAIR can generate high-energy beams, reaching up to 30 AGeV for protons and 12 AGeV for heavy ions. The key objective of this simulation is to estimate the particle rates across the entire area of the second station module.

In CBM experiment, the interaction rate will go up to 10 MHz. A simulation has been performed using 100,000 minimum bias Au-Au UrQMD events at energies ranging from 4 AGeV to 12 AGeV. These events are simulated through the CBM experiment setup using the Geant3 transport engine. The selected geometry represents a more realistic configuration of the MuCh detector setup as shown in Figure 2.4a. This setup includes improvements such as a latest readout shape, the incorporation of FEBs, C Plate, G10 material, and CNC holes. The detector planes of the second station can be seen in Figure 2.4b.

The primary goal of this study is to compute the particle rate at different stages of the simulation process Monte Carlo (MC), Digitization and Reconstruction for the Muon Chamber Detector.

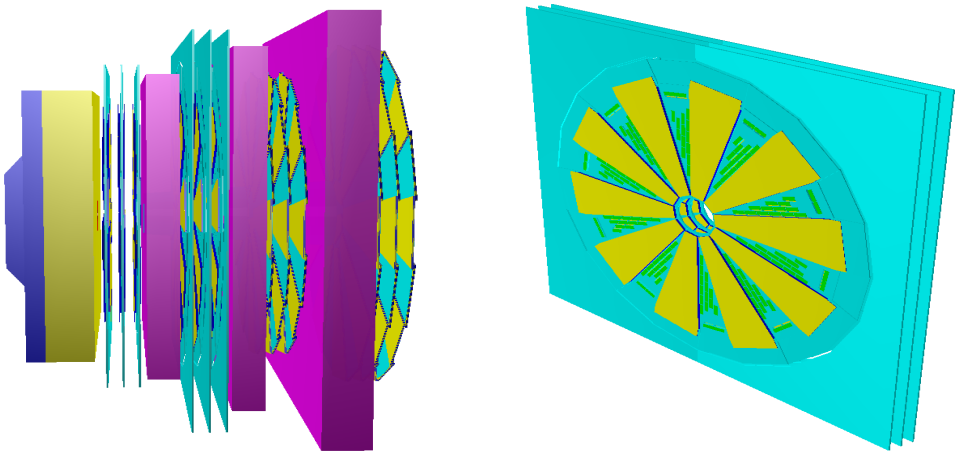

(a) (b)

Figure 2.4: (a) Muon Chamber detector setup. (b) Detector Planes geometrical setup of Muon Chamber Second Station.

The UrQMD-generated events are transported through the detector setup using the Geant3 engine, which produces Monte Carlo (MC) points on the detection layers. Figure 2.5a shows the Z-distribution of MC points and the entries around 200 cm come from the 3 detector layers of the second station. The XY distribution of MC points is shown in Figure 2.5b, which shows a decreasing point density as we go radially outwards.

The MC points have been converted into digis on the detector based on predefined digitization parameters. These parameters include a spot radius of 500μm, a charge threshold (Q$threshold$) of 6 fC, a charge saturation (Qmax) of 81 fC, a mean gas gain of 5000 and 32 ADC channels. Each layer of second station is radially segmented into sectors with a one-degree segmentation, as illustrated in Figure 2.5c and the same has been implemented in the readout PCB gerber.

The radial point density distribution is analyzed based on the expected interaction rate of 10 MHz. Since the numbers in the plot represent values per event, so they are scaled by a factor of 10^7.

The variation of MC point rate per event per cm^2 with radius is illustrated in Figure 2.6a, which goes up to a maximum value of 75 kHz/cm^2 at 12 AGeV.

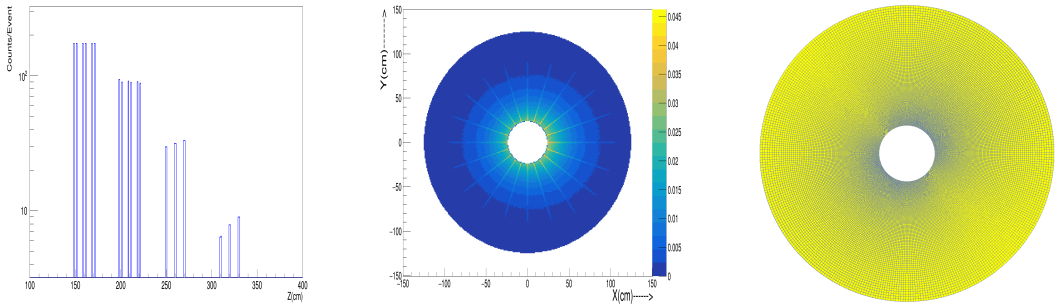

(a) (b) (c)

Figure 2.5: (a) Z distribution of Muon Chamber Station. (b) XY distribution of MC points on Second Station. (c) Segmentation of Second Station.

The digi density is calculated by determining the number of digis per sector and then dividing this value by the pad area within the corresponding sector, as shown in Figure 2.6b. The maximum value of digi rate goes up to 90 kHz/cm^2 at 12 AGeV. Further, the digis have been utilized to generate hits on the MuCh detector using reconstruction algorithms. The particle hit density is illustrated in Figure 2.6c and the maximum hit density goes upto 66 kHz/cm^2 at 12 AGeV. Figure 2.7 shows the peak rates of MC point density, digi and hits. So, from this simulation study, it has been found that the maximum digi rate will go up to 90 kHz/cm^2 at 12 AGeV and this rate can well be handled by GEM based detectors.

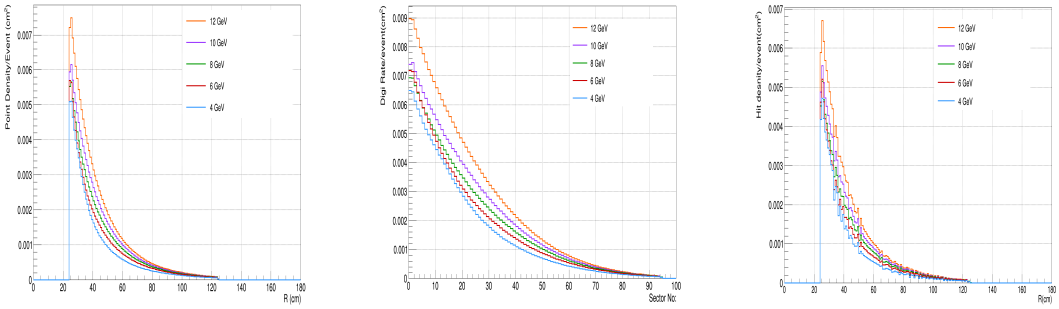

(a) (b) (c)

Figure 2.6: (a) Radial density distribution of MC ponits. (b) Sector wise digi rate distribution. (c) Radial density distribution of Reconstructed Hits

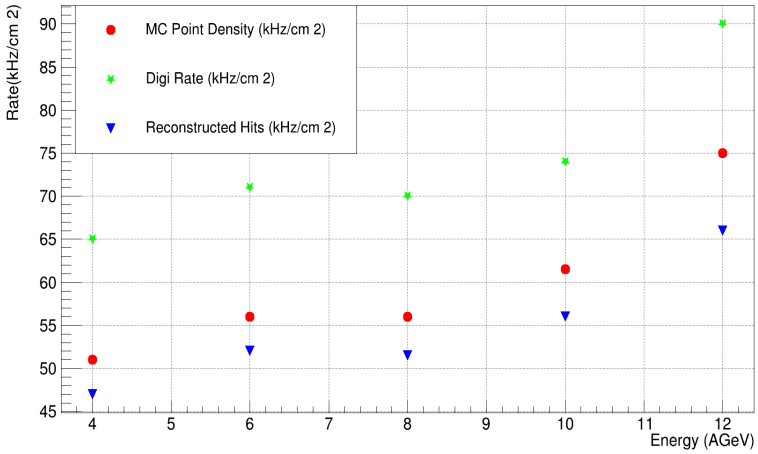

Figure 2.7: Peak rates at different energy.

2.5 Data acquisition chain and Front End Board (FEB)

As the incident particle rate in CBM will be very high, the traditional triggered electronics are not suitable for data acquisition. Therefore, for the CBM-MuCh-GEM detectors, a self-triggered readout architecture has been adopted [5]. Front End Boards (FEB) with STS/MUCH-XYTER ASIC are being used for data acquisition. This ASIC is designed for

readout via a GBTx. However, in our test setup at VECC, a custom FPGA-based GBTx emulator board is used instead. Unlike the GBTx, this emulator board offers a standard 10 Gbps back-link and 42 front-end links, each capable of handling a 320 Mbps data rate. The data from these links is collected using an FPGA-based HiTech Global development board, which is installed in the DAQ server PC via a PCIe slot and can manage up to eight AFCK boards. The data stream generated by the ASIC includes 7-bit channel identifiers, 5-bit ADC values, 14-bit timing information, and a 2-bit data type identifier. Operating at a clock frequency of 320 MHz, the ASIC provides a timing resolution of 3.125 ns. This timing information is used to form time clusters, which, combined with spatial data, enable the construction of real-time clusters for further analysis. The ASIC employs a flash ADC, with each of its 32 channels having a configurable threshold set via a 8-bit DAC. Calibration of all 32 Channels are performed using an external pulse generator, within a charge range of 6 fC to 81 fC in 2.5 fC steps.

Each FEB generates 5 W heat, so a total of 5 W x 15 = 75 W heat gets generated by the readout electronics of one GEM module. Now as the entire second station will consist of 60 modules, a total 4.5 KW heat will be generated. This amount of heat can raise the temperature of the cave and the readout ASIC performace will also deteriorate, so this needs to be extracted from the cave. A cooling arrangement to cool down the FEBs for smooth operation has been developed. A 10 mm thick trapezoidal shaped aluminum plate with water channels grooved inside has been designed and fabricated for cooling of the electronics. Chilled water of 17^0 C is circulated through those water grooves, which in turn cools down the entire aluminum plate surface area. The FEBs are mounted on this cooling plate such that the heat gets transferred to the plate and gets carried away by chilled water. On the other side of the same cooling plate the detector module is mounted, such that this plate works as a support structure. Inside CBM cave, 20 such trapezoidal aluminum plates will be joined together to make a circular support structure for each layer of 2^{nd} station.

2.6 Measurement of Detector Gain with ^{55}Fe X-ray Source

The gain of the second station MuCh module has been measured using a ^{55}Fe X-ray source at lab. A gain up to 4274 is measured at summed GEM voltage of 1014 Volts, beyond this voltage the cluster charge spectra gets saturated as the ASIC has been calibrated upto 81 fC. Figure 2.8a shows the cluster charge (fC) spectra of ^{55}Fe at a summed foil voltage of 977 V. The main peak of the spectra is fit with a Gaussian and the mean value (in fC) is taken for the gain calculation. As the number of primary electrons generated is around 212, the gain is calculated by dividing the clustered charge by 212. Figure 4.1c shows the schematic of the hole positions on the drift plane. Gain has been measured at several hole positions. The Figure 2.8c shows the Gain variation with HV at two different positions (hole 6 and hole 18) on the detector. The plot shows that the gain increases exponentially with HV. As the two holes are located in two halves of the detector, so it can be seen that both halves show similar gain behaviour. The gain uniformity has been measured at several hole locations across the detector, at fixed summed HV of 964 V. The values are shown in Figure 2.8d, and a variation of 43% is observed across the entire module. This variation is observed due to charge sharing among the smaller pads. If the shared charge goes below 6 fC (threshold value) then it can't be detected and so it won't be the part of the cluster charge, hence the gain will show a lower value.

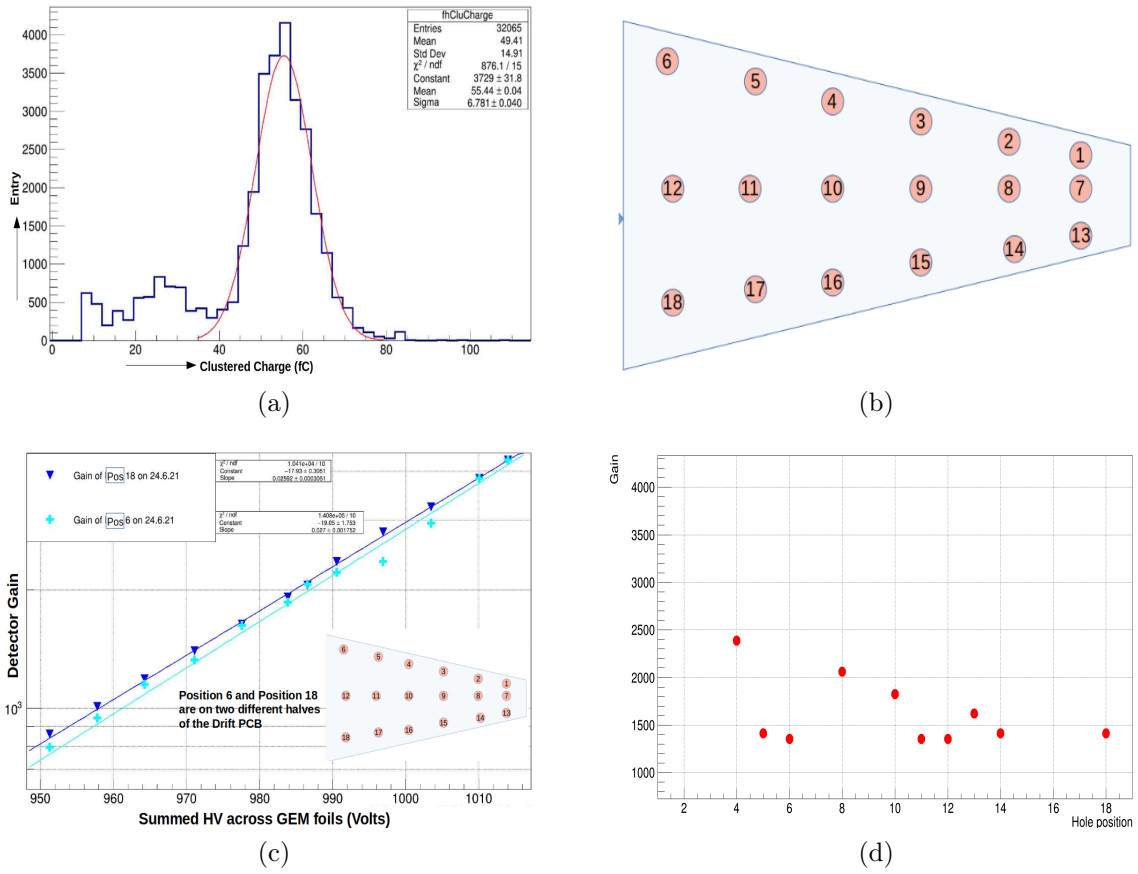

Figure 2.8: (a) Cluster Charge (fC) spectra of ^{55}Fe at 977 V. (b) Hole Layout (c) Detector Gain Variation with HV at 2 positions on the detector. (d) Gain Variation

2.7 Noise performance of the module

The entire area of the detector can be read out by 15 FEBs, but due to limited available electronics resources, we could read out an area corresponding to 5 FEBs at a time only. The 5 FEBs has been connected to the broader region of the detector. One annular ring of pads, just above the joining line of the PCB shows noise. Figure 2.9a shows the readout pad mapping of the detector module with 19 columns and 96 rows. Ring no. 88 just above the joining line show noise. As this is a joined PCB so the ground plane gets disconnected at the joining position,

so this particular ring of pads pick up noise from surrounding. To take care of this we shielded the 88^{th} annular ring by copper tape and the tape was soldered to ground plane of both side of the joining line, this makes the shielding of the entire PCB complete as shown in Figure 2.9b. After this modification, the data is acquired and found to be noise-free. Now, to get the noise profile of the entire detector module, one particular FEB is used to get the noise data over all the connectors. Figure 2.9c shows the readout areas corresponding to 15 connectors in different colors. All these areas are readout by 1 FEB at a time. The detector is kept at operating voltage and from each connector, noise data is acquired for fixed time duration of 4000 TS (Approx 8 mins) and the combined noise data is shown in Figure 2.9d. One particular zone around 40^{th} row and 10^{th} column shows noise, the reason maybe due to long tracks in this area.

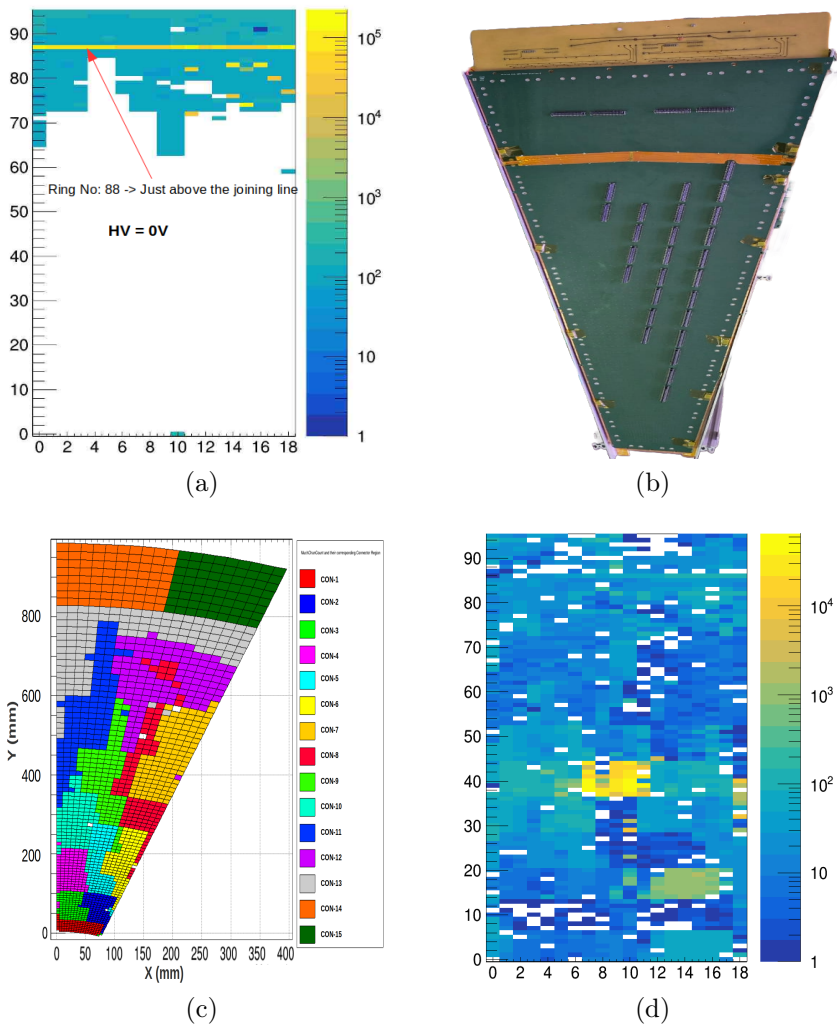

Figure 2.9: (a) Mapping of readout PCB showing noisy annular ring just above the joining line. (b) Shielding of readout PCB joining line. (c) Readout area corresponding to various connectors. (d) Noise profile of the module.

2.8 Measurement of Detector Efficiency and gain with Cosmic muons

A threefold cosmic coincidence setup is prepared for measurement of various characteristics of the detector as shown in Figure 2.10a. 3 plastic scintillators of size 2.5 cm x 2.5 cm, 3.5 cm x 3.5 cm and 8 cm x 8 cm, are used; out of which the first 2 are kept on the top of the module and last one is kept below the module such that the module readout area comes under proper geometrical acceptance. The scintillators are coupled to photomultiplier tubes (PMT) for voltage signal output. The output of PMTs is given to a 16-channel leading edge discriminator (CAEN N841) and further a quad coincidence logic unit (CAEN N1145) is used to get an AND logic with a time window of 500 ns. The final output is read by STS/MUCH-XYTER electronics. So whenever a cosmic muon passes through all the 3 scintillators a trigger signal is generated. On an average 2 coincidence muons are observed per minute. The detector is placed in such a way that the readout area around the coincidence region has no dead pad. Figure 2.10b shows a clean spot of cosmic muons for measurement at position 2 (Inset of Figure 2.12a). Figure 2.11a shows a typical time difference spectrum between trigger signal and the second station module response at summed HV of 1084 V. The detector signal reaches faster as the readout electronics is directly coupled to the detector, but the scintillator signals are processed through NIM modules and afterwards it is given to readout electronics, so the trigger gets delayed and thats why the time difference spectrum shows a mean of 1101 ns. The time resolution of the detector comes out to around 18 ns.

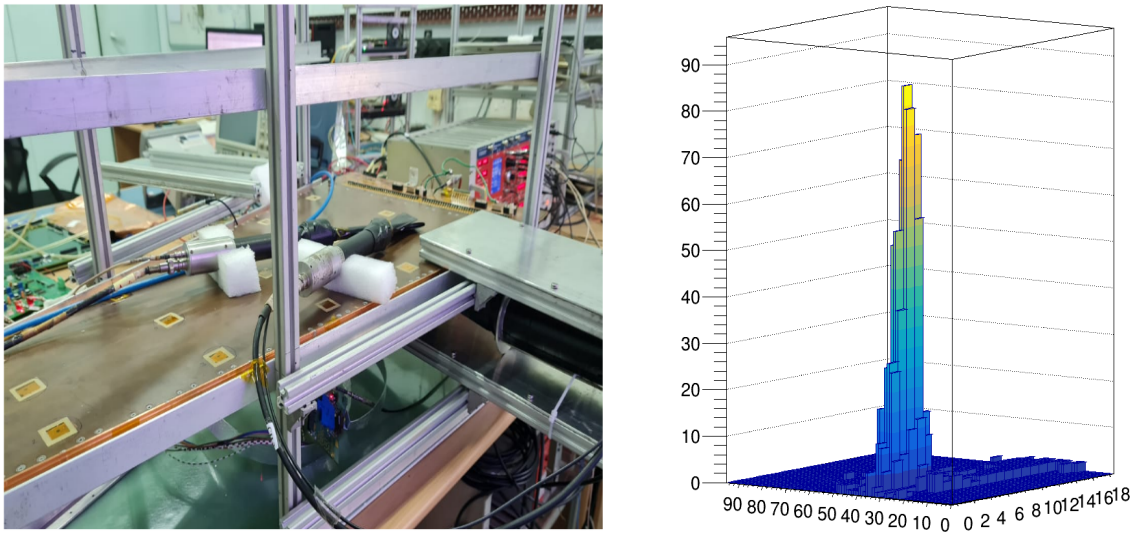

(a) (b)

Figure 2.10: (a) 3 fold cosmic coincidence setup. (b) Cosmic hit mapping at position 2 of the module

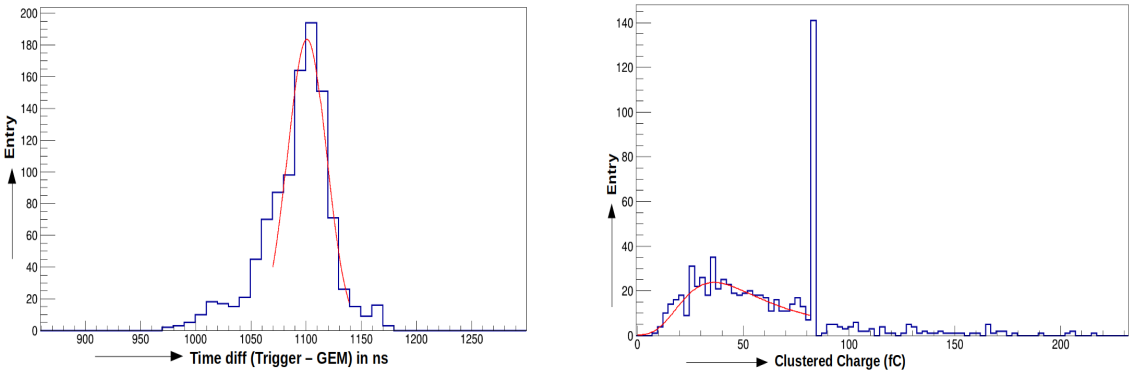

(a) (b)

Figure 2.11: (a) Time difference spectra of GEM hits and scintillator trigger at 1084V (b) Typical cluster charge spectra of cosmic muons at 1084V.

A typical cluster charge spectrum for the cosmic muon is shown in Figure 2.11b. The spectrum is fitted with a Landau distribution and a peak is observed at 39 fC, which corresponds to 2.4

x 10^5 number of electrons, now we assumed that 30 number of primary electrons get generated for each incident cosmic muon. Now if we divide the total number of electrons by 30 then we get detector gain of 8125. We see a peak at 81 fC corresponding to saturation of cluster charge.

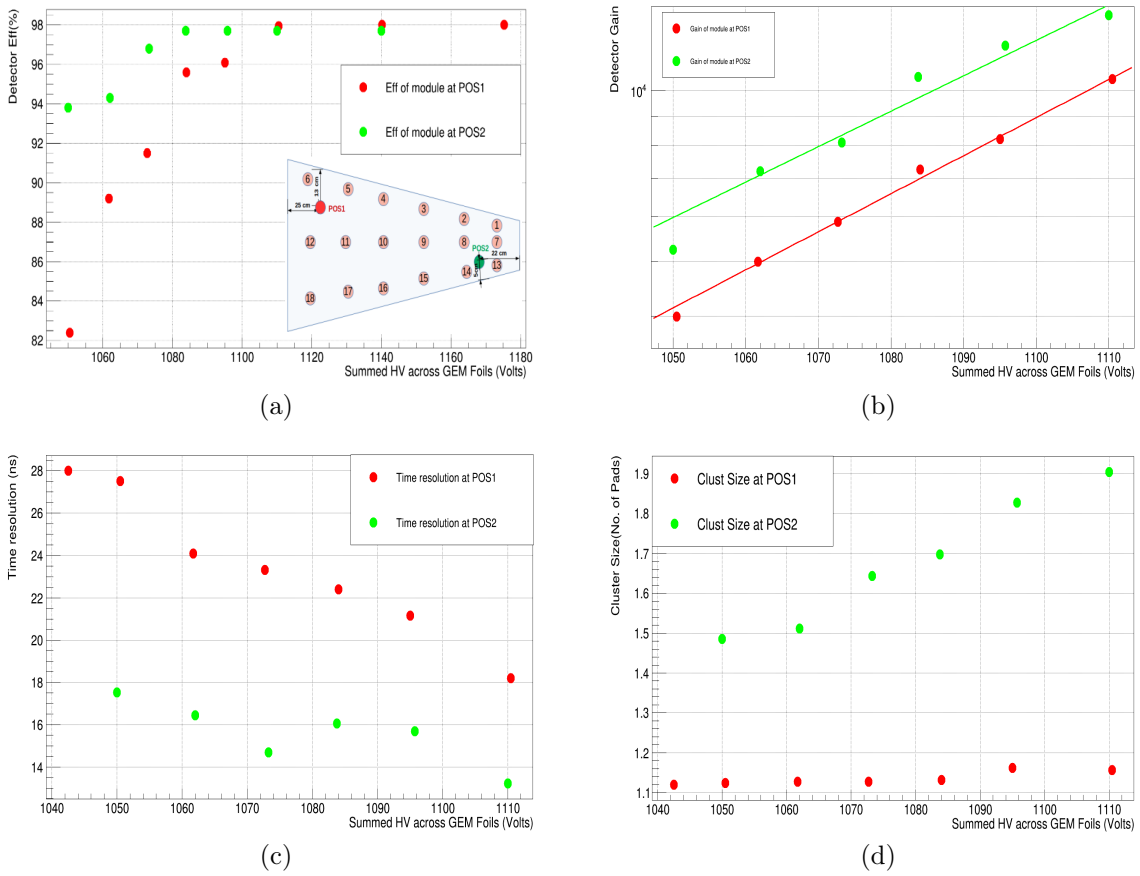

Figure 2.12: (a) Cosmic muon detection efficiency variation with HV at 2 positions (Inset: Location at which efficiency measured). (b) Detector gain calculated from cosmics cluster charge. (c) Time Resolution. (d) Cluster Size.

The cosmic muon detection efficiency is measured for the module at different operating voltages. Figure 2.12a shows the increasing trend of efficiency with HV of the module, red color refers to the efficiency at position 1 (pad size $\sim$ 19 mm) of the detector and the green color refers to the efficiency at position 2 (pad size $\sim$ 7.7 mm). A maximum efficiency of 98% at 1110V

is measured and the plateau starts around 1070V. The efficiency along the joining line of the PCB is also measured, and found to be around 98% at 1110V.

The gain of the detector is measured from cluster charge spectra at various voltages. The variation of detector gain with HV is shown in Figure 2.12b and it can be seen that position 2 shows a gain of 13572 at 1110V. Beyond this voltage the cluster charge spectra get saturated and it could not be fit to get a proper peak.

The variation of time resolution with summed HV is shown in Figure 2.12c, the value can be seen decreasing with increasing voltage. At position 1 the value of time resolution is around 18 ns.

Figure 2.12d shows the cluster size variation with HV. Position 1 falls on the row number 92 of the readout pcb, which corresponds to pad size of 19 mm, so the cluster size of 1.1 pads corresponds to 21 mm. Similarly, Position 2 falls on the row number 38 of the readout pcb, which corresponds to pad size of 7.7 mm, so the cluster size of 1.9 pads corresponds to 14.6 mm. So the cluster size of the 2 different zones is within 30%.

2.9 Summary

The Compressed Baryonic Matter (CBM) experiment at FAIR aims to study strongly interacting nuclear matter at extreme baryon densities using heavy-ion collisions at interaction rates up to 10 MHz. The Muon Chamber (MuCh) system of CBM is designed for efficient identification of rare probes in a high rate forward rapidity environment. To meet these requirements, Gas Electron Multiplier (GEM) based detectors are employed in the first two MuCh stations.

This thesis reports the design, fabrication, simulation studies, and laboratory performance of the first full size prototype of the MuCh second station triple-GEM detector module, developed at VECC. The trapezoidal detector module has an active length of 1 m and represents the final

CBM geometry. Due to fabrication constraints of large area multilayer PCBs, a novel PCB joining technique was developed, enabling realization of an 8-layer readout PCB with minimal dead area and ensured gas tightness.

The detector employs a triple-GEM configuration with a 3-2-2-2 mm gap structure and operates with an Ar:CO_2 (70:30) gas mixture. Large area single mask GEM foils from CERN were assembled using the NS-2 technique, eliminating gluing and reducing mechanical stress. Each foil is segmented into 24 high voltage sectors, powered through an optocoupler based biasing scheme for enhanced operational reliability.

Monte Carlo simulations using UrQMD events and Geant3 transport were performed to estimate particle rates in the second MuCh station. The studies predict maximum digi rates of 90 kHz/cm^2 at 12 AGeV, confirming the suitability of GEM detectors for CBM conditions.

The detector was characterized using self-triggered STS/MuCh-XYTER readout electronics. Gain measurements with a ^{55}Fe X-ray source showed stable operation with gains exceeding 4 x 10^3, while gain uniformity variations were mainly due to charge sharing in regions with smaller pad sizes. Noise originating near the PCB joining region was successfully mitigated through additional grounding and shielding.

Cosmic muon studies demonstrated a maximum detection efficiency of 98% with an efficiency plateau above 1070 V and a time resolution of 18 ns. Cluster size and gain measurements across different pad geometries showed consistent detector performance.

This work establishes that large-area triple-GEM detectors with joined multilayer PCBs can be used for high-rate tracking in the CBM MuCh system and form a strong basis for future beam tests and final deployment at FAIR.

Bibliography

[1] Subhasis Chattopadhyay, Yogendra Pathak Viyogi, Peter Senger, Walter F. J. Muller, and Christian J. Schmidt, editors. *Technical Design Report for the CBM : Muon Chambers (MuCh). GSI, 2015*, `https://repository.gsi.de/record/161297`

[2] A. Kumar et al, *Commissioning and testing of pre-series triple GEM prototypes for CBM-MuCh in the mCBM experiment at the SIS18 facility of GSI*, *JINST 16 P09002* (2021). doi:https://doi.org/10.1088/1748-0221/16/09/P09002

[3] A.K. Dubey et al, *GEM detector development for CBM experiment at FAIR*, *Nucl. Instrum. Meth. A 718 (2013) 418.* doi:https://doi.org/10.1016/j.nima.2012.10.043

[4] A.K. Dubey et al, *Testing of triple-GEM chambers for CBM experiment at FAIR using self-triggered readout electronics.*, *Nucl. Instrum. Meth. A, 755:62, 2014.* doi:https://doi.org/10.1016/j.nima.2014.04.027

[5] J. Saini et al, *Test and characterisation of STS/MuCh-XYTER and integration with multiple detectors of CBM-MuCh detector systems.*, *2023 JINST 18 P01009.* doi:https://doi.org/10.1088/1748-0221/18/01/P01009

[6] L. Franconi and A. Marinov, *Status of no-stretch no-spacer GEM assembly, the NS2 technique method and experiment result*, `https://indico.cern.ch/event/176664/contributions/1442160/`

[7] A. Kumar et al, *Operating large size GEM detectors using a novel optocoupler based biasing scheme for the Muon Chamber system of CBM experiment*, *Nucl. Instrum. Meth. A 958 (2020) 162905*. doi:https://doi.org/10.1016/j.nima.2019.162905

Chapter 3

Detector performance test in mini-CBM high intensity particle beam

3.1 Introduction

The Compressed Baryonic Matter (CBM) experiment at FAIR is designed to explore the properties of strongly interacting matter at high net-baryon densities using relativistic nucleus nucleus collisions at interaction rates unprecedented in heavy ion physics. To achieve its physics goals, CBM employs fast, radiation hard detectors, a novel self triggered front end readout architecture, and a free streaming data acquisition system capable of handling raw data rates up to the terabyte per second scale. The successful implementation of this concept requires not only robust detector modules but also optimized readout chain performance, real time data processing, and coordinated operation of all subsystems under realistic high rate conditions. Before the installation of the full CBM detector at SIS100, it is therefore essential to validate these technologies in an integrated environment. The mini-CBM (mCBM) experiment at SIS18 has been conceived specifically to meet this requirement by providing a full system test setup

using prototype or pre-series detector modules from all major CBM subsystems: STS, MUCH, TRD, TOF, RICH, PSD, and ECAL, together with their corresponding front end electronics and DAQ infrastructure. Installed in the HTD cave at GSI, the mCBM setup arranges the detectors downstream of a fixed target at approximately 25° with respect to the incident beam direction, reproducing the compact geometry foreseen for CBM while operating without a magnetic field [1]. This configuration enables straight line tracking and allows systematic studies of detector behaviour, hit rates, data throughput, synchronization, and online/offline reconstruction performance. A central objective of mCBM is to test the free streaming readout chain, in which all registered detector signals time-stamped at the front end, are transmitted continuously via GBT optical links to Data Processing Boards (DPBs) and then forwarded to the First Level Event Selector (mFLES) in the Green IT Cube. Here, time slice building, online track reconstruction, event identification, and physics based data selection are executed in real time. This approach represents a paradigm shift compared to conventional triggered experiments and must be extensively validated under SIS18 beam conditions up to interaction rates of 10^7 events/s. To benchmark the performance of the integrated system, mCBM focuses on the reconstruction of Λ hyperons produced in heavy ion collisions at SIS18 energies. The Λ yield is low of order 10^{-5} per event making it an excellent probe to test the sensitivity and efficiency of the reconstruction algorithms. Simulations with the full mCBM geometry demonstrate that Λ candidates can be identified using straight line tracking in STS, hit association in TRD and MUCH, and velocity measurements from TOF information, despite the absence of a magnetic field. The feasibility studies show clear Λ invariant mass peaks for reactions such as Ni+Ni at 1.93 AGeV and Au+Au at 1.24 AGeV, validating the reconstruction strategy and confirming the scientific utility of the test setup. The work presented in this chapter reports on the performance test of GEM based MUCH detector modules and associated electronics during high intensity beam operation as part of the mCBM program. Operating within a complex multi-detector environment featuring high hit multiplicities, substantial background, and stringent timing constraints, the MUCH subsystem offers a unique opportunity to evaluate

stability, rate capability, thermal behaviour, and data integrity under realistic CBM like conditions. Particular emphasis is placed on signal characteristics, hit rate distributions, long term stability, and the impact of intense beam flux on electronics and cooling solutions. This chapter is structured as follows. First, the mCBM experimental layout and beam conditions relevant to the test campaign are described. Next, the detector configuration, data acquisition chain, and online monitoring framework used during the run are outlined. Detailed performance results are then presented. Finally, a discussion is provided on the implications of these results for the full CBM experiment and the readiness of the MUCH subsystem for large-scale production and integration.

3.2 Experimental Setup

3.2.1 mini-CBM layout and beam conditions

The detector performance tests were carried out within the mini-CBM (mCBM) setup installed in the HTD cave at SIS18. The configuration closely follows the geometry foreseen for the full CBM experiment: a fixed target is placed at the coordinate origin, and all detector subsystems are arranged downstream at a polar angle of about 25° with respect to the incident beam direction.

The MuCh prototype stations under investigation were positioned between the Silicon Tracking System (STS) and the Transition Radiation Detector (TRD), as shown in Figure 3.1, i.e. in the region where the muon absorber and muon chambers will be located in the final experiment.

Figure 3.2 shows the acual setup at mCBM cave, at GSI. The measurements discussed in this chapter were performed with high intensity heavy ion beams at SIS18. The beam species, kinetic energy and typical intensity were chosen to reproduce CBM like interaction conditions

while staying within the safe operational envelope for the prototype detectors and front end electronics.

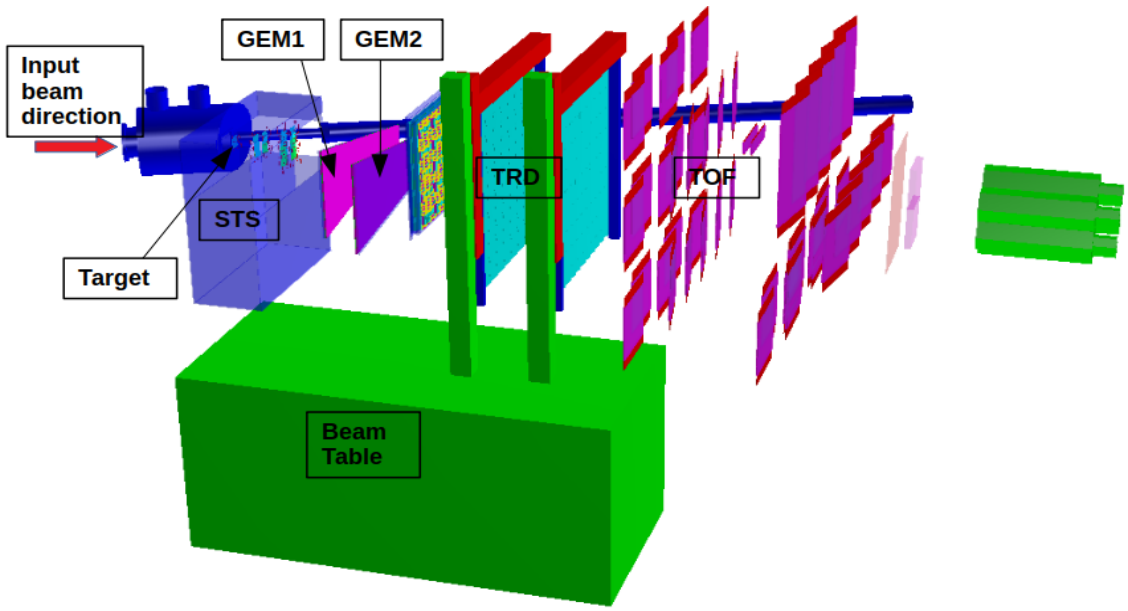

Figure 3.1: Geometry of mCBM setup showing all the detector subsystems.

In mCBM, May, 2025 beamtime we got $^{209}Bi^{68+}$ beam at 1.1 AGeV from SIS18 accelerator. Gold (Au) target of thickness 2.5 mm corresponding to approximately 10% interaction probability was employed. The maximum particle intensity we received upto $8 \times 10^8/6$ sec spill. The beam was extracted in slow extraction mode with spill lengths of the order of several seconds, resulting in quasi continuous streams of interactions in time. The interaction rate for the performance tests reached upto 13 MHz for mCBM, thereby providing a realistic environment to stress the detectors and readout chain.

The mCBM setup was installed in the HTD cave at SIS18, with all detector subsystems aligned along the fixed-target beam line at an angle of 25° with respect to the primary beam. The MuCh prototype stations were positioned downstream of the target, in between the STS and TRD stations, closely following the geometry foreseen for the full CBM experiment as shown in Figure 3.1. The measurements presented in this chapter were performed with $^{56}Fe^{25+}$ and

$^{209}Bi^{68+}$ at a kinetic energy of 1.7 AGeV and 1.1 AGeV respectively and typical intensities upto 8×10^8/ spill in slow-extraction mode with a spill length of 6 seconds.

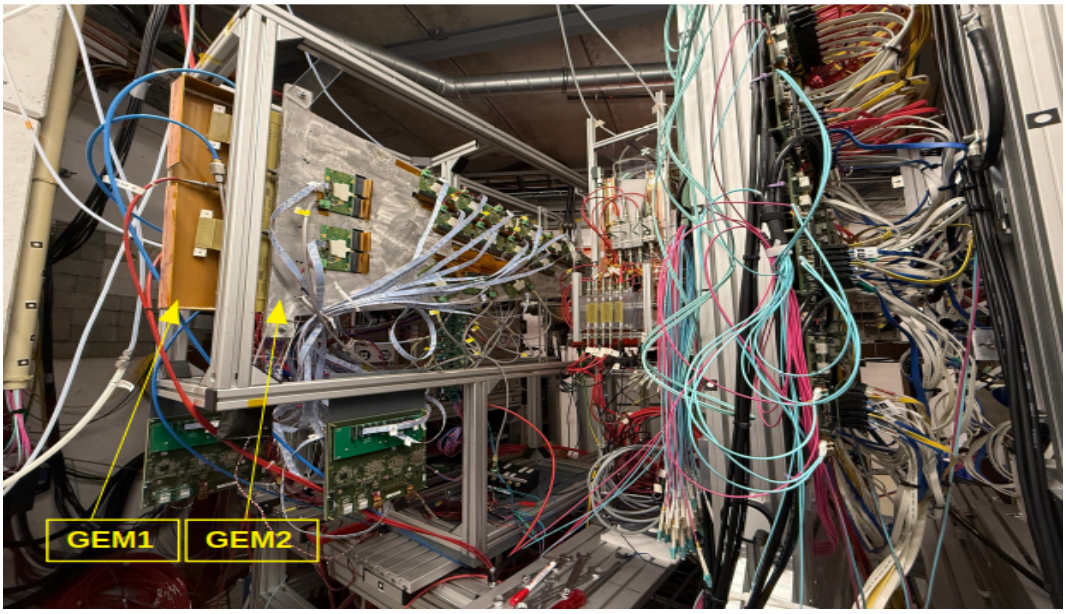

Figure 3.2: Side view of the mini-CBM setup showing the relative positions of the detectors.

3.2.2 MuCh detector configuration in mini-CBM

The MuCh subsystem in the mCBM setup consisted of two trapezoidal triple-GEM detector modules positioned at different distances from the target. The first module (GEM1) corresponds to the dimensions of Station 1, while the second module (GEM2) matches the geometry of Station 2. Both modules were placed within the common acceptance of the other detector subsystems. The detectors were operated with an Ar:CO_2 (70:30) gas mixture at a total gain adjusted to ensure high detection efficiency for minimum-ionising particles while maintaining an acceptably low discharge probability. Figure 3.3a and Figure 3.3b show close-up photographs of the GEM1 and GEM2 detectors, respectively, mounted on their aluminium cooling plates. As visible in the images, 18 FEBs are installed on the cooling plate for GEM1 and 15 FEBs for GEM2, providing readout for all detector channels, while the detector modules themselves

are positioned on the opposite side of the plates. Both cooling-plate assemblies, together with the detectors, were mounted on a common support frame. This complete structure was then installed on the beam table inside the mCBM cave, as illustrated in Figure 3.2.

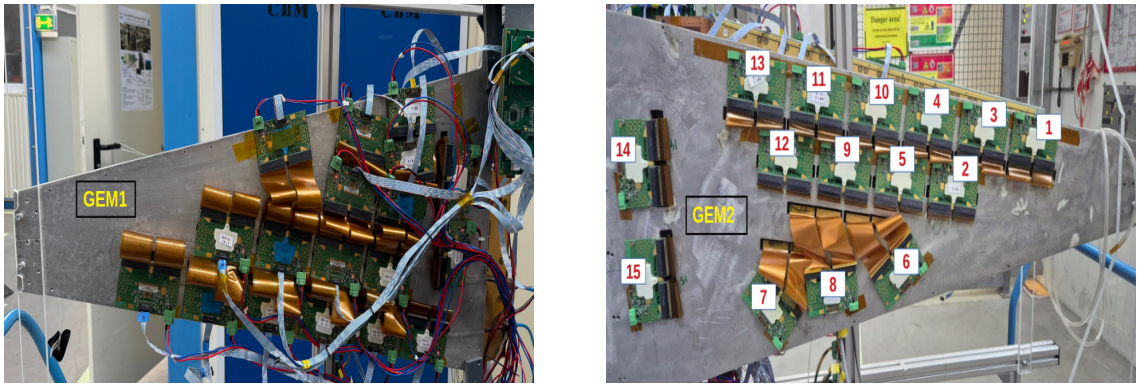

(a) (b)

Figure 3.3: (a) GEM1 mounted on aluminum cooling plate with FEBs. (b) GEM2 mounted on aluminum cooling plate with FEBs.

The FEBs were mounted onto the aluminium cooling plate using screws inserted into carefully tapped holes, ensuring that the embedded water channels remained fully sealed. During installation, particular care was required to avoid applying mechanical stress to the FEBs, as excessive strain could damage the wire bonds of the ASICs. Similar attention was given to the Low Voltage (LV) connections to prevent accidental contact with the aluminium plate, which could otherwise lead to electrical short circuits. Since the heat generated by each FEB is predominantly concentrated beneath the ASIC, small copper blocks were glued at these locations to provide an efficient thermal bridge, enabling effective heat transfer from the ASIC to the cooling plate. The FEBs were connected to the detector readout connectors through flexible copper cables, which transmit the charge signals from the detector pads to the ASICs. Data from each group of six FEBs were routed to an FMC board via copper patch-bus cables, and the FMCs subsequently forwarded the data to a GBTx-based CROB (Common Readout Board). Finally, the CROB transmitted the data to the storage nodes through high-speed optical links.

The readout plane of each GEM detector was segmented into pads with progressive geometry and the granularity matched to the expected particle flux. Details of the Fabrication and testing of Station-1 module is reported in [2] and for the second station it is reported in second chapter of this thesis.

3.2.3 Readout chain, DAQ and run configuration

The MuCh detectors in mCBM were read out using the free streaming data acquisition concept developed for CBM. Signals crossing the programmable threshold in the MUCH-XYTER ASIC were time stamped and multiplexed onto electrical e-links. These e-links were received by GBTx-based Readout Boards (ROB-3), where the data streams from many channels were aggregated and transmitted via 4.48 Gbit/s optical GBT links to the Data Processing Boards (DPBs) located in the DAQ container. On the DPBs, subsystem specific preprocessing such as time ordering, zero suppression and framing into micro slices was performed. The resulting streams were forwarded via FLIB (or CRI) boards to the FLES input nodes in the Green IT Cube, where time slices were built and handed over to the compute farm for online and offline processing. All detector subsystems in mCBM shared the same timing and fast control (TFC) system, which distributed a common clock and synchronisation signals, thus ensuring a global time stamp alignment at the nanosecond level. For the MuCh performance studies, several dedicated runs with stable beam, target in place, and all relevant subsystems operational were selected. The dataset comprises runs at different interaction rates and detector settings (high voltage and threshold scans), which allowed a systematic investigation of the detector response and stability.

3.3 Data Analysis Results

3.3.1 Basic QA plots

During the mCBM beamtime campaign in May 2025, approximately 230 runs were recorded with the MuCh subsystem in conjunction with the other detector systems. For detailed analysis, Run 3887 was selected, corresponding to data taken with GEM1 operated at 4100 V and a branch current of 1520 μA. The beam consisted of $^{56}Fe^{25+}$ ions incident on a 4 mm nickel target, yielding an interaction rate of about 10 %. The average beam intensity during this run was 10^7 particles per 10 second spill.

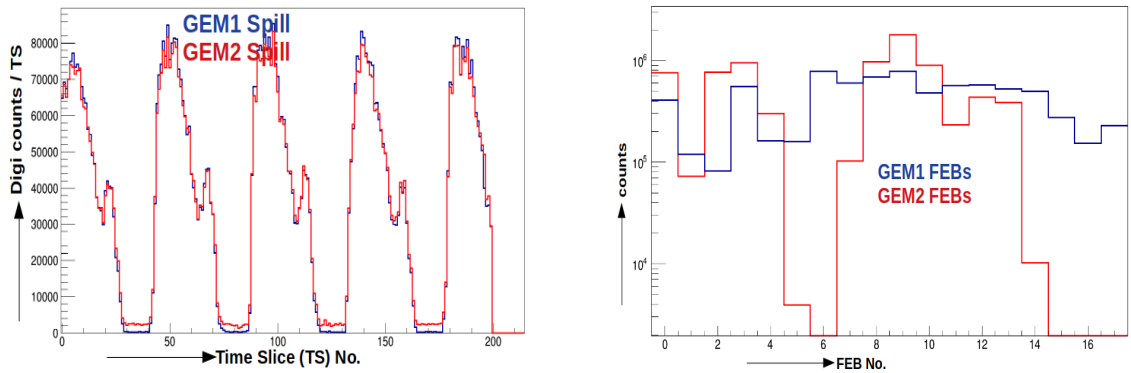

(a) (b)

Figure 3.4: (a) Spill Structure of GEM1 (Blue) and GEM2 (Red). (b) Number of active FEBs during data taking.

Figure 3.4a presents the spill structure as observed by GEM1 and GEM2, illustrating the temporal profile of the incoming particle bunches. Figure 3.4b displays the number of FEBs that were active during this data-taking period. Once the data are recorded, they are stored as raw ".tsa" files, which are subsequently processed using the CBMROOT framework to produce the corresponding ".root" files. In these rootified datasets, the fundamental time unit is the Time Slice (TS). For performance evaluation, the number of digis per TS is examined for the

detector, as shown in Figure 3.5. This distribution provides the mean digi rate for the selected run, which is expected to scale with the beam intensity.

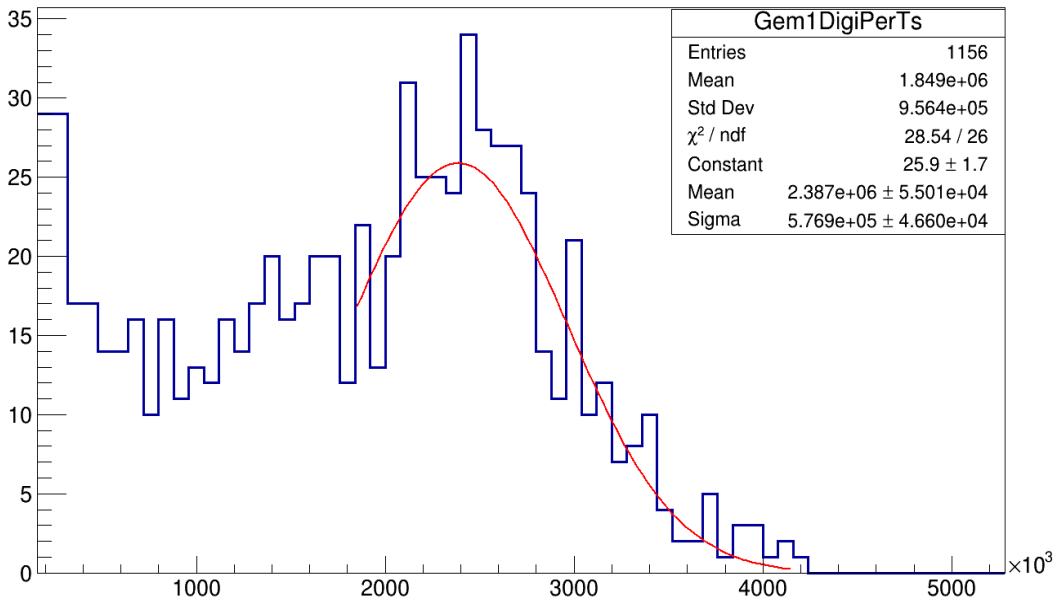

Figure 3.5: Digi per TS profile.

During the recent mCBM beamtime, data were collected at six distinct beam intensities. Figure 3.6 illustrates the sequence of run numbers together with the corresponding intensities, providing an overview of the beam conditions under which the measurements were performed.

All recorded runs are organized according to their run numbers and corresponding beam intensities. The complete listings are provided in Figure 3.7 for GEM1 and in Figure 3.8 for GEM2.

3.3.2 Detector Noisy Channel listing

During detector operation, it was observed that a subset of channels contributed disproportionately to the overall data rate. To prevent excessive data throughput and ensure stable DAQ performance, these high noise channels were masked at the hardware level so that their data

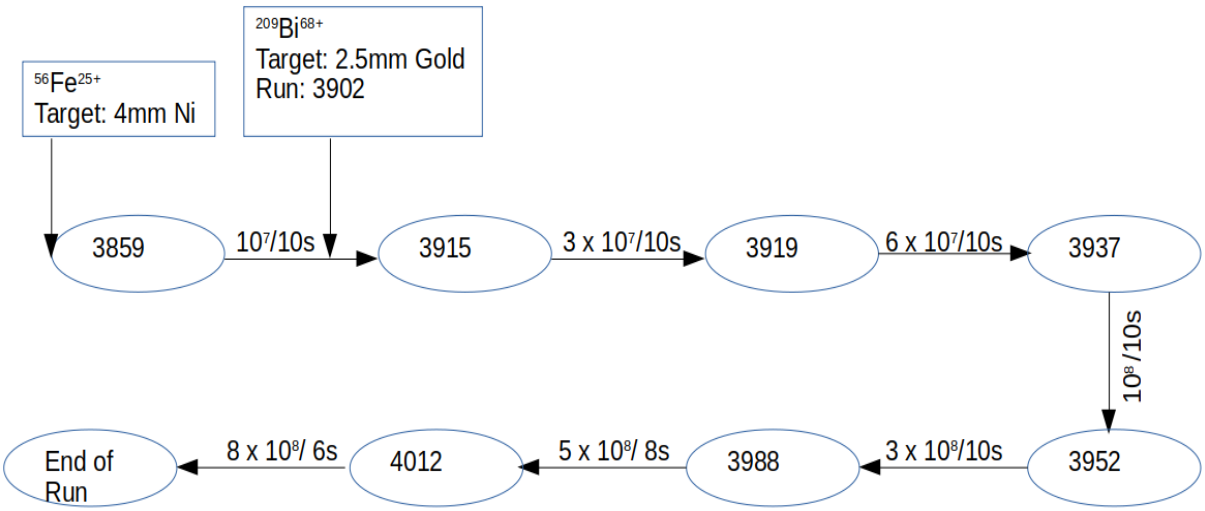

Figure 3.6: Overview of the run sequence, indicating the corresponding beam intensities, ion species, and target materials used during the measurement campaign.

	3700 V, 1371 .5 uA	3800 V, 1408 .6 uA	3825 V 1443 .05	3850 V 1442 .85	3875 V 1461 .75	3900 V, 1445 .7 uA	3925 V 1480 .85	3950 V, 1464 .2 uA	3960 V 1445 .1uA	3975 V 1499 .4	4000 V, 1482 .75 uA	4025 V 1518 .5	4050 V, 1501 .4 uA	4075 V, 1487 .81	4100 V, 1519 .9 uA	4125 V, 1527 .8 uA	4148 V 1537 .35 uA	4150 V, 1538 .35 uA	4175 V, 1547 .7 uA	4200 V, 1555 .8 uA
I = 10^7 / 10s	3890	3889				3883 3891		3884			3885 3893 upto 3898		3886 3875		3887 3876			3888 3877	3878	3892
I = 3 x 10^7 / 10s											3916				3917 3918					
I = 6 x 10^7 / 10s						3930 3936		3935			3919 3928 3934				3920 3929	3932		3921 3931		3922 3924
I = 10^8 / 10s						3937		3941			3939		3943 3944 3945		3938		3940			
I = 3 x 10^8 / 10s						3952 3959			3969 3970 3971 3972		3960 3987		3961	3968 3973	3962 3963 3966 3981 3982	3965 3967		3964 3975 3979 3980	3976 3977 3978	
I = 5 x 10^8 / 8s						3990	3991 4008	3992		3993 4007	3994 3988 3989	3995 4005 4006	3996	3997 4004	3998 upto 4003					
I = 8 x 10^8 / 6s		4014	4015	4016	4017	4018	4019	4020		4021	4022	4023		4024	4025 upto 4037					

Figure 3.7: Run listing for GEM1.

were not recorded. After establishing this nominal operating condition, data were collected and further processed offline. For the offline noise evaluation, a low intensity run was selected, and the data were unpacked to identify persistently noisy channels. The analysis focused on the

	3700 V, 1371 .5 uA	3750 V, 1371 .05	3800 V, 1410 .1 1413 .4	3825 V 1443 .05 1419 .2	3850 V 1407 .56 1428 .5	3875 V 1461 .75 1439 .7	3900 V, 1447 .6	3925 V 1480 .85 1456 .35	3950 V, 1445 .21 1465 .85	3960 V 1445 .1uA	3975 V 1499 .4 1474 .95	4000 V, 1462 .75 1484 .6	4025 V 1518 .5 1493 .6	4050 V, 1480 .86 1503 .05	4075 V, 1487 .81	4100 V, 1499 .4 1521 .7	4125 V, 1527 .8 1530 .8	4148 V 1537 .35 uA	4150 V, 1517 .66 uA	4175 V, 1547 .7 uA	4200 V, 1559 .2 uA
I = 10^7 / 10s		3890	3894		3889		3876 3891		3877 3883			3878 3884 3893		3885		3886 3917			3887		3888 3892
I = 3 x 10^7 / 10s							3916														
I = 6 x 10^7 / 10s			3930				3919 3936		3931 3935			3920 3929 3934		3921 3933		3922 3924 3928	3932				
I = 10^8 / 10s			3937				3938 3939 3942 3943 3944		3941			3940		3945 upto 3951							
I = 3 x 10^8 / 10s					3962 3963 3964		3952 to 3961 and 3965 to 3972 3987		3976 3978 3979 3982			3973 3975									
I = 5 x 10^8 / 8s			3990	3991 4008	3992	3993 4007	3994 3988 3989	3995 4005 4006	3996		3997 4004	3998	3999 upto 4003								
I = 8 x 10^8 / 6s			4014	4015	4016	4017	4018	4019	4020		4021		4022	4023 4024 4025							

Figure 3.8: Run listing for GEM2.

off-spill periods, time intervals when the beam is absent, during which the expected digi rate per channel should ideally be close to zero. In practice, however, some channels exhibit significantly higher off-spill activity. To classify a channel as noisy, a threshold of 50 Hz was applied: any channel producing more than 50 digis per second during the off-spill interval was marked as noisy. Using this criterion, complete noisy channel lists were generated separately for GEM1 and GEM2. These identified channels were subsequently excluded from all further analyses. Importantly, the same noisy channel map was applied consistently across all runs to ensure uniform acceptance and maintain comparability of the results. This procedure guarantees that variations observed in detector performance or digi rates across different beam intensities originate from physical effects rather than from changes in channel quality. We observe that the noise baseline of both TOF and GEM1 detectors increases noticeably with beam intensity, as illustrated in Figure 3.9. In Figure 3.9(a), the red line indicates the off-spill digi level of the TOF detector for Run 3885, recorded at an intensity of 10^7/spill. When the intensity is increased to 5×10^8/spill in Run 3994, the corresponding off-spill baseline, shown in Figure

3.9(b), rises from approximately 3×10^3 digis/TS to 3×10^4 digis/TS, representing nearly an order of magnitude increase.

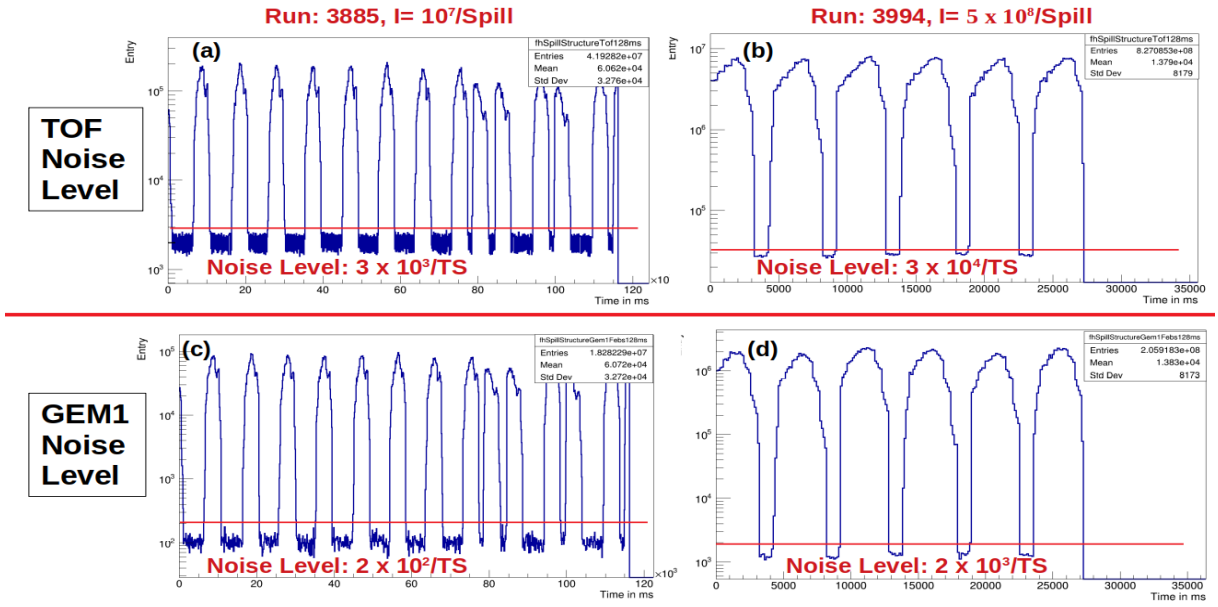

Figure 3.9: Off-spill noise levels of TOF and GEM1 detectors at low and high beam intensities. A clear upward shift in the noise baseline is observed as the beam intensity increases from 10^7 / spill (Run 3885) to 5×10^8/spill (Run 3994).

A similar behaviour is observed for GEM1, as shown in Figures 3.9(c) and Figures 3.9(d), where the off-spill noise level increases from roughly 2×10^2 digis/TS at low intensity to about 2×10^3 digis/TS at the highest intensity. This systematic upward shift in the baseline with increasing beam flux suggests the presence of enhanced radiation induced background during off-spill periods. At higher intensities, activation effects, and residual interactions in the target and surrounding materials can contribute to additional ionisation in the detector gas, thereby elevating the off-spill digi rate.

3.3.3 Detector Digi behaviour w.r.t Intensity

Our objective is to study the response of the detector as a function of increasing particle intensity. For this purpose, a subset of runs from Figure 3.7 was selected, specifically those in which GEM1 was operated at 4000 V. The chosen runs: 3916, 3919, 3987, and 3994 correspond to progressively higher beam intensities. The spill structures recorded by GEM1 for these runs are shown in Figure 3.10.

To quantify the detector performance, we evaluated the number of digis recorded per spill and examined how this quantity varies with beam intensity. Ideally, such a comparison requires identical detector acceptance across all runs. However, due to a few non-operational FEBs in some runs, the effective acceptance was not uniform. To ensure a fair comparison, the study was therefore performed on a zone-by-zone basis. The overall readout segmentation of GEM1 is shown in Figure 3.11a, consisting of 23 columns along the X-axis and 97 rows along the Y-axis, forming the trapezoidal active area of the detector. The lower sector numbers (near 0) correspond to the narrow end of the trapezoid, while higher sector numbers (near 96) represent the wider region of the module.

From this segmentation, three representative zones were selected for the analysis:

- $nx = 0$, corresponding to the narrow region,
- $nx = 7$, corresponding to the middle region, and
- $nx = 17$, corresponding to the broad region of the detector.

These selected regions are illustrated in Figure 3.11b, Figure 3.11c, and Figure 3.11d, respectively.

The average number of digis per spill was plotted as a function of the beam intensity for the three selected detector regions, as shown in Figure 3.12a Figure 3.12b, and Figure 3.12c for

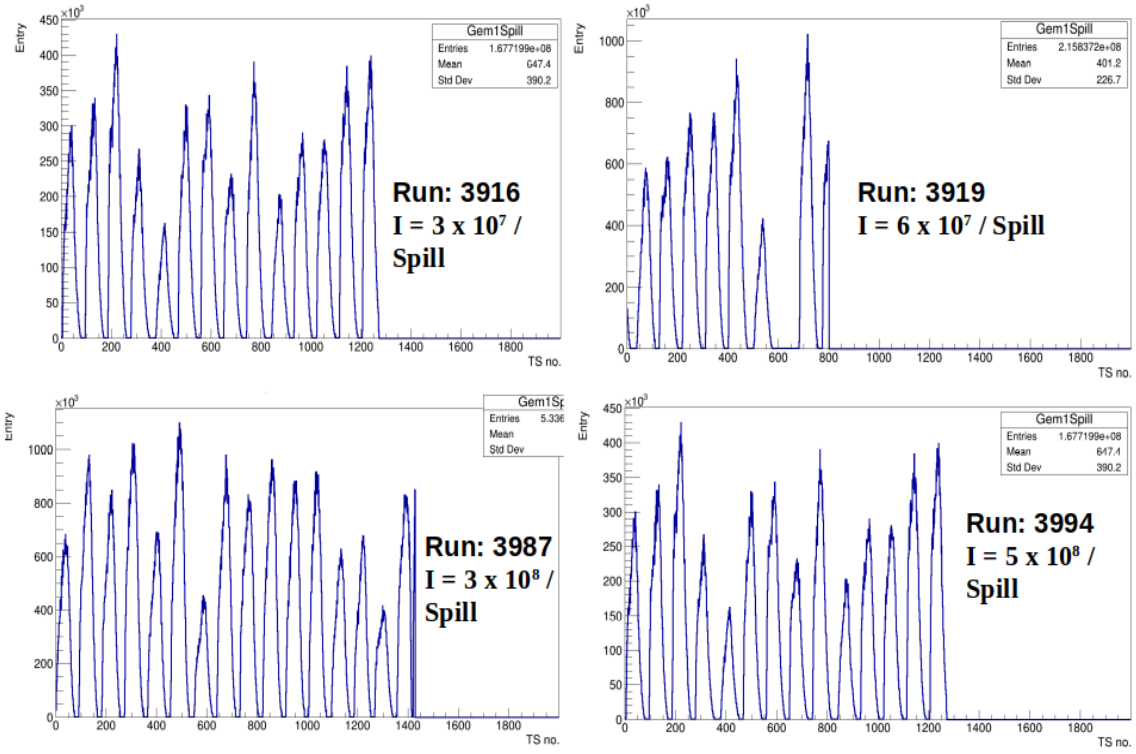

Figure 3.10: GEM1 Spill structure at several intensities but at fixed voltage of 4000 V.

nx=0, nx=7, and nx=17, respectively. In all three zones of the detector, the digi yield was observed to increase linearly with beam intensity up to approximately 5×10^8 particles per spill. This consistent linear trend across the narrow, middle, and broad regions indicates that the detector response remains proportional to the particle flux within this intensity range.

Such behaviour is expected for a well operated GEM detector, as linearity of the digi rate with incident particle count reflects stable gas gain, uniform charge collection, and the absence of significant space charge effects or electronics saturation. These observations collectively suggest that, up to the tested intensities, the detector maintains stable gain, and no onset of rate induced non linearities.

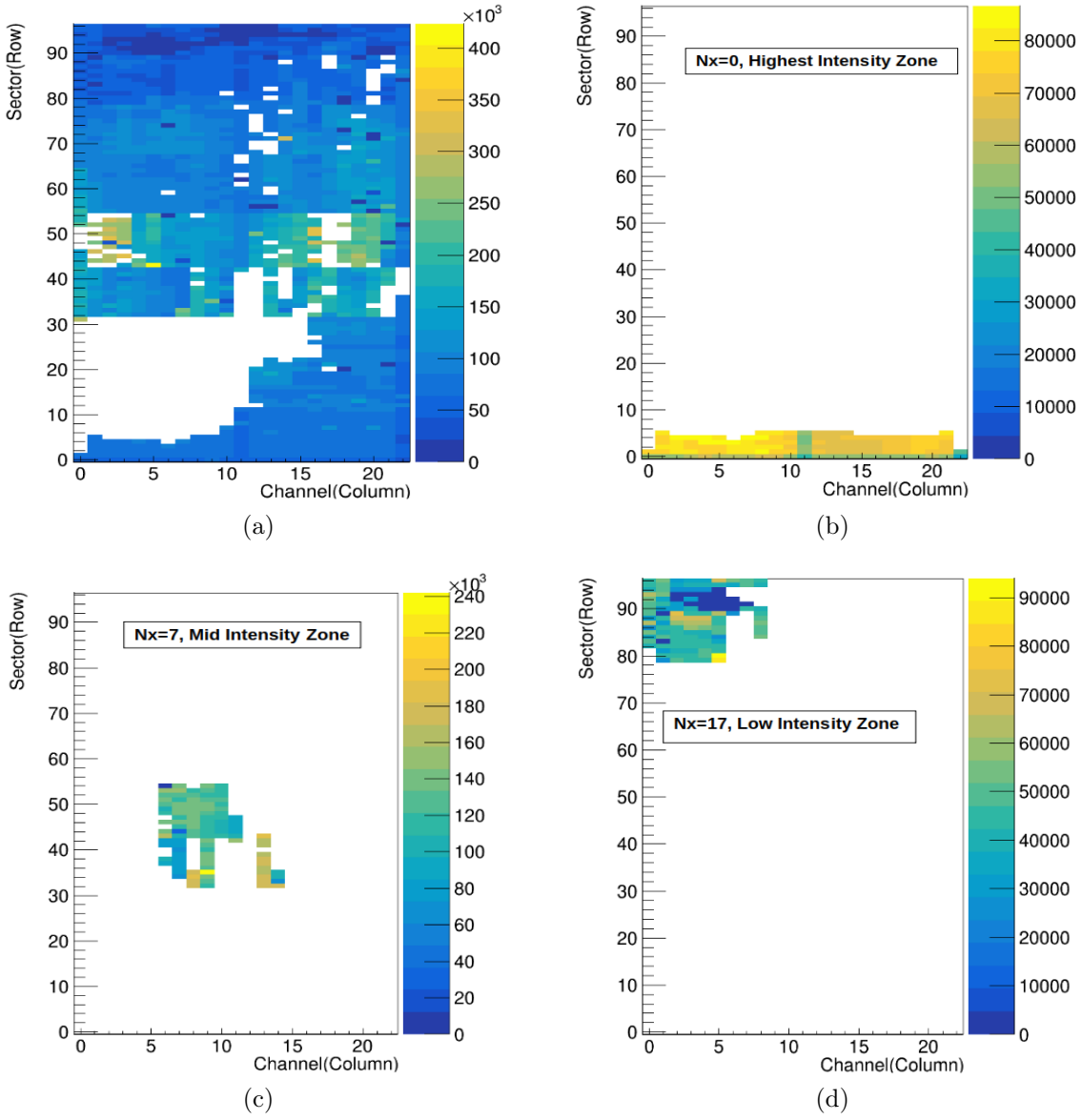

Figure 3.11: (a) Full coverage availabe for the detector. (b) nx = 0, corresponding to the narrow region. (c) nx = 7, corresponding to the middle region. (d) nx = 17, corresponding to the broad region of the detector.

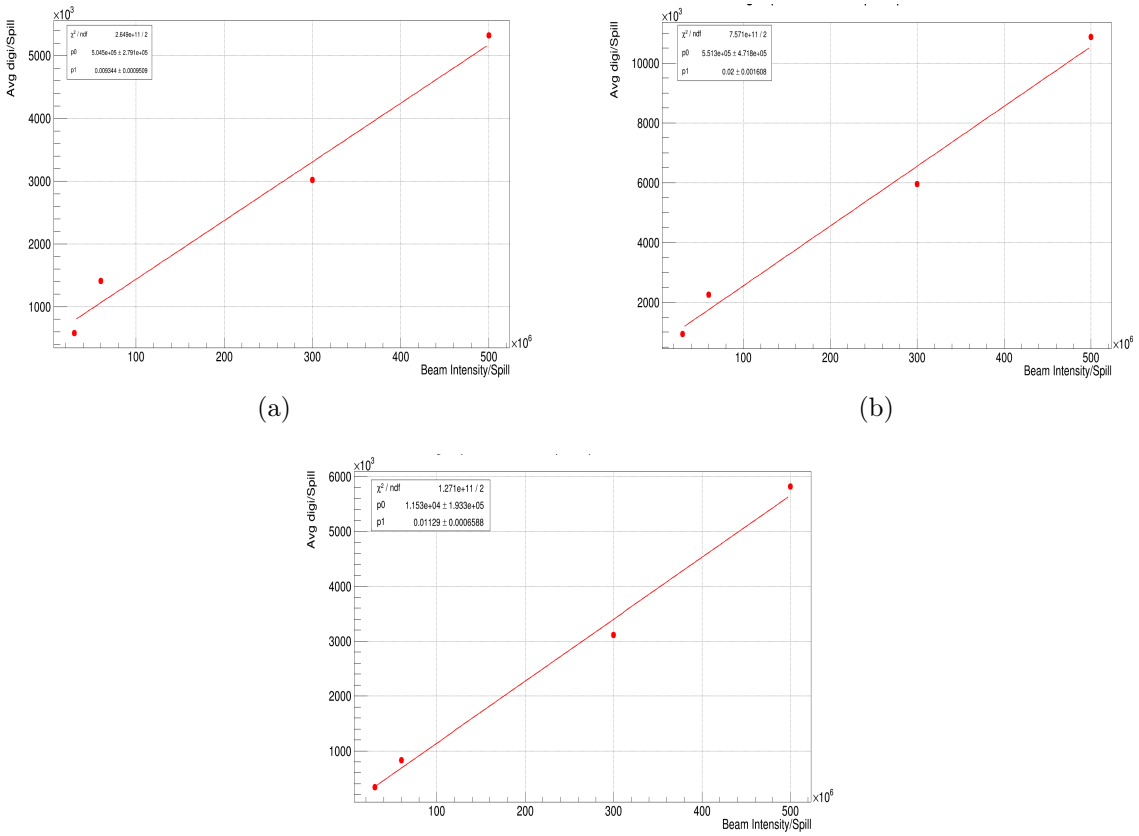

Figure 3.12: (a) Average digi vs Beam intensity for narrow zone (nx=0). (b) Average digi vs Beam intensity for mid zone (nx=7). (c) Average digi vs Beam intensity for outer zone (nx=17).

3.3.4 Time offset stability

Since all mCBM subsystems operate in a common data taking mode and are synchronized in time at the beginning of each run, a fixed time correlation is expected between them. When a charged particle traverses both the MuCh and TOF detectors, the timestamps generated in the two systems should differ by a constant offset, reflecting their relative electronics and cable delays.

The time difference between TOF and MuCh was computed for Run 3887, and the corresponding spectrum is shown in Figure 3.13a. A clear peak is observed, indicating a stable time

offset of approximately 706 ns, with a timing resolution of about 19 ns. This offset remains constant throughout the entire duration of the run. The stability of this correlation is further demonstrated in Figure 3.13b, where the time difference is plotted as a function of the Time Slice (TS). The time offset shows no significant drift over the full run length. Such temporal stability is essential for downstream physics analysis, as any fluctuation in time correlation would make it impossible to associate hits from different subsystems reliably. Consequently, for every recorded run, the first validation step is to determine and confirm the TOF - MuCh time offset before proceeding to higher level reconstruction or physics interpretation.

A similar timing correlation study was carried out between the two MuCh stations, GEM1 and GEM2. Figure 3.13c shows the distribution of the time difference T_{GEM1} - T_{GEM2} for all correlated hits recorded in the run. A well defined peak is observed at approximately 10 ns, with a timing resolution of about 49 ns. This clearly demonstrates that both detector stations remain synchronised within a stable time offset throughout data taking.

The stability of this offset over the duration of the run is illustrated in Figure 3.13d, where the time difference is plotted as a function of the TimeSlice (TS) number. The band remains centered around the same offset value without any drift or broadening. This stability is essential for event building and cross detector correlation: if the relative timing between stations fluctuates, the assignment of hits to the same physical particle becomes unreliable, ultimately degrading reconstruction quality. The observed constant time alignment therefore confirms that GEM1 and GEM2 operated in a fully synchronised, time stable mode during the mini-CBM beamtime.

3.3.5 Spatial Correlation

The spatial correlation between detector subsystems is a crucial indicator of their mutual alignment and common geometric acceptance. To evaluate this for the MuCh system, we examined the hit distributions of GEM1 and GEM2 using their digi maps. Figure 3.14a shows the two-

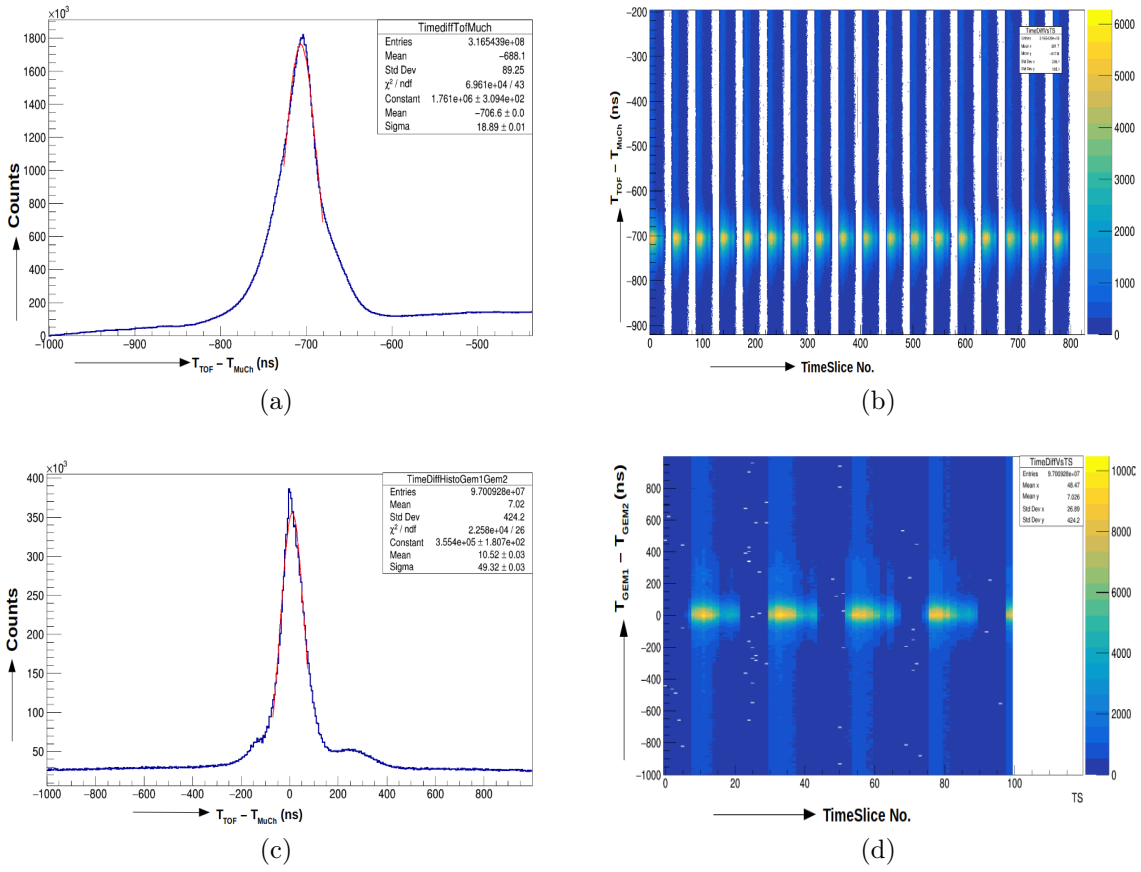

Figure 3.13: (a) Time difference (TOF - MuCh) spectrum showing a well defined offset of 706 ns with a timing resolution of 19 ns, obtained from all FEBs of MuCh. (b) Stability of the TOF - MuCh time difference over the full duration of the run, plotted as a function of Time Slice (TS). (c) Time-difference spectrum between GEM1 and GEM2 digis, exhibiting a peak at around 10 ns and a resolution of approximately 49 ns. (d) Corresponding time difference vs. TimeSlice plot demonstrating that the relative timing between the two stations remains stable over the full duration of the run.

dimensional occupancy map of GEM1, where the X-axis corresponds to the readout columns (channels) and the Y-axis to the readout rows (sectors). Regions without entries correspond to channels that were not read out due to non-functional FEBs or disabled channels. A similar oc-

cupancy map for GEM2 is shown in Figure 3.14b. To visualise the geometrical overlap between the two detector planes, the readout pad positions of GEM1 and GEM2 are superimposed in Figure 3.14c. As expected from their design, the Station-1 module (GEM1) is shorter in length but wider than the Station-2 module (GEM2). Despite this size difference, both detectors were installed in a common acceptance region during the mini-CBM beamtime. Consequently, particles traversing one detector are expected to pass through the other as well, enabling track correlations across the two planes. The consistent spatial patterns observed in the occupancy maps confirm this overlap and demonstrate correct alignment and stable geometrical correlation between GEM1 and GEM2.

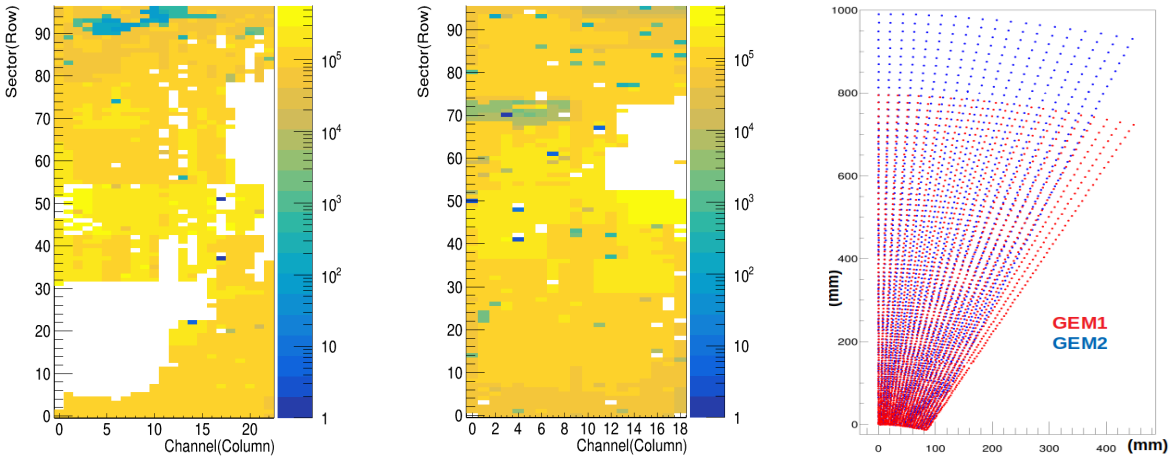

(a) (b) (c)

Figure 3.14: (a) Two-dimensional occupancy map of GEM1 showing the distribution of digis across channels (X-axis) and sectors (Y-axis). Empty regions correspond to non-functional or masked channels arising from FEB related issues. (b) Two dimensional occupancy map of GEM2 using channel-sector representation as GEM1. The blank areas indicate regions not read out due to inactive FEBs or disabled channels during data taking. (c) Geometrical overlap of GEM1 (red) and GEM2 (blue) readout pad positions. The Station-1 detector (GEM1) is wider but shorter compared to the Station-2 detector (GEM2).

Using the time-sorted data streams from GEM1 and GEM2, we first constructed crude events, each containing approximately 50 combined digis from both detectors. A time correlation was then performed among the digis within each event, yielding a clean and well defined correlation peak, as shown in Figure 3.13c. To extract only physically meaningful coincidences, we applied a time difference selection window of -200 ns to +200 ns. Digis satisfying this temporal coincidence criterion were subsequently used to study the spatial correlation between the two detector modules. Figure 3.15a presents the correlation matrix of GEM2 sector versus GEM1 sector, which shows a narrow and well-defined diagonal band. A similar trend is observed in millimetre coordinates in Figure 3.15b. This behaviour clearly indicates that both GEM1 and GEM2 are well aligned in space, such that particles passing through the common acceptance region of the apparatus produce consistent and correlated hit positions in both detectors. In other words, the detectors are geometrically matched so that a particle trajectory observed in GEM1 can also be traced reliably through GEM2.

The channel-to-channel correlation between GEM2 and GEM1 is shown in Figure 3.15c, while Figure 3.15d displays the corresponding position correlation in millimetre scale. As discussed earlier, the right half of GEM2 exhibited reduced activity during this run; hence, the channel-channel and spatial correlations do not extend across the full detector width. Nevertheless, the regions with valid data demonstrate a clear one to one spatial correspondence, further confirming the relative alignment and proper functioning of the two GEM stations.

3.3.6 Digi Correlation

To further assess the stability and linearity of the MuCh detector response under varying beam conditions, we investigated the correlation between the number of digis per Time Slice (TS) recorded by GEM1, GEM2, and the TOF subsystem. Such inter detector correlations are essential, as they reflect whether the MuCh subsystem behaves consistently with the global

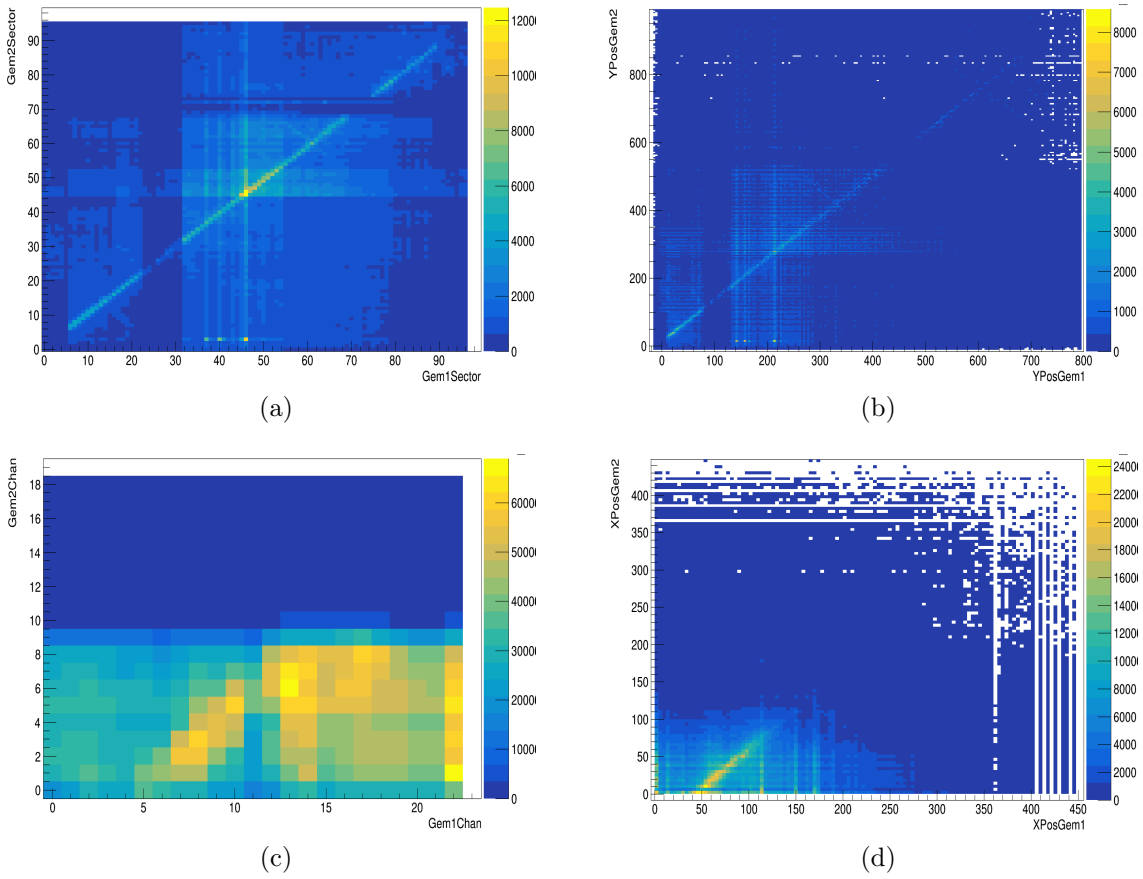

Figure 3.15: (a) Sector-sector spatial correlation between GEM2 and GEM1 after applying the time-coincidence cut (-200 ns $<$ Δt $<$ 200 ns). A strong and narrow diagonal band is observed, indicating that hits produced by the same particle in the two detectors fall on geometrically corresponding sectors. (b) Digi position correlation along the Y direction (in millimetres) for GEM2 versus GEM1. (c) Channel to channel correlation between GEM2 and GEM1 for digis satisfying the temporal coincidence requirement. (d) Digi position correlation along the X direction (in millimetres) between GEM2 and GEM1.

event activity observed by the other detectors in mCBM. After removing all noisy channels identified through the off spill masking procedure, we evaluated the digi multiplicity on a TS by TS basis and compared it across subsystems. Figure 3.16a presents the correlation between

GEM2 and GEM1 digi counts. A clear linear relationship is observed over the full range of TS occupancies, indicating that both GEM detectors respond proportionally to changes in particle flux and operate coherently within the common acceptance region. Figure 3.16b shows the correlation between GEM1 and TOF digi multiplicity, while Figure 3.16c shows the corresponding GEM2 vs TOF comparison. Both plots exhibit strong linearity, confirming that the MuCh detectors scale uniformly with the global event activity measured by TOF.

We performed the same check across different beam intensities, and consistently observed linear behaviour for GEM1 and GEM2. This demonstrates that both GEM1 and GEM2 remain linear over the full tested intensity range. These correlations strongly support the conclusion that the MuCh detectors exhibit stable gain, uniform response across their active area, and no observable saturation effects up to intensities of 5×10^8 particles per spill.

3.3.7 Digi Rate Estimation

The incident particle rate is a crucial operational parameter for the CBM experiment, as it directly influences detector occupancy, data throughput, and the long term stability. In this context, we determined the instantaneous particle load on the MuCh detectors during the highest intensity runs of the mCBM 2025 beam campaign. The geometrical orientation of the MuCh modules, shown earlier in Figure 3.1, indicates that the narrow end of each trapezoidal detector faces the beam pipe. Consequently, this region is expected to experience the highest particle flux.

Figure 3.17a presents the rate distribution for GEM1 as a function of TimeSlice (TS) number on the x-axis and the combined FEB channel index on the y-axis. GEM1 requires 2,231 electronic channels to read out its active area, and each channel is mapped to a unique index in this combined scale. For every TS (128 ms), the number of digis recorded in each channel is counted and divided by the TS duration to obtain the channel rate in Hz. The resulting

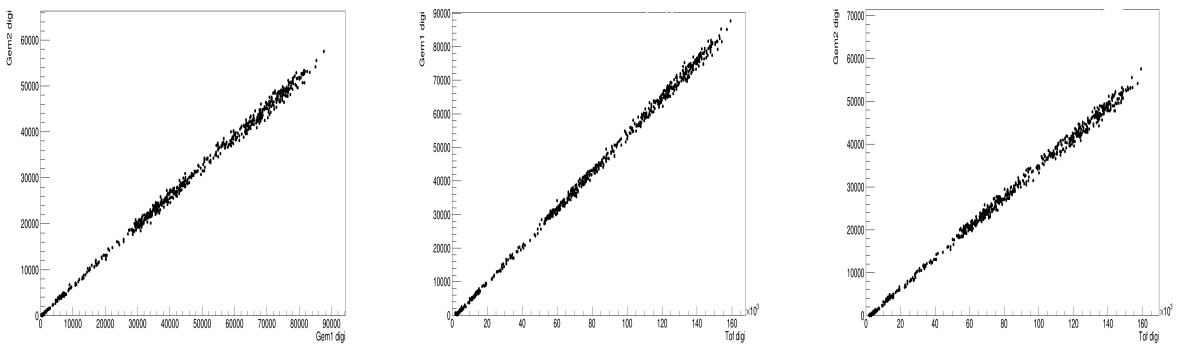

(a) (b) (c)

Figure 3.16: (a). Scatter plot showing the number of digis recorded in GEM2 versus GEM1 on a TS by TS basis after noisy channel removal. The strong linear trend demonstrates that both GEM detectors respond proportionally to the instantaneous particle rate and behave consistently within the common acceptance region. (b) The digi counts observed in GEM1 are plotted against those in the TOF detector for each TS. The linear relationship confirms that GEM1 scales coherently with the global event activity measured by TOF, indicating stable detector performance over the full intensity range. (c) Scatter plot illustrating the digi multiplicity in GEM2 versus TOF for each TS. The observed linear trend shows that GEM2 maintains a stable and proportional response to variations in event activity, similar to GEM1. This further supports the linear behaviour of the MuCh subsystem under increasing beam intensities.

two dimensional rate map exhibits a clear spill structure: within each spill the particle rate gradually rises, reaches a maximum, and subsequently decreases before entering the off spill period, where essentially no beam particles are present. From Figure 3.17a, it is observed that the maximum rate handled by GEM1 electronics reaches approximately 100 kHz per channel.

Since the pad dimensions of the readout pads increase progressively from the narrow to the wider region of the detector, the electronic channel occupancy alone does not directly reflect the particle flux density. Therefore, each channel rate was normalized to the corresponding pad

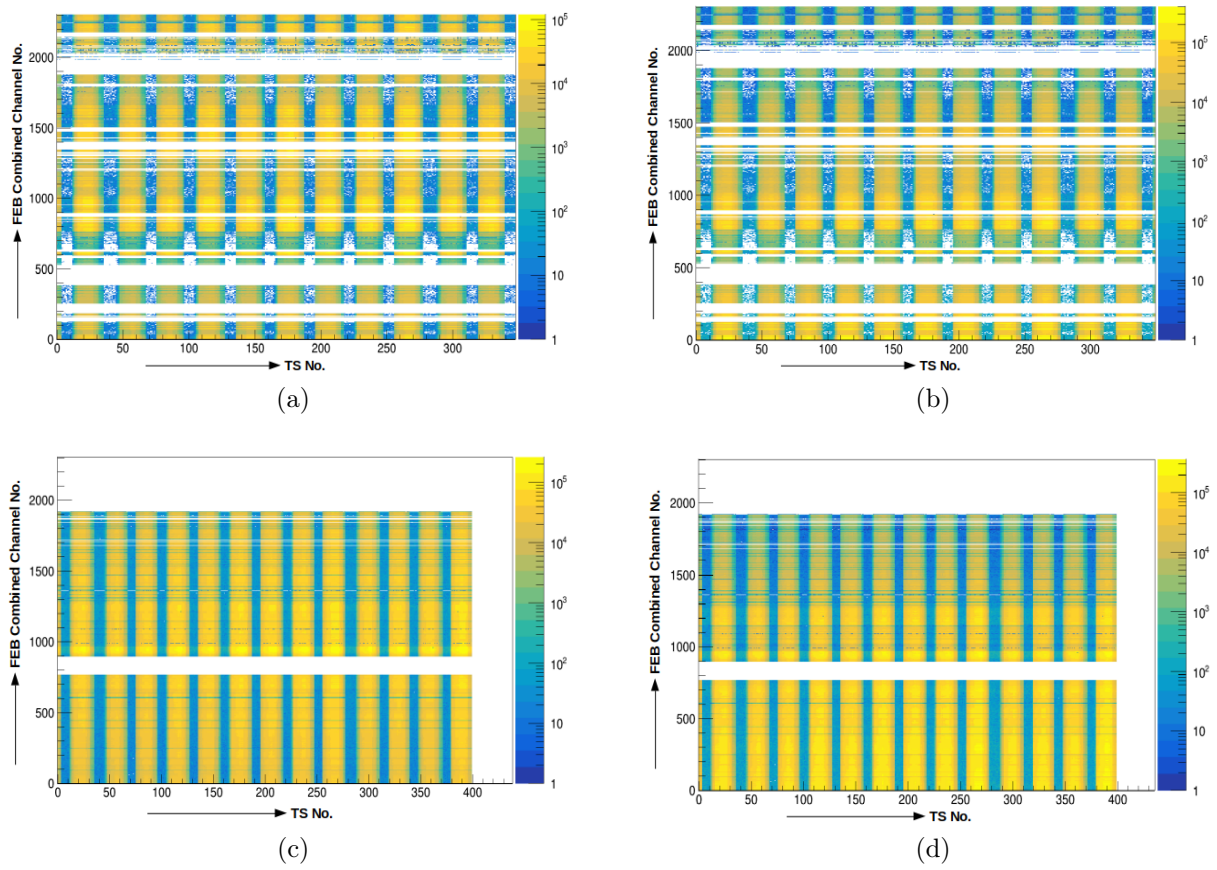

Figure 3.17: (a) GEM1 digi rate per electronic channel as a function of TimeSlice (TS) number for the highest intensity run. (b) GEM1 particle flux distribution normalized to pad area (Hz/cm^2). (c) GEM2 digi rate per electronic channel as a function of TimeSlice (TS) number. (d) GEM2 particle flux distribution normalized to pad area (Hz/cm^2).

area to obtain the incident particle rate in units of Hz/cm^2. Figure 3.17b shows the resulting GEM1 rate distribution per unit area. For the highest intensity run (Run 4022), the peak flux reaches nearly 4×10^5 Hz/cm^2 or 400 kHz/cm^2. This value represents the maximum particle density sustained by GEM1 during the mCBM campaign.

A similar analysis was performed for GEM2, whose readout is served by 15 FEBs corresponding to a total of 1,920 channels. Figure 3.17c and Figure 3.17d show the per channel and per area

rate maps, respectively. The highest flux observed in GEM2 reaches approximately 3×10^5 Hz/cm^2 or 300 kHz/cm^2. As expected, Figure 3.17d clearly shows that the largest particle rate is concentrated in the channels associated with the narrow side of the detector, those facing the beam pipe. The rate gradually decreases toward the outer (broader) region of the detector, consistent with the geometrical acceptance and angular distribution of the incoming particle flux. These measurements demonstrate that both GEM1 and GEM2 handled the extreme rate conditions of the mCBM beamtime, validating their readiness for the CBM experiment.

3.3.8 Hit reconstruction and event building in MuCh

At the digi level, the MuCh data processing chain begins with event building, followed by cluster formation and hit reconstruction, and finally correlation studies using the reconstructed hits. The overall reconstruction sequence can be summarized as: Digis $\rightarrow$ Event Building $\rightarrow$ Clusters $\rightarrow$ Hits.

Event building is performed using the time-stamped digis produced by the detector front-end electronics. Prior to event reconstruction, time offset corrections are applied to the digis from different GEM front-end boards (FEBs) with respect to the reference time provided by the T0 detector. This step is essential to bring all sub-detector digis into a common time frame.

The event reconstruction in mCBM is based on a time-based event building approach. In the present analysis, a Fixed Time Window (FTW) algorithm is employed, with a time window of 120 ns optimized for the GEM detectors. First, the time stamps of all digis from the various sub-detectors are sorted in chronological order. Event building is then initiated using the T0 detector as the reference. Starting from a valid T0 digi, a time window of 120 ns is opened, and all digis primarily from the GEM detectors that fall within this window are grouped together and treated as a single event. This procedure is applied sequentially over the entire data set.

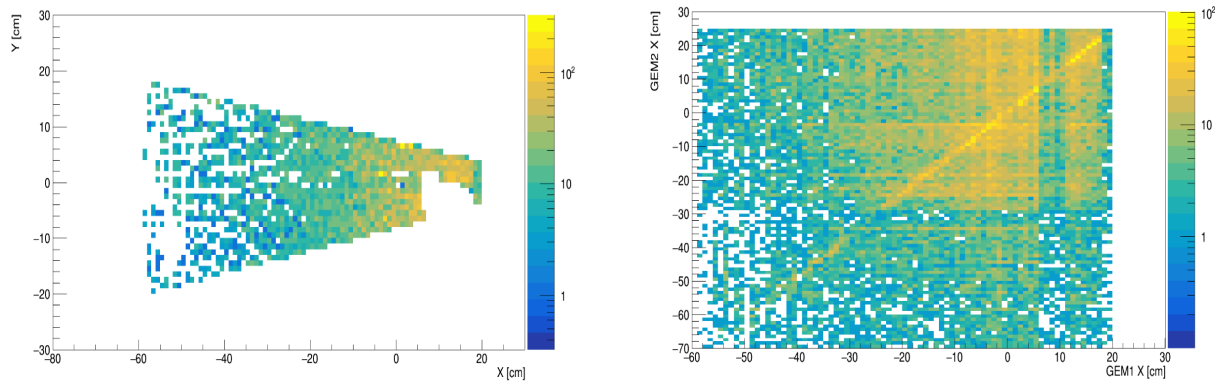

(a) (b)

Figure 3.18: (a) Two-dimensional X-Y hit distribution of the GEM1 detector obtained after time-based event building and hit reconstruction. The trapezoidal active area of the detector is clearly visible, while empty regions correspond to inactive or masked FEBs during data taking. (b) X-coordinate correlation between reconstructed hits in GEM1 and GEM2 for hits belonging to the same reconstructed event. The clear diagonal structure indicates a strong spatial correlation and confirms proper relative alignment of the two MuCh stations along the horizontal direction.

The FTW algorithm is operated in No-Overlap mode, where each digi is allowed to belong to only one event. If a new event seed appears within the time window of a previously defined event, it is ignored. As a consequence, this mode can lead to partially reconstructed or missed events in the presence of event pile-up. Therefore, the No-Overlap mode is suitable mainly for low event-rate conditions and serves as a robust starting point for validating the event reconstruction chain.

Once events are built, hit reconstruction is carried out using standard clustering algorithms. Neighboring digis in space and time are grouped into clusters, and cluster centroids are calculated to form reconstructed hits. The resulting two-dimensional (XY) hit distributions for GEM1 is shown in Figure 3.18a which represents the active detector regions clearly. Empty

regions observed in the distribution corresponds to dead or inactive areas, which arise from non-functioning GEM FEBs during the data-taking period.

As a first-level validation of the event reconstruction and tracking performance, spatial correlation studies are performed between the two MuCh stations, GEM1 and GEM2. Correlations are constructed using reconstructed hits from both stations within the same event. The resulting XX correlation plot is shown in Figure 3.18b, exhibit clear diagonal bands, indicating strong spatial correlations between GEM1 and GEM2. These diagonal structures demonstrate that hits in both stations originate from the same charged particles and are correctly associated within a single reconstructed event.

Overall, these results confirm the proper functioning of the time-based event building, the reliability of the hit reconstruction procedure, and the suitability of the MuCh GEM detectors for charged-particle tracking in the high-rate environment of mCBM.

3.3.9 Summary

This chapter presents a comprehensive performance evaluation of the GEM-based Muon Chamber (MuCh) detector prototypes operated during the mini-CBM (mCBM) experiment at SIS18. The measurements were carried out under realistic CBM-like conditions using high-intensity heavy-ion beams, reaching interaction rates of up to several tens of MHz. Two trapezoidal triple-GEM modules corresponding to MuCh Station-1 (GEM1) and Station-2 (GEM2) were operated in a fully integrated multi-detector environment together with STS, TOF, TRD, and other subsystems.

The detector response was studied over a wide range of beam intensities and operating voltages. A systematic procedure for identifying and masking noisy channels was developed using off-spill data, ensuring stable data acquisition and uniform acceptance across all runs. The analysis demonstrates that, after noise mitigation, both GEM detectors exhibit a linear response with

respect to beam intensity up to 5×10^8 particles per spill, with no indication of gain saturation or rate-induced non-linearities.

Time correlation studies between MuCh and TOF, as well as between GEM1 and GEM2, reveal stable and well-defined timing offsets throughout the full duration of data taking. The observed stability at the nanosecond level confirms reliable synchronization of the MuCh subsystem within the free-streaming readout architecture of CBM. Spatial correlation analyses further show strong one-to-one correspondence between hits in GEM1 and GEM2, demonstrating correct geometrical alignment and common detector acceptance.

Digi-level correlation studies between MuCh and TOF confirm that both GEM stations scale linearly with global event activity across different beam intensities. Rate capability studies show that GEM1 and GEM2 successfully handle extreme particle fluxes of up to approximately 400 kHz/cm^2 and 300 kHz/cm^2, respectively, with the highest rates observed at the narrow ends of the detectors facing the beam pipe.

Finally, time-based event building and hit reconstruction using a fixed time window algorithm were validated using reconstructed hit distributions and inter-station hit correlations. The clear diagonal structures observed in the X-X and Y-Y hit correlation plots confirm correct event association and reliable hit reconstruction.

Overall, the results presented in this chapter demonstrate that the MuCh GEM detectors, together with their front-end electronics and readout chain, operate stably and linearly under high-rate conditions representative of the CBM experiment. These findings validate the readiness of the MuCh subsystem for large-scale deployment in CBM and provide confidence in its performance for future high-luminosity heavy-ion physics measurements.

Bibliography

[1] mCBM@SIS18, CBM Collaboration (Collaboration author), GSI 58 S. (2017) https://doi.org/10.15120/GSI-2019-00977

[2] A. Kumar et al, Commissioning and testing of pre-series triple GEM prototypes for CBM-MuCh in the mCBM experiment at the SIS18 facility of GSI, JINST 16 P09002 (2021). https://doi.org/10.1088/1748-0221/16/09/P09002

[3] Ghosh, C., Dubey, A.K., Kumar, J., Kumar, A., Chattopadhyay, S. (2021). Design and Development of Various Cooling Arrangements for Muon Chamber Detector Electronics. In: Behera, P.K., Bhatnagar, V., Shukla, P., Sinha, R. (eds) XXIII DAE High Energy Physics Symposium. DAEBRNS HEPS 2018 2018. Springer Proceedings in Physics, vol 261. Springer, Singapore. https://link.springer.com/chapter/10.1007/978-981-33-4408-2

Chapter 4

Gas system development for CBM-MuCh GEM detector system

4.1 Introduction

The international Facility for Antiproton and Ion Research (FAIR) in Darmstadt, Germany provides unique research opportunities in the field of hadronic and leptonic physics. The upcoming Compressed Baryonic Matter (CBM) experiment at FAIR is designed to investigate the dense nuclear matter in nucleus-nucleus collision with an interaction rate up to 10 MHz. The identification of rare probes like low mass vector mesons (LMVM), multi-strange hyperons, charmonia etc, requires very high interaction rate and efficient background suppression. CBM will initially use proton beam from SIS100 synchrotron with an energy of 2-29 AGeV and heavy ion beam with an energy of 2-14 AGeV. Finally it will continue using beam from SIS300 synchrotron with an energy up to 90 AGeV for proton and upto 45 AGeV for heavy ions [1]. The CBM-MuCh detector system is an essential part of this experiment, designed to detect muons produced during high-energy collisions. The muon detection capabilities of the system heavily

depend on the performance of the GEM detectors [2] [3], which require precise control of the gas mixture ratio and gas flow rate within the detector chambers. Thus, the development of a reliable and cost-effective gas mixing unit system and a gas flow monitoring system for the CBM-MuCh detectors is necessary. In this article, we have reported the details of the design, development, and testing of a gas mixing unit and a gas flow monitoring system for the CBM MuCh GEM detectors [4] [5].

4.2 Detector design and Fabrication

The detector module used in this study consists of one drift PCB, one readout PCB, and three GEM foils, arranged in a 3-2-2-2 mm gap configuration corresponding to the drift, two transfer, and induction gaps, respectively [7] [1]. Figure 4.1a shows the schematics of the High Voltage (HV) distribution scheme. The readout PCB is an eight-layer board comprising 1824 pads, distributed across 19 columns and 96 rows.

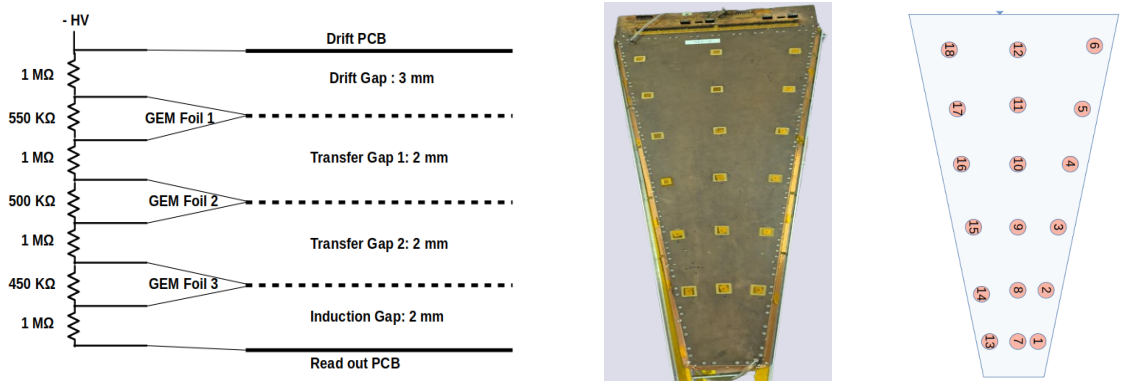

(a) (b) (c)

Figure 4.1: (a) Schematics of the HV distribution scheme for Triple GEM detector. (b) Real size MuCh second station GEM chamber. (c) Hole layout on drift PCB of the module.

The trapezoidal single-mask GEM foils were procured from CERN and stretched using the "NS-2" technique, which avoids the use of glue and facilitates re-tensioning if required. The

foils are segmented into 24 sectors to minimize capacitance and limit the discharge probability. Each segment of all three foils was tested at 550 V, with the requirement of no shorts and a leakage current below 5 nA.

All assembly steps and measurements were carried out at an ambient temperature of 23^0 C and a relative humidity of 50 % in a class-1000 clean room at VECC. After passing the quality assurance (QA) tests, the three GEM foils were assembled together with the required spacers and screws between the drift and readout PCBs [9]. Figure 4.1b shows the assembled GEM detector module for the second station of the MuCh. For gain measurements with the ^{55}Fe X-ray source, through-holes were provided across the drift PCB to allow source irradiation at different locations; the positions of these holes are indicated in Figure 4.1c.

In the adopted HV distribution scheme, a detector operating voltage of 3800 V corresponds to a branch current of 664 micro Amp. Under this configuration, the voltages across the three foils are 365 V, 332 V and 299 V, respectively, resulting in a sum total of 996 V across the three GEM foils.

4.3 Gas Mixing Unit

The charge amplification in a GEM detector depends heavily on the properties of the input gas. So, it is crucial to understand how the detector response varies with the ratio of Ar:CO_2 mixture. Earlier we have observed drastic gain variation in the same detector module, but with different cylinders of premixed Ar:CO_2 gas. This happens due to the gas purity variation and different tolerances in mixture ratio for different premixed cylinders. So, to overcome this issue a gas mixing unit has been developed. The detector properties have been studied systematically by varying the gas mixture ratio and the gas flow rate. Figure 4.2a shows the schematic layout of the gas mixing and delivery system. Figure 4.2b shows the full-size GEM prototype used for testing.

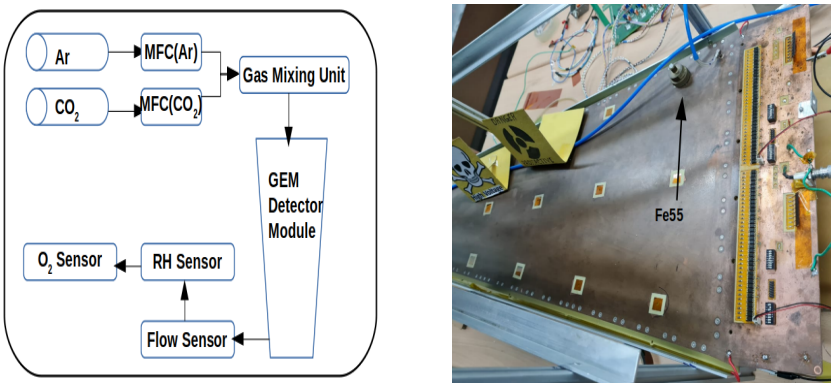

(a) (b)

Figure 4.2: (a) Schematic of the gas delivery and monitoring system used in the experiment. (b) Detector Under test: Real size prototype of MuCh second station GEM chamber

This schematic shows that the input gases are taken from two ultra high pure (UHP) gas cylinders containing Argon and Carbon Dioxide (CO_2) respectively. Those gases are given to 2 MFCs and the output controlled gases are sent into a gas mixing unit for proper blending. Then the output of the mixing unit is given to the GEM detector as active medium and the output of the detector is passed through a flow sensor. This flow sensor is discussed in section 5 in details. Afterwards a relative humidity sensor and an oxygen monitoring system is used. The detector under test is shown in Figure 4.2b, which is a real size GEM prototype for CBM MuCh second station .

A gas mixing unit has been developed using two commercial Aalborg GFC17 Mass Flow Controllers and the setup is shown in Figure 4.3a. The MFCs are controlled via a controller circuit using a 15 connector D - pin attached to it as shown in Figure 4.3b. The MFC output values can be seen via the LCD display. Each MFC is calibrated using a commercial flow meter, to ensure precise control over the flow rates of Argon and CO_2.

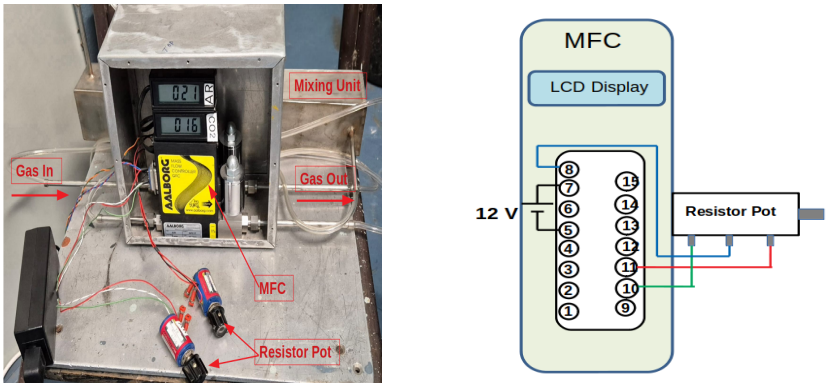

(a) (b)

Figure 4.3: (a) MFC Setup. (b) MFC Control circuit.

4.3.1 Calibration

For the calibration of the MFCs, two high-purity gas cylinders containing Argon and Carbon Dioxide (CO_2) are used and each gas is individually allowed to flow through its respective MFC. Each MFC is connected to a resistance potentiometer equipped with an adjustable knob, which is used to fine-tune the gas flow rate, thereby achieving specific, predetermined gas mixture ratios. Each MFC has been calibrated by comparing its setpoint output with a standard flow meter, for gas mixture ratios of 60:40, 70:30, 80:20, and 90:10 (Ar:CO_2).

Figure 4.4 shows the calibration graph at different gas mixing ratio. This plot shows the required flow rate (L/hr) in X-axis and the MFC setpoints of Argon and CO_2 by different colors in Y-axis.

Once calibration is completed and the MFC readings are verified, the flow rates of Argon and CO_2 are set to the desired values for the target gas mixture ratios. The output gases from both MFCs are then combined through a gas mixing unit as shown in Figure 4.3a. The mixed gas flow is monitored using a gas flow sensor to confirm that the overall flow rate matches the experimental requirements.

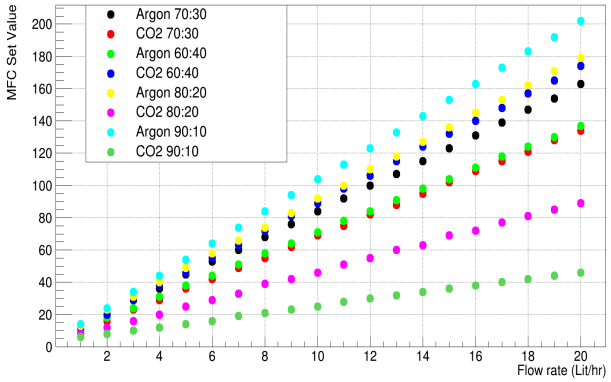

Figure 4.4: Calibration graph for different mixing ratio.

Following confirmation, the gas mixing unit is flushed continuously for 3 hours to remove any impurities or residual gases, ensuring that only a clean and homogenous gas mixture enters the GEM detector module. Subsequently, the outlet of the gas mixing unit is connected to the GEM module inlet, and the detector is flushed again for 3 hours to purge any contaminants present within the detector volume.

After the flushing procedures, high voltage is applied to the GEM detector. A ^{55}Fe radioactive source is positioned at the desired location on the detector surface, and data acquisition is initiated to determine the high voltage value at which the ^{55}Fe signal becomes detectable.

Finally, measurements are performed at different high voltage settings, and the detector gain is calculated from the collected data.

4.3.2 Data Analysis and Results

A ^{55}Fe X-ray source is used as ionizing radiation to the real size CBM MuCh second station GEM chamber module. The source is placed on hole-18 position of the drift PCB as shown in Figure 4.1c and the data is acquired using self-triggered STS/MUCH-XYTER Front End Boards (FEB) [6].

The gain characteristics of the GEM detector module are studied for the 70:30 Argon to CO_2 gas mixture ratio at varying gas flow rates. A typical clustered charge spectra of ^{55}Fe is shown in Figure 4.5a, which shows the main peak at 77 fC. The main peak of the spectra is fit with a Gaussian and the mean value (in fC) is taken for the gain calculation. As the number of primary electrons generated is around 212, the gain is calculated by dividing the clustered charge by 212.

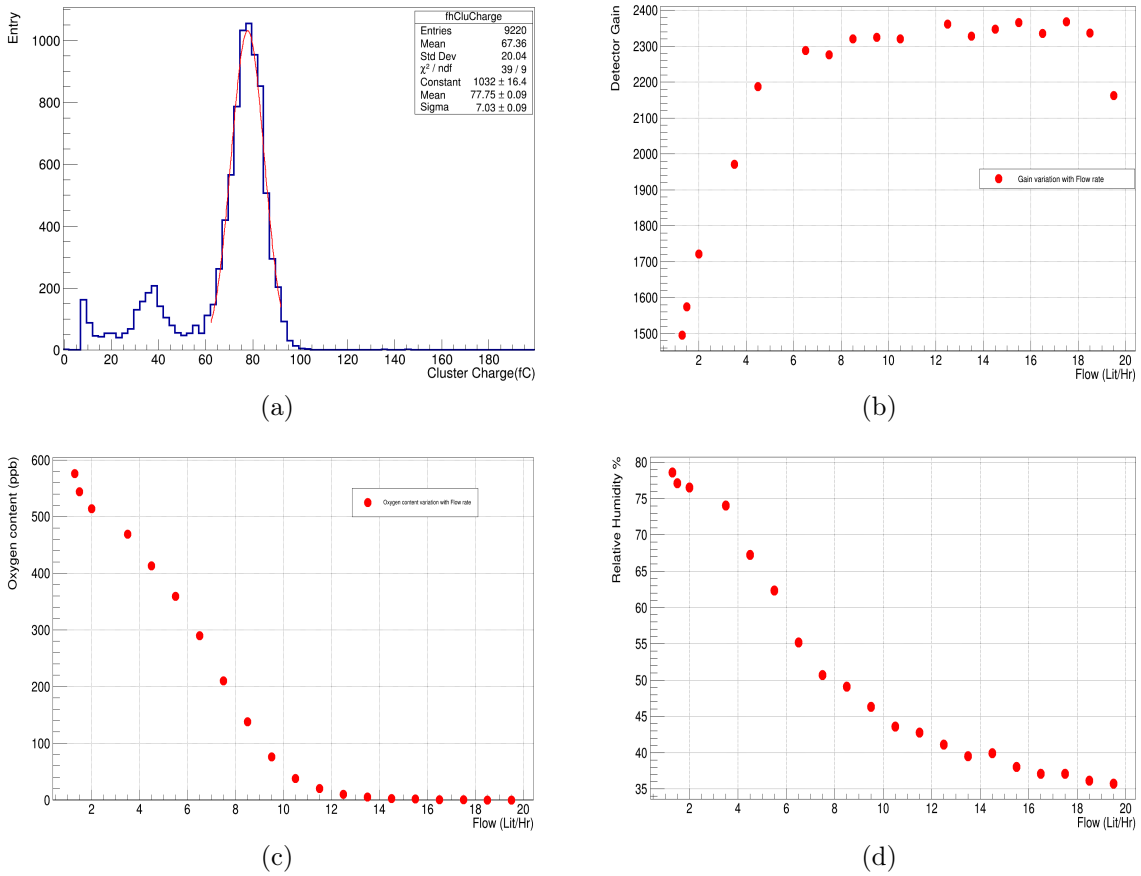

Figure 4.5: (a) Typical clustered charge spectra at HV = 855.90 V, I_{mon} = 1141.20 μA, MPV = 77.75 fC. (b) Gain of the GEM detector as a function of gas flow rate for 70:30 Argon:CO_2 gas mixture. (c) Variation of Oxygen content (ppb) with flow rate. (d) Variation of Relative Humidity with flow rate.

It is observed that as the gas flow rate is increased, the gain of the GEM module also increases up to a flow rate of 8 L/hr and then gain saturates as shown in Figure 4.5b. In the low flow rate region, the impurities (O_2, H_2O) play a significant role in gas medium which leads to lower gain. As the flow rate increased to an value of 8 L/hr, the gain becomes optimal.

These results indicate the presence of an optimal flow rate that balances gas purity and detector response, which is critical for stable and efficient operation of the GEM modules. The present results are based on gain measurements taken at a single position on the detector. Since it is a large-area trapezoidal module, measurements at multiple positions may provide additional insight and could further refine the determination of the optimum flow value [9].

The O_2 content in the output gas from the detector module has also been measured using a Hach orbisphere 410 dissolved oxygen monitor. The amount of oxygen is found to decrease with higher flow rate, as shown in Figure 4.5c. At a flow rate of 8 L/hr the oxygen level drops below 160 ppb, at which the maximum detector gain is observed. Which further confirms the reason of lower gain at low gas flow rate. Figure 4.5d shows the variation of relative humidity (RH) with flow rate. This shows that as the flow rate is increased upto 8 L/hr, the RH comes down below 50 % from the ambient RH of 80 % and accordingly the detector gain is maximized. For leak characterization of the detector module, gas was supplied at a flow rate of 8 L/hr and a 3 % lower flow rate at the output has been observed, using the same calibrated flow measuring device. This indicates an estimated module leak rate of about 3 %.

Based on our initial findings for the 70:30 Argon:CO_2 gas mixture, where the maximum gain is observed at a flow rate of 8 L/hr, we select this flow rate as the operating point for further studies. The subsequent analysis involves investigating the gain characteristics of the GEM detector for various gas mixture ratios, namely 60:40, 70:30, 80:20, and 90:10 - all conducted at a fixed flow rate of 8 L/hr. For each gas mixture, we varied the applied high voltage and recorded the corresponding gain to understand the detector's response under different gas compositions.

4.3.3 Comparison of Gain for Different Gas Mixture Ratios

Figure 4.6 presents the variation of gain as a function of the GEM summed-up high voltage for all Ar:CO_2 gas mixture ratios: 60:40, 70:30, 80:20, and 90:10.

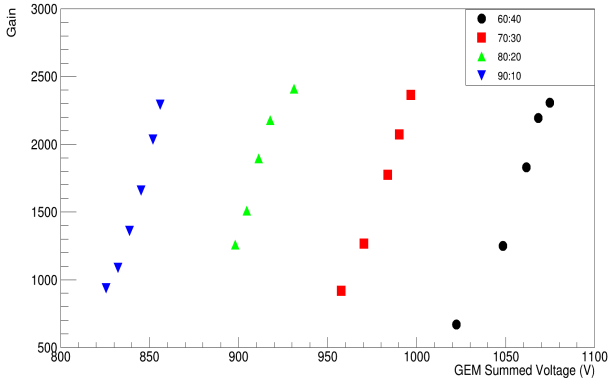

Figure 4.6: Measured gain of the GEM detector as a function of summed-up applied high voltage for various Ar:CO_2 gas mixtures at fixed flow rate of 8 L/hr. The 90:10 mixture shows the highest gain.

The plot clearly shows that the gain increases with voltage for each mixture, with higher argon content mixtures generally exhibit higher gain at comparably lower voltages. Notably, the 90:10 mixture demonstrates the highest gain values, consistent with the enhanced ionization properties of argon-rich mixtures. This comparison highlights the trade-off between gas composition and detector performance, essential for optimizing operational parameters in GEM detectors.

4.4 CBM Muon Chamber Gas Layout

The first two stations of the CBM Muon Chamber detector will consist of GEM detectors, with each station comprising three layers of detectors. In each layer of the first station, 16 detector modules will be installed, totaling 48 modules in the first station. Initially, it was proposed

to connect four consecutive GEM modules in a daisy-chain gas configuration. However, a laboratory study using three full-size GEM modules connected in a daisy-chain (shown in Figure 4.7) revealed significant performance degradation.

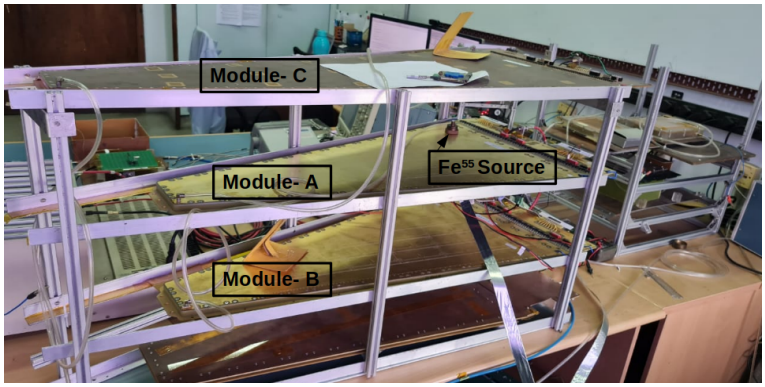

Figure 4.7: Photograph of three full-size GEM modules used to study gain performance under daisy-chained (series) and parallel gas configurations.

Specifically, the gain of the second and third modules dropped by approximately 35 % compared to the first module. Furthermore, if a leaky module was placed at the first position in the chain, it maintained normal gain, but the downstream modules exhibited nearly zero gain. This finding strongly suggests that daisy-chaining is not suitable for the CBM MuCh setup, particularly due to its susceptibility to upstream gas impurities or leaks. To address this, we tested a parallel gas configuration using two real-size GEM modules connected in parallel. In this setup, both modules achieved their expected gain values, independent of the leak condition in either module. Based on this observation, it is concluded that each GEM module in the CBM MuCh detector should be supplied with gas through an independent parallel gas line. However, in the actual detector environment, modules will be installed at different heights and distances from the central gas distribution line, which will result in variable line resistances. If all modules are connected in a simple parallel configuration without flow regulation, these differences in line resistance could lead to unequal gas flow rates, causing gain variation across modules (as observed in Figure 4.5b). To ensure uniform flow, we plan to install a manual

flow controller in each input gas line, allowing us to regulate the flow rate individually for each module. Additionally, to monitor flow stability and detect any leakage, a gas flow sensor will be installed on both the input and output lines of each module.

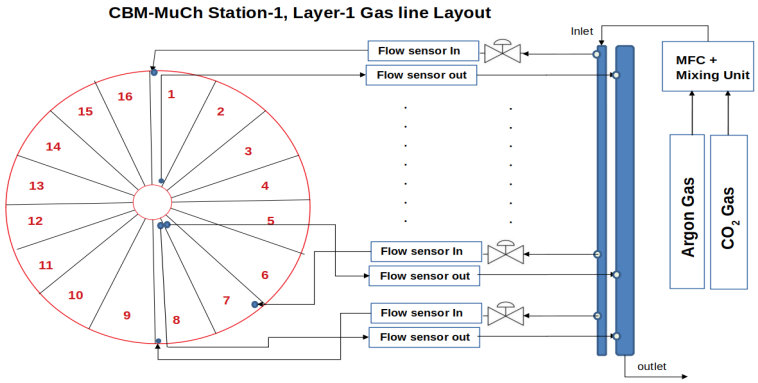

Figure 4.8: Schematic of the proposed gas distribution system for the CBM-MuCh GEM detectors. Each module receives gas through an independent line equipped with flow controllers and sensors to enable uniform distribution, leak detection, and real-time monitoring.

A schematic of the proposed gas distribution system for the CBM-MuCh GEM modules is shown in Figure 4.8. Ultra high purity (UHP) Argon and CO_2 gases will be blended in precise ratios using a calibrated MFC-based gas mixing unit. The mixed gas will be distributed into 16 channels for each layer. Each channel will pass through a manual flow controller and then an input flow sensor before entering the detector module. After exiting the module, the gas will pass through an output flow sensor. The difference between the input and output sensor readings provides a measure of gas leakage in each module. Finally, the output gas from all modules will be collected and exhausted outside the experimental cave. In total, 108 GEM modules will be used across the first two stations. Therefore, to monitor both input and output flow rates, 216 flow sensors will be required. Data from all flow sensors will be collected by a concentrator board and recorded remotely via ethernet.

4.5 Gas Flow Monitoring System

A gas flow monitoring system has been developed for CBM-MuCh GEM detectors using a Honeywell AWM92100 commercial gas flow sensor, as shown in Figure 4.9a.

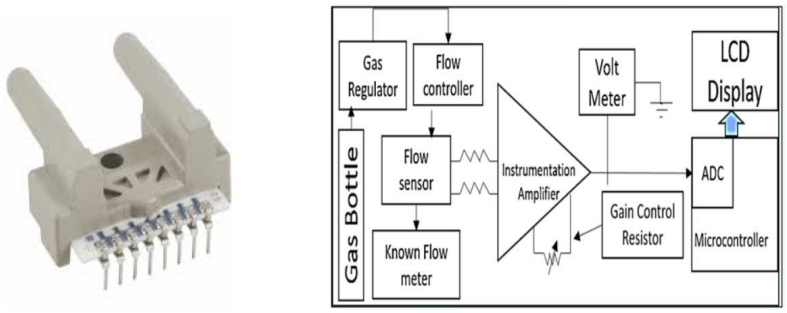

(a) (b)

Figure 4.9: (a) Honeywell AWM92100 flow sensor. (b) Schematic of the gas flow sensor setup

This flow sensor is selected due to its high sensitivity, fast response time and the desired flow measurement range. This sensor has a range of 200 Standard Cubic Centimeters per Minute (SCCM) with a response time of 1 ms. The sensor works based on thermal principle, where the gas flow induces a change in the temperature of a sensing element. This temperature change is then converted into an electrical signal that is proportional to the flow rate. This sensor provides an analog output that needs to be processed for displaying a readable output. The schematic of the gas flow sensor calibration setup and monitoring scheme can be seen in the Figure 4.9b. The gas sensor is put in series to the gas line via a gas regulator and a flow controller. The output of the gas flow sensor is first amplified using an instrumentation amplifier (INA141U). The amplifier plays a vital role in processing the weak signal produced by the sensor and enhancing its amplitude so that it can further be processed by a microcontroller. The INA141U amplifier is chosen for its low noise and high precision. This amplifier can be configured to provide a dual gain mode, which allows for measuring different ranges of gas flow. With the lower gain of 10, the sensor can achieve the range of 0 to 200 SCCM which will be

required for the GEM detector system, whereas with higher gain of hundred the range can be confined within 0 to 2 SCCM.

4.6 Flow Sensor Integration and Calibration

A Printed Circuit Board (PCB) has been designed for the control circuitry of the flow sensor as shown in Figure 4.10a, and after fabrication the PCB is shown in Figure 4.10b.

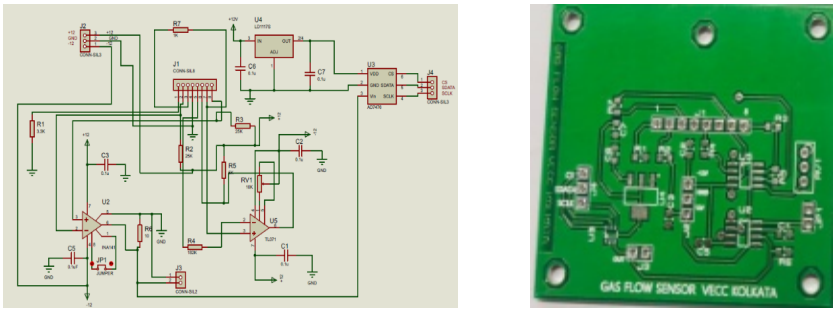

(a) (b)

Figure 4.10: (a) PCB layout for control circuit (b) The real PCB.

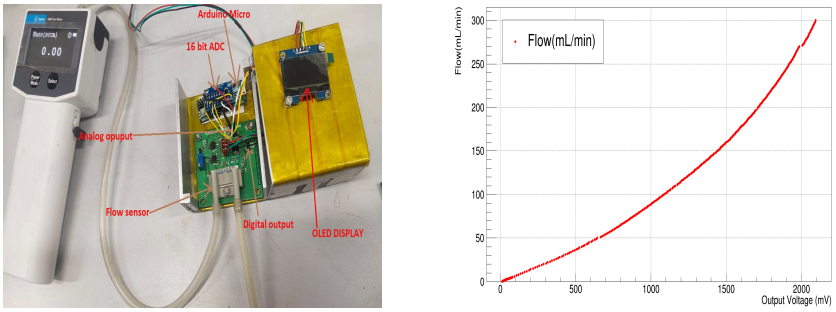

(a) (b)

Figure 4.11: (a) Calibration setup of the Flow sensor (b) Calibration Curve.

The PCB is populated with the flow sensor and with all the other necessary electronics components as shown in Figure 4.11a. The output of the flow sensor is connected to a commercial

Agilent ADM flow meter for calibration of the sensor. An OLED display has been attached with the setup to read the flow values given by the sensor.

Now the gas flow is increased using a manual controller and the output voltage of the sensor is logged. The Figure 4.11b shows the calibration curve of the sensor for different flow rates. A python script based online data monitoring and logging system has also been developed. This system can be controlled over ethernet, so it will be useful to monitor all the flow sensors, that will be connected to MuCh detectors in CBM experiment.

These flow sensor systems, once fully deployed, will provide real-time monitoring of gas flow conditions across all 108 GEM modules in the CBM-MuCh detector system. This infrastructure ensures not only consistent detector operation but also enables early detection of gas flow anomalies or potential leaks. The integration of individual flow sensing and remote data acquisition thus plays a critical role in maintaining the long-term stability and reliability of the CBM experiment's muon detection subsystem.

4.7 Summary

A Mass Flow Controller (MFC) based gas mixing system has been designed, implemented, and characterized for the CBM-MuCh GEM detectors. Each MFC was calibrated by comparing its set-point output with a standard flow meter for Ar:CO_2 gas mixtures of 60:40, 70:30, 80:20, and 90:10 ratio. Systematic gain measurements using a ^{55}Fe X-ray source were performed on a large size trapezoidal GEM module of $\sim$2800 cm^2 area and having 3-2-2-2 mm gap configuration. The oxygen content in the output gas was found to decrease with increasing flow rate, reaching below 160 ppb at 8 L/hr, where the maximum detector gain was observed. A similar trend was seen for relative humidity, which dropped from 80 % ambient to below 50 % at 8 L/hr, consistent with the conditions required for stable detector operation. The detector gain was also measured for different gas mixture ratios, and in all cases, the gain was found to increase with applied

voltage. Mixtures with higher argon content exhibited higher gain at comparatively lower voltages. From these studies, a 70:30 mixture operated at 8 L/hr was identified as providing the most stable gain response. Based on a dedicated gas distribution study, a parallel gas layout with individual flow regulation has been proposed to avoid the gain degradation observed in daisy-chain configurations. To ensure uniform and stable gas flow across all 108 modules of the first two MuCh stations, a comprehensive gas monitoring solution has been implemented. This system employs 216 calibrated flow sensors with remote data acquisition, enabling real-time monitoring of input and output flow rates, leak detection and long-term operational stability. These developments ensure uniform gas delivery, long-term stability and reliable operation of the CBM-MuCh subsystem. The proposed architecture can be readily adapted for other large-scale GEM-based systems and gaseous detectors in high-rate experiments, offering a precise gas handling and monitoring.

Bibliography

[1] Subhasis Chattopadhyay, Yogendra Pathak Viyogi, Peter Senger, Walter F. J. Muller, and Christian J. Schmidt, editors. Technical Design Report for the CBM : Muon Chambers (MuCh). GSI, 2015, https://repository.gsi.de/record/161297

[2] F. Sauli, GEM: A new concept for electron amplification in gas detectors, Nucl. Instrum. Meth. A 386 (1997) 531. https://doi.org/10.1016/S0168-9002(96)01172-2

[3] F. Sauli, The gas electron multiplier (GEM): Operating principles and applications, Nucl. Instrum. Meth. A 805 (2016) 2. https://doi.org/10.1016/j.nima.2015.07.060

[4] A.K. Dubey et al., GEM detector development for CBM experiment at FAIR, Nucl. Instrum. Meth. A 718 (2013) 418. https://doi.org/10.1016/j.nima.2012.10.043

[5] A. Kumar et al, Commissioning and testing of pre-series triple GEM prototypes for CBM-MuCh in the mCBM experiment at the SIS18 facility of GSI, JINST 16 P09002 (2021). https://doi.org/10.1088/1748-0221/16/09/P09002

[6] J. Saini et al, Test and characterisation of STS/MuCh-XYTER and integration with multiple detectors of CBM-MuCh detector systems. JINST 18 P01009 (2023). https://doi.org/10.1088/1748-0221/18/01/P01009

[7] S. Bachmann et al, Performance of GEM detectors in high intensity particle beams, Nuclear Instruments and Methods in Physics Research A 470 (2001) 548-561. https://doi.org/10.1016/S0168-9002(01)00802-6

[8] Apar Agarwal et al, Testing a large size triple GEM detector for the first station of the CBM-Muon Chambers with a high-intensity gamma source at GIF++ under large-area illumination, 2025 JINST 20 P04022. https://doi.org/10.1088/1748-0221/20/04/P04022

[9] Chandrasekhar Ghosh et al, First prototype of MuCh second station GEM module: design, fabrication and testing for CBM experiment at GSI, Germany, 2025 JINST 20 P09005. https://doi.org/10.1088/1748-0221/20/09/P09005

Chapter 5

Testing of various cooling arrangement for CBM-MuCh GEM detector electronics

5.1 Introduction

The Compressed Baryonic Matter (CBM) experiment at the Facility for Antiproton and Ion Research (FAIR) is designed to investigate the phase structure of strongly interacting matter at high baryon densities. The Muon Chamber (MuCh) subsystem plays a central role in identifying low momentum muons originating from the decays of light vector mesons. The MuCh system employs large area Gas Electron Multiplier (GEM) detectors equipped with MUCH-XYTER front end electronics boards (FEBs). Each FEB dissipates approximately 5 W of power. A detector module in the first station contains 18 FEBs, while a second station module contains 15 FEBs. Consequently, the combined thermal load from the first and second stations amounts to nearly 8.82 kW.

Reliable thermal extraction is therefore critical for maintaining stable operation of the readout electronics [1]. This chapter presents a comprehensive and systematic evaluation of the various

cooling schemes investigated at VECC: (i) Water cooling using grooved aluminium channels, (ii) Forced air cooling using ducted airflow, (iii) Peltier based thermoelectric cooling, and (iv) water cooling employing a molded aluminium plate with an embedded steel pipe. The design methodology, experimental setups, and corresponding thermal performance measurements are presented in this chapter.

5.2 Cooling Requirements of MuCh Electronics

The MuCh system consists of trapezoidal GEM detectors distributed across two stations, with the first station comprising three concentric detector layers, as illustrated in Figure 5.1a. Each station requires a high degree of thermal stability to prevent FEB drift, electronic noise, and long term degradation. The first station of the MuCh system contains 48 detector modules, each requiring 18 FEBs (as shown in Figure 5.1b) for data readout, yielding an aggregate of 864 FEBs. At a dissipation rate of 5 W per FEB, the corresponding thermal load for the station is calculated to be 4.32 kW. Similarly, for the MuCh second station, a total of 60 detector modules are used, each equipped with 15 FEBs, resulting in a heat load of approximately 4.5 kW.

According to the cooling requirement summary, the expected heat loads are:

- Station-1: 48×90 W ≈ 4.32 kW
- Station-2: 60×75 W ≈ 4.5 kW
- Total heat load: ≈ 8.82 kW

The electronics must be maintained below 25°C for optimal performance and it is proposed to connect 4 plates (quadrant) in daisy chain water cooling. Using basic heat transfer principles, the water mass flow requirement for a quadrant is computed using:

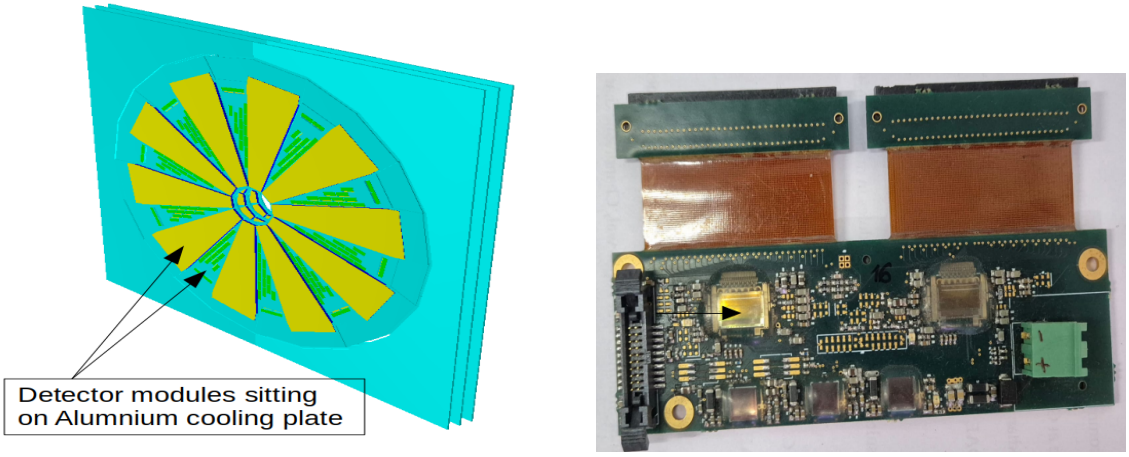

(a) (b)

Figure 5.1: (a) Schematic of the three detector layers of the first MuCh station (b) MuCh Front End Board (FEB)

$$m = \frac{Q}{(\rho\, C\, \Delta T)}$$

where Q is heat load (4 x 90 W = 360 W), C is heat capacity of water (4186 J/kg.°C), and ΔT is allowable rise (2°C). This yields 0.043 kg/s or 2.6 L/min. This requirement forms the baseline for designing embedded water channels.

5.3 Water cooling using grooved aluminium channels

The primary cooling strategy investigated at VECC employed water channels machined into a 10 mm thick aluminium plate. In this method, a 10 mm aluminium sheet was milled to create a 5 mm T-shaped groove, as illustrated in Schematic 5.2a, and the resulting cut geometry is shown in Figure 5.2b. The groove was subsequently sealed by brazing a 2 mm aluminium strip over its surface, after which the entire plate was precision machined to achieve a smooth and planar finish.

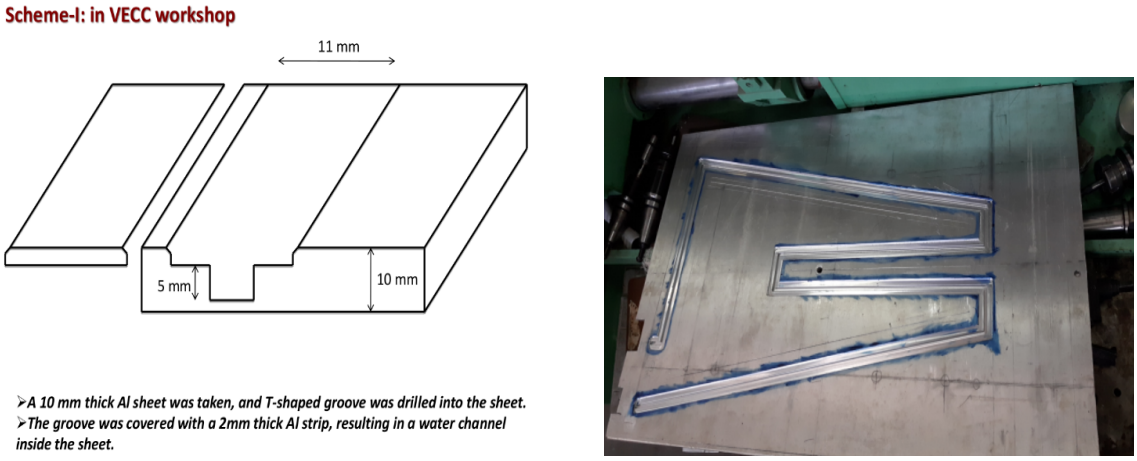

(a) (b)

Figure 5.2: (a) Schematic of the T-shaped machined groove. (b) Aluminium cooling plate after groove machining.

5.3.1 Aluminium Plate performance test:

To evaluate the performance of the cooling plate, heating resistors with a power dissipation of 5 W each were mounted on the aluminium surface to emulate the thermal load of the FEBs. A DC voltage was applied across the series connected resistors so that each resistor generated a heat load of 5 W. Concurrently, chilled water from a laboratory water chiller was circulated through the embedded channels using a submersible pump, with the outlet flow returned to the chiller to maintain a closed loop system. Temperature control and monitoring were carried out using an Arduino based microcontroller system. The schematic of the experimental arrangement is presented in Figure 5.3a, and the corresponding laboratory setup is shown in Figure 5.3b.

In the absence of water circulation, continuous heating causes the aluminium plate to reach temperatures of approximately 50°C. Since the FEBs must be maintained below 25°C to ensure stable and accurate data acquisition, active cooling is required throughout detector operation. To assess the temperature uniformity across the plate, eighteen temperature sensors were positioned at different locations, and their readings were continuously monitored and

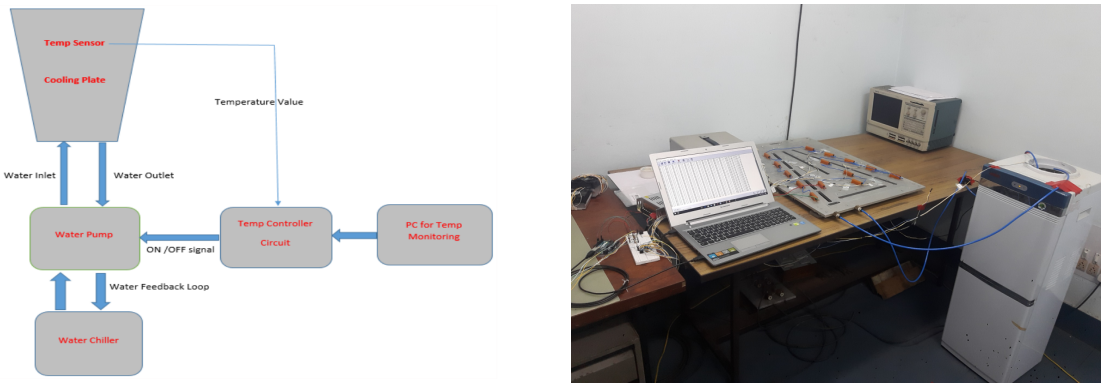

(a) (b)

Figure 5.3: (a) Schematic of the laboratory cooling setup. (b) Photograph of the fabricated cooling-plate test assembly.

logged using an Arduino based system. Custom Arduino firmware was developed for this purpose. DS18B20 digital temperature sensors were selected owing to several advantages over conventional analog sensors: they support cable lengths up to 100 m without loss of accuracy, and up to 255 sensors can be connected on a single one wire bus, as each device possesses a unique internal address. The circuit diagram of the temperature monitoring and control unit is shown in Figure 5.4a.

Figure 5.4b illustrates the temperature stability of the aluminium plate over a continuous 100 hour operation. The red data points represent the plate temperature; initially, the plate was allowed to heat up to approximately 35°C without cooling. Once the cooling system was activated, the temperature rapidly decreased to around 25°C and remained regulated at this value through the temperature feedback control circuit. The blue data points correspond to the chiller water temperature, while the black data points indicate the ambient laboratory temperature.

The cooling plate fabricated at the VECC workshop was subsequently deployed at the CERN SPS H4 test beam line for thermal management of the detector electronics [2]. In this configu-

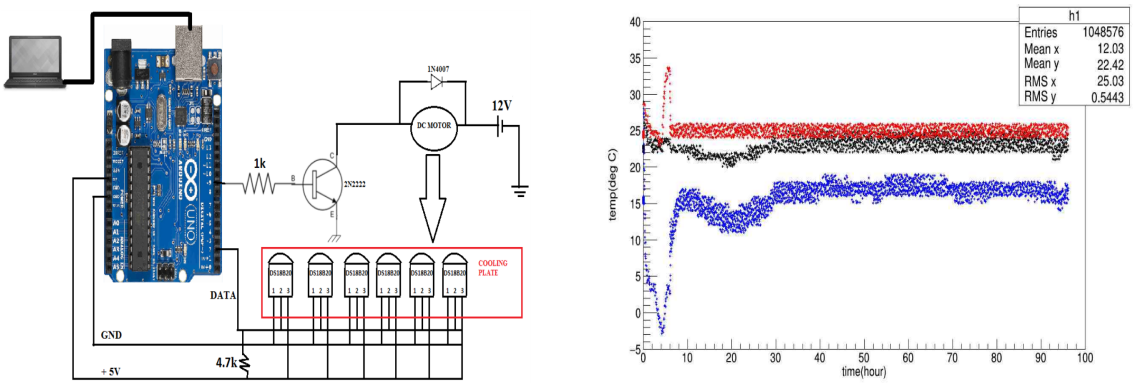

(a) (b)

Figure 5.4: (a) Temperature measuring, controlling and logging unit. (b) Temperature stability over 100 hours operation at lab.

ration, the detector was mounted on one side of the plate, while the FEBs were installed on the opposite side and connected to the detector via flexible cables. The cooling plate successfully maintained the temperature of all FEBs below 25°C throughout the beam test operation.

5.4 Forced air cooling using ducted airflow

After establishing the effectiveness of the aluminium water cooling plate, an alternative cooling approach was explored that would not rely on liquids such as water, which may pose leakage risks over long term operation. To mitigate such concerns, various air cooling configurations were investigated. A dummy model of the trapezoidal GEM detector, equipped with seating positions for 18 FEBs, was fabricated using G10 material, as shown in Figure 5.5a. To reproduce the thermal load of the FEBs, eighteen resistors were mounted on the G10 surface, and a DC voltage was applied across their series connection, resulting in a power dissipation of approximately 5 W per resistor. A single axial fan was employed to extract heat from the system, as indicated in the Figure 5.5a. The measurements were conducted under ambient conditions of 23°C and 58% relative humidity. Initially, the resistors were allowed to heat without cooling until their

temperatures stabilized at elevated values; the fan was then switched on, and the temperatures were monitored until a steady state was reached. All temperature readings were recorded using DS18B20 digital sensors, and the corresponding temporal profiles are presented in Figure 5.5b.

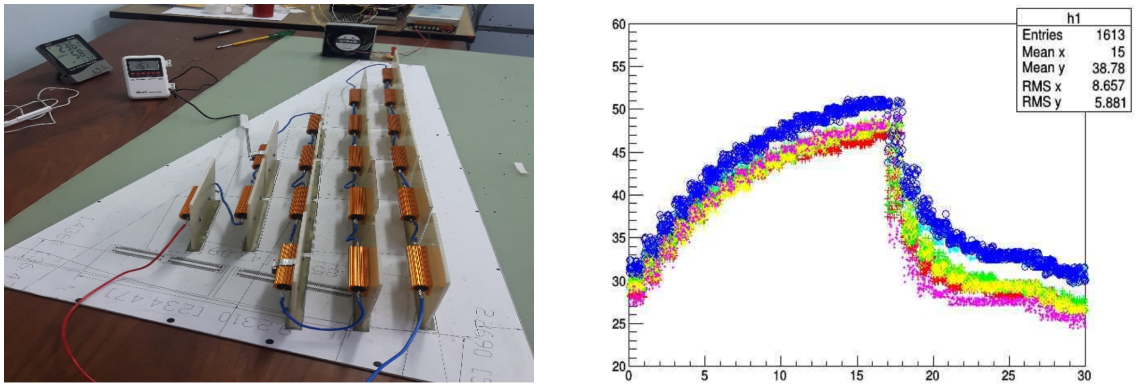

(a) (b)

Figure 5.5: (a) Dummy air cooling setup using G10. (b) Temperature profile of 6 different heating element with time(minutes) in X-axis and Temp(°C) in Y-axis.

The results show that, in the absence of forced airflow, the resistor temperatures rise to approximately 50°C. Upon activation of the fan, the temperatures decrease significantly, stabilizing within the range of 25°C to 31°C. Notably, most elements cool to below 28°C; the element corresponding to the blue temperature sensor exhibits a slightly higher temperature due to its position being marginally outside the primary airflow path.

5.4.1 Channelized Air flow:

A second air-cooling prototype incorporating a channelized airflow geometry was developed using a G10 structure as shown in Figure 5.6a. In this configuration, the effect of an upper cover on the overall cooling performance was investigated by conducting measurements with and without the top enclosure. As in the previous study, eighteen resistors were used to emulate the thermal load of the FEBs, with a voltage applied across their series connection to achieve a heat

dissipation of 5 W per resistor. A single fan was employed to extract heat from the assembly, as illustrated in the corresponding schematic. The experiments were carried out under ambient conditions of 23°C and 58% relative humidity. Initially, the resistors were heated without cooling until their temperatures reached a steady high value; the fans were then turned on, and temperature readings were recorded until stabilization. All measurements were obtained using DS18B20 digital temperature sensors, and the resulting temperature-time profiles are shown in the accompanying figures.

The thermal response demonstrates that, without airflow, the heating elements reach temperatures exceeding 50°C due to the imposed 5 W thermal load per resistor. The data as shown in Figure 5.6b and Figure 5.6c also indicate that the cooling efficiency decreases when the upper cover is installed. The presence of the cover leads to the formation of localized hot pockets particularly at the location corresponding to the red sensor attributed to restricted airflow in that region.

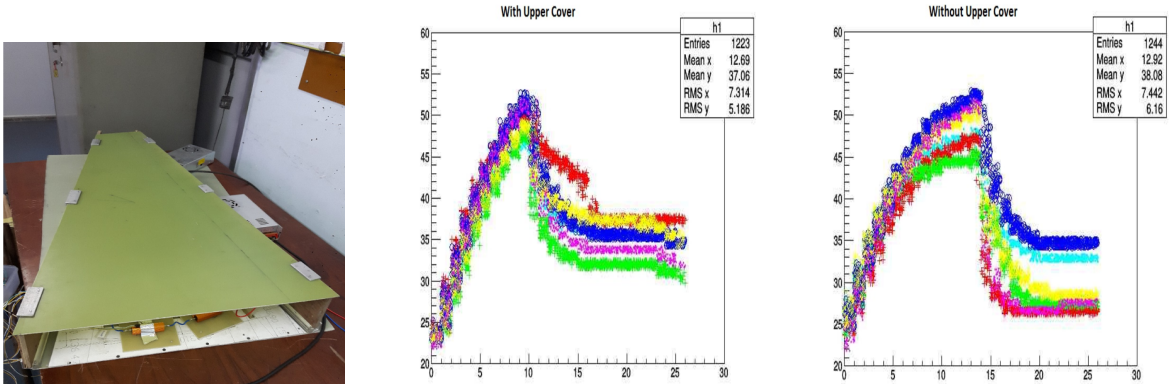

(a) (b) (c)

Figure 5.6: (a) Channelized air-cooling test setup with upper cover. (b) Cooling performance with top cover installed with time (minutes) in X-axis and Temp(deg C) in Y-axis. (c) Cooling performance without top cover with time (minutes) in X-axis and Temp(deg C) in Y-axis.

The fan speed was reduced from 14,900 rpm to 9,023 rpm by lowering the supply voltage from 12.6 V to 10 V in order to examine the impact on acoustic noise. However, the reduction in noise level was not significant. Although the fan can operate at voltages as low as 8 V, the available power supply has a minimum output of 10 V. Given the negligible change in noise characteristics, no additional data were recorded for the fan operated at 10 V.

Despite its apparent simplicity, air cooling exhibits several critical limitations that render it unsuitable for long term use in the MuCh detector system. High speed fans generate substantial acoustic noise, which can disrupt neighboring subsystems, interfere with sensitive instrumentation, and complicate operational conditions in the experimental hall. Additionally, the continuous high velocity airflow introduces mechanical vibrations that propagate through the mounting structures and FEB connectors. Over extended periods, these vibrations can loosen electrical contacts, compromise connector integrity, and increase the likelihood of intermittent signal failures.

Furthermore, the effectiveness of air cooling is highly sensitive to the geometry of the detector enclosure; airflow obstructions or the formation of stagnant air pockets can lead to non uniform temperature distributions, with some FEBs consistently operating at elevated temperatures. Dust accumulation within the airflow channels presents another long term reliability concern, as it degrades cooling efficiency and necessitates frequent maintenance; an undesirable requirement for an inaccessible, large scale detector system. Taken together, these issues: noise, vibration, non uniform cooling and susceptibility to dust, demonstrate that air cooling is not a viable option for the final CBM MuCh installation.

5.5 Peltier based thermoelectric cooling

Peltier thermoelectric coolers were investigated to assess whether localized heat extraction from the aluminium plate could improve the overall cooling performance. For this study, a 2 mm

thick aluminium plate was instrumented with fourteen resistors, each dissipating 5 W when a voltage was applied across their series connection, thereby reproducing the thermal load of the FEBs. Three Peltier modules were mounted in direct contact with the aluminium plate, as illustrated in Figure 5.7a. The experiment was conducted in two stages. First, the resistors were allowed to heat without any cooling until their temperatures stabilized; temperature sensors were then placed on the resistor surfaces to record the steady state values. Subsequently, the Peltier modules were activated, and the temperatures of the same resistor locations were again measured after stabilization. In a second set of measurements, sensors were positioned directly on the aluminium plate to monitor the corresponding plate temperatures before and after Peltier operation.

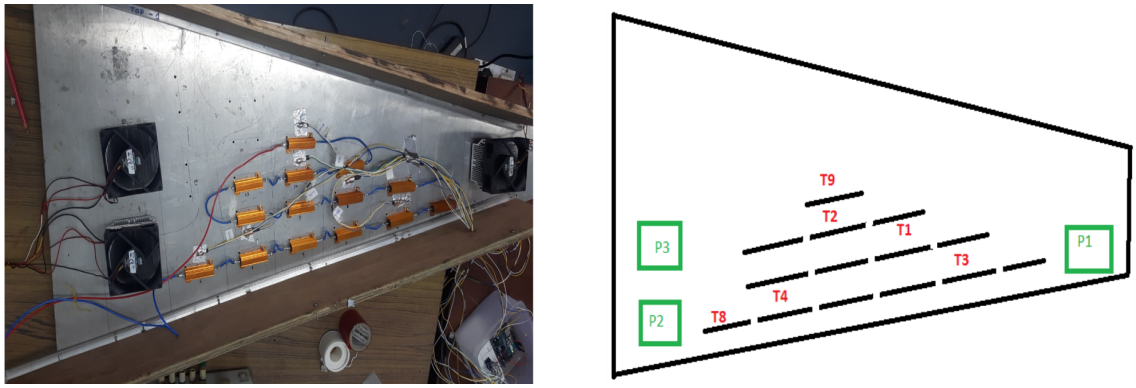

(a) (b)

Figure 5.7: (a) The peltier cooling setup. (b) Schematic of the sensor (Red) and Peltier (Green) positions.

The results show that Peltier cooling produces only a modest reduction in temperature, typically in the range of 3°C to 7°C. Notably, the temperature at one of the monitored positions (T1) remained relatively high at approximately 34°C, owing to its greater distance from the Peltier modules. This indicates that the cooling effect is highly localized, limited by the small effective contact area of the three modules (approximately 48 cm^2 in total). Although the arrangement was intended as a crude approximation of dual water channels placed along the plate

edges, the thermal performance remains insufficient for realistic detector operation. Moreover, Peltier devices introduce additional challenges, including significant electrical power consumption and the need to dissipate the substantial heat generated on the hot side of the modules. These limitations collectively indicate that Peltier cooling may serve only as a supplementary technique and is not viable as a standalone solution for the MuCh detector system.

5.6 Water cooling employing a molded aluminium plate with an embedded steel pipe and Integration into mini-CBM experiment at GSI

In addition to the machined aluminium cooling plates, a new fabrication approach based on a molding technique has recently been developed. In this method, a stainless steel pipe of 6 mm outer diameter and 3 mm inner diameter is arranged within a trapezoidal mold in a zig-zag configuration, as illustrated in Figure 5.8a.

The pipe is bent such that it traverses all FEB mounting locations, enabling efficient heat extraction as chilled water flows through it. Once the pipe is positioned, molten aluminium is poured into the mold to form a monolithic cooling plate. Since aluminium melts at approximately 660°C while the steel pipe remains solid up to around 1400°C, the pipe retains its structural integrity during casting and becomes permanently embedded within the aluminium matrix. This approach eliminates brazing defects and ensures fully enclosed leak-tight channels.

Following fabrication, each cooling plate is subjected to a hydrostatic pressure test in the range of 5 to 10 bar to verify the integrity and leak tightness of the embedded cooling channel. Using this technique, full scale cooling plates corresponding to the geometries of both the first and

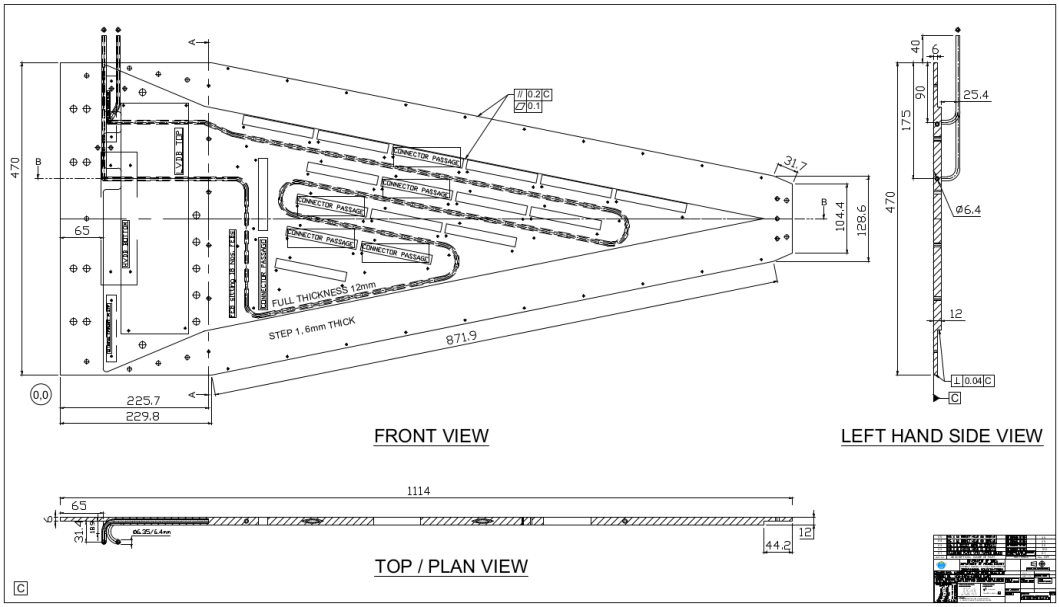

(a)

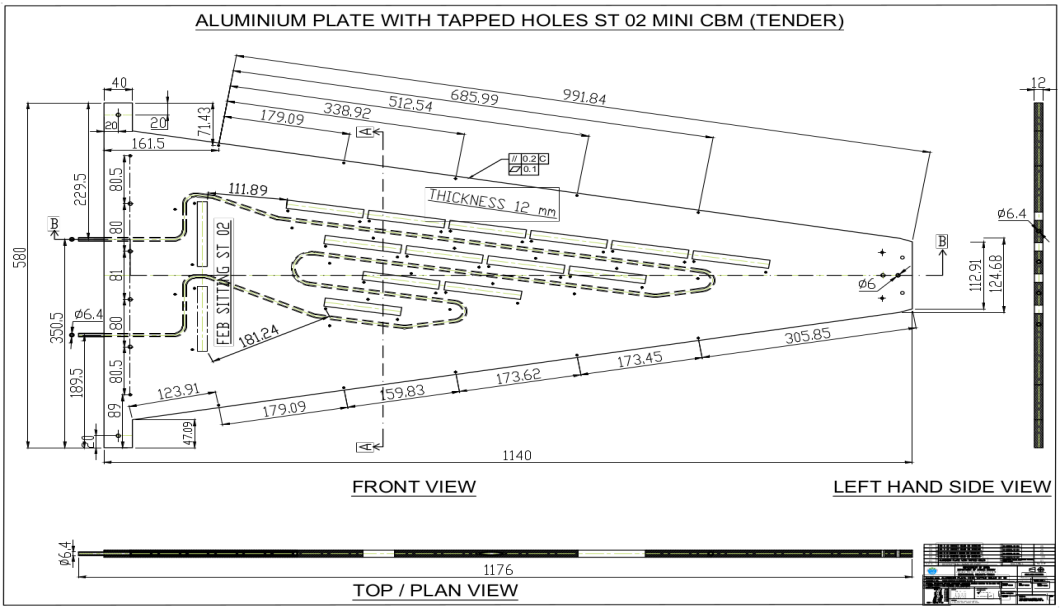

(b)

Figure 5.8: (a) Engineering drawing of the first-station molded aluminium cooling plate. (b) Engineering drawing of the second-station molded aluminium cooling plate.

second MuCh stations have been successfully produced. The engineering drawings for these plates are shown in Figure 5.8a and Figure 5.8b, respectively.

During the recent mini-CBM beamtime campaign, the molded aluminium cooling plate was deployed for the second station module, as shown in Figure 5.9a. Throughout the three days of continuous beam operation, the cooling plate performed reliably, maintaining the electronics temperature within the required operational limits and demonstrating its suitability for long-duration experimental conditions.

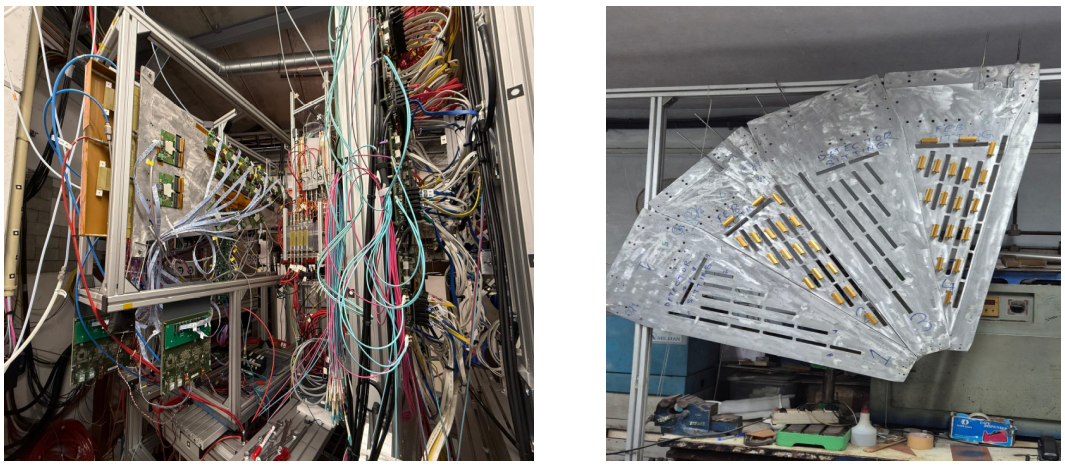

(a) (b)

Figure 5.9: (a) Molded aluminium cooling plate installed in the mini-CBM experiment at GSI. (b) Quadrant composed of four molded cooling plates under laboratory testing.

The next objective is to assess the cooling performance of a complete quadrant consisting of four molded aluminium plates connected in a daisy chain water flow configuration. To emulate the physical orientation used in the actual CBM experiment, the four plates were mounted on a vertical support frame in a staggered arrangement, as shown in Figure 5.9b. This vertical configuration reproduces the full hydraulic resistance and gravitational effects that the cooling water will experience in the final detector installation. Heating resistors were affixed to each plate, as indicated in the Figure 5.9b, to simulate the thermal load from the FEBs. In this arrangement, the first plate on the left is oriented such that the FEBs would be mounted on its rear surface and the detector on the front. The adjacent plate is oriented oppositely, with the FEBs on the front and the detector on the back, and this alternating pattern continues across

the quadrant. This staggered geometry accurately reflects the layout of the full MuCh system. The ongoing experimental study aims to evaluate the thermal stability and cooling efficiency of the complete quadrant under full heat-load conditions.

5.7 Summary

A comprehensive investigation of multiple cooling strategies for the CBM MuCh GEM detector electronics has been carried out, with the objective of identifying a reliable, long term, and scalable solution suitable for large scale deployment in the CBM experiment. The thermal load associated with the MuCh system is substantial, exceeding 8.8 kW across the first and second stations; hence, effective thermal management is a critical prerequisite for stable detector operation. Water cooling using machined aluminium plates with embedded channels demonstrated excellent thermal uniformity, operational stability, and compatibility with FEB temperature requirements. Long duration laboratory measurements confirmed that the system can maintain the temperature of all heating elements below 25°C, and its successful deployment in the CERN SPS beamline further validated its robustness under realistic experimental conditions. Air cooling configurations, although simple in design, were found to be unsuitable for CBM. The inherent limitations including high acoustic noise, mechanical vibrations affecting connector integrity, non uniform temperature profiles, sensitivity to enclosure geometry, and long term dust accumulation render air cooling incompatible with the stringent reliability requirements of the experiment. Peltier based thermoelectric cooling provided only localized and limited temperature reduction, with insufficient cooling capacity for full detector modules and substantial additional power dissipation on the hot side. These factors preclude its use as a primary cooling mechanism. A molded aluminium cooling plate design incorporating embedded stainless steel pipes has emerged as a promising alternative to machined plates. This method provides a structurally uniform monolithic plate, eliminates brazing related imperfections, and ensures

a robust, leak tight cooling path. Its successful operation during the mini CBM beamtime, demonstrates its potential for use in the final detector installation. Overall, the studies presented in this chapter establish water cooling via integrated metal channels, either machined or molded, as the only viable approach for reliable long term thermal management of the MuCh detector electronics. Future work will focus on large scale implementation, optimization of hydraulic resistance across full quadrants, and integration into the CBM detector's mechanical and services infrastructure.

Bibliography

[1] Ghosh, C., Dubey, A.K., Kumar, J., Kumar, A., Chattopadhyay, S. (2021). Design and Development of Various Cooling Arrangements for Muon Chamber Detector Electronics. In: Behera, P.K., Bhatnagar, V., Shukla, P., Sinha, R. (eds) XXIII DAE High Energy Physics Symposium. DAEBRNS HEPS 2018 2018. Springer Proceedings in Physics, vol 261. Springer, Singapore. https://link.springer.com/chapter/10.1007/978-981-33-4408-2

[2] Sumit Kumar Kundu et. al., Development of a water-based cooling system for the Muon Chamber detector system of the CBM experiment,Nuclear Instruments and Methods in Physics Research Section A: Accelerators, Spectrometers, Detectors and Associated Equipment, Volume 1050,2023,168143, https://doi.org/10.1016/j.nima.2023.168143.

Chapter 6

Production testing and planning: X-ray test and Other QA

6.1 Introduction

The Compressed Baryonic Matter (CBM) experiment at the Facility for Antiproton and Ion Research (FAIR), Darmstadt, Germany, is dedicated to exploring the phase diagram of strongly interacting matter in the regime of high net-baryon density. Within this framework, the Muon Chamber (MuCh) system constitutes a vital subsystem, responsible for the identification and tracking of muons originating from the decay of vector mesons (such as J/ψ) and low-mass dimuon pairs. To meet the stringent physics requirements of CBM, the MuCh system employs large-area Triple Gas Electron Multiplier (Triple-GEM) detectors, chosen for their excellent spatial resolution, high-rate handling capability, and robust operational efficiency. Before deployment in the high-radiation environment of the CBM experiment, each Triple-GEM detector undergoes an extensive program of quality assurance and performance characterization. These procedures involve the examination of several key operational parameters, including gain uni-

formity across the active area, long-term stability under sustained irradiation, and the I vs HV characteristics under controlled ionization conditions. This chapter presents the X-ray based characterization of CBM MuCh Triple-GEM detectors, utilizing a compact miniature X-ray tube. The studies were conducted primarily at the dedicated detection laboratory and X-ray characterization facility established at the Variable Energy Cyclotron Centre (VECC), Kolkata.

6.2 Motivation for X-ray Based GEM Characterization

The primary purpose of detector characterization is to ensure stable and uniform performance across the entire active area [1]. While cosmic rays provide an uniform, low rate ionization source for basic functionality checks, a controlled, highly stable, and reproducible source of higher-energy radiation is essential for comprehensive testing.

X-ray sources offer several key advantages for GEM detector characterization:

6.2.1 Controllable Flux:

The X-ray flux (photon count rate) can be precisely adjusted by varying the tube current and voltage , allowing for systematic studies of detector response across a wide range of operational conditions, including high-rate environments relevant to CBM.

6.2.2 Stable Energy Spectrum:

The energy spectrum consists of a continuous Bremsstrahlung background and distinct characteristic peaks determined by the target material. These well-defined energies are crucial for calibrating the detector's energy response and confirming the gas gain.

6.2.3 Local Probing:

The small focal spot size and collimation capabilities of the source allow for localized irradiation of the detector, enabling mapping of the gain uniformity across different regions of the large-area GEM modules.

6.3 Principles of X-ray Production

X-rays are generated when high-energy electrons are rapidly decelerated in a target material. The resulting X-ray spectrum is composed of two distinct components:

6.3.1 Bremsstrahlung (Braking Radiation):

This continuous spectrum is produced by the deceleration of incident electrons in the electric field of the target nuclei. The maximum X-ray energy is equal to the kinetic energy of the incident electrons, which is directly proportional to the accelerating high voltage (HV) applied across the tube.

6.3.2 Characteristic X-rays:

These appear as sharp peaks superimposed on the Bremsstrahlung spectrum. They are produced when an incident electron knocks out an inner shell electron of the target atom. The resulting vacancy is filled by an outer shell electron, and the energy difference is emitted as a characteristic X-ray photon, unique to the target material. For the Mini-X2, the relevant characteristic lines are the K and L series of the target material (e.g., Silver (Ag) or Gold (Au)).

6.4 Mini-X2 Silver Target X-ray Tube

The Amptek Mini-X2 X-ray tube system is employed as the controlled source of ionization. This miniature X-ray tube system is a compact, reliable source optimized for applications requiring stable, USB controlled output. The system consists of the Mini-X2 X-ray tube module and the Mini-X2 Controller as shown in Figure 6.1.

Figure 6.1: Mini-X2 X-ray tube module and the Mini-X2 Controller.

The dedicated X-ray testing facility at VECC employs the Amptek Mini-X2 X-ray tube system. This source is a compact, air-cooled system with a grounded anode and a Silver (Ag) target. The key operational specifications of the Mini-X2 X-ray tube are summarized in Table 6.1.

The Mini-X2 generates a conical X-ray beam with an opening angle of approximately 120^0. The system is fully controlled through an USB interface, enabling precise adjustment of operating parameters such as tube voltage and current. To ensure safe operation under high-voltage conditions, the unit incorporates multiple hardware interlocks and visual warning indicators.

The characteristic X-ray spectrum produced by the Silver (Ag) target at various operating voltages is presented in Figure 6.2. As expected, the spectrum consists of a broad Bremsstrahlung continuum superimposed with distinct characteristic emission peaks corresponding to the Ag K-series transitions.

Parameter	Value (Mini-X2 System)
Target Material	Silver (Ag)
Peak Characteristic Energy	22 keV
Tube Voltage	10 kV to 50 kV
Tube Current Range	5 μA to 200 μA
Typical Dose Rate	1 Sv/hr (100 rem/hr) at 50 kV and 80 μA (4 W)
Typical Flux	6 x 10^4 photons/s/mm^2/μA @ 30 cm on axis (at 50 kV)
Focal Spot	Approx. 2mm
Window Material	125 μm Beryllium (Be)
HV Stability	$< 0.1\%$

Table 6.1: Specifications of the Mini-X2 X-ray tube.

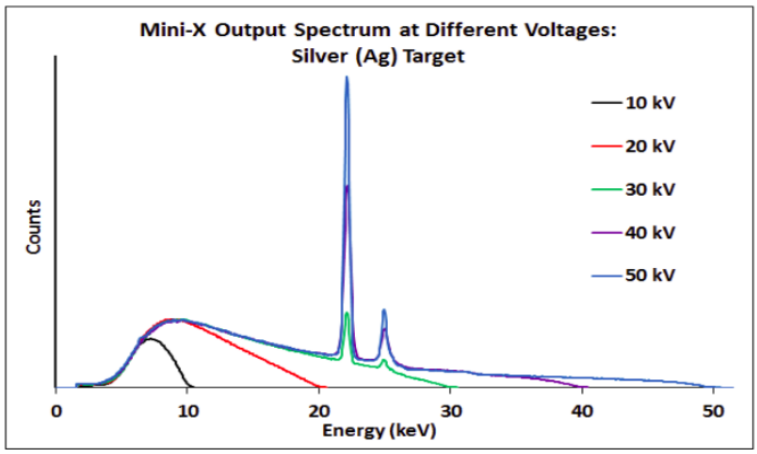

Figure 6.2: X-ray spectrum for the Silver target.

6.5 Experimental Setup at VECC

The characterization of the Triple-GEM detector at VECC was carried out inside a purpose-built X-ray cabinet specifically designed for high-radiation and high-voltage experiments. This enclosure provides a controlled and stable environment for detector testing while ensuring comprehensive radiation shielding and compliance with safety protocols. The setup enables reliable operation of the X-ray source and the detector under well regulated conditions essential for accurate performance measurements.

6.5.1 Test Environment and Safety:

The X-ray tube installation at VECC is located on the terrace of the main building and utilizes a robust, radiation shielded cabinet, as shown in Figure 6.3. The cabinet measures 2 m x 2 m and is constructed using 15 mm thick lead (Pb) sheets. A lead lined sliding door provides additional shielding, ensuring safe operation during high intensity X-ray irradiation.

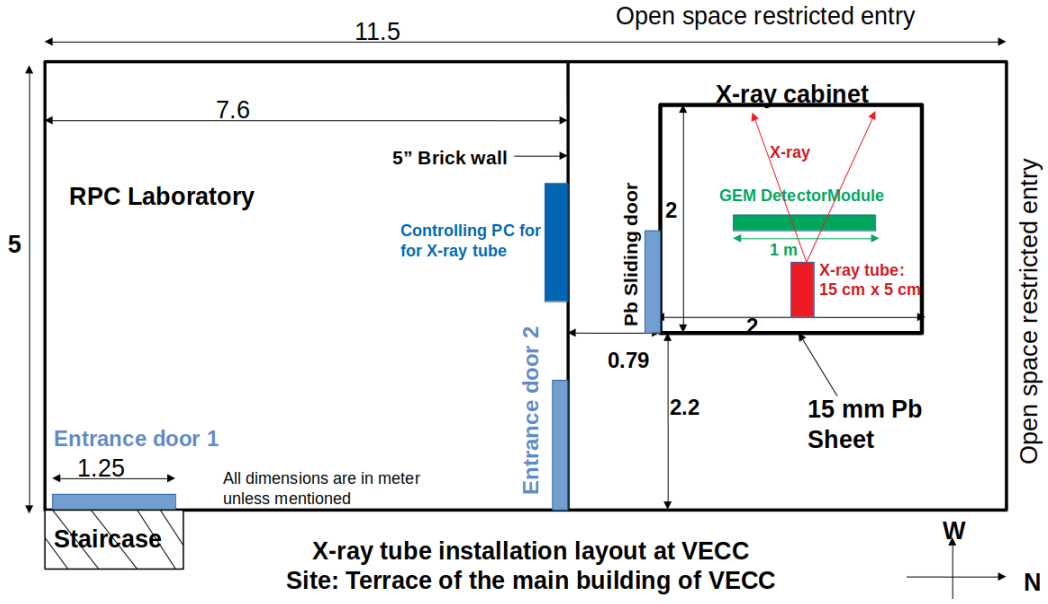

Figure 6.3: X-ray cabinet layout.

The installation includes restricted access to the open area surrounding the X-ray cabinet to ensure operational safety. The detector module is mounted inside the shielded chamber (indicated in green), while the Mini-X2 controller unit (indicated in red) is operated remotely from an external computer. To validate safe usage conditions, radiation survey measurements were conducted by the Health Physics Group at VECC prior to and during operation.

6.5.2 Detector and Setup:

A large trapezoidal CBM MuCh Triple GEM detector module is mounted inside the shielded enclosure, as shown in Figure 6.4. The detector is supplied with an Ar:CO_2 (70:30) gas mixture from an MFC based gas mixing unit, which serves as the active medium. The X-ray tube is fixed on a stationary frame, whereas the detector is mounted on a movable platform, allowing it to be translated across the active area for systematic characterization.

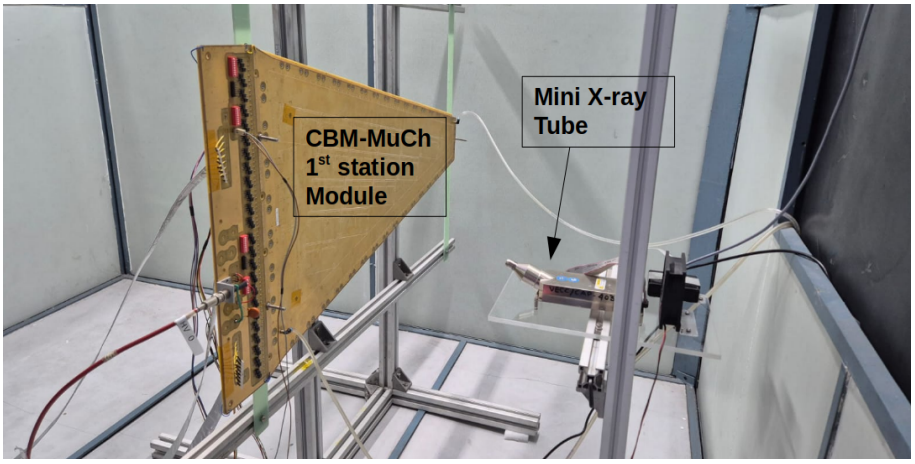

Figure 6.4: Detector setup inside X-ray cabinet at VECC.

6.5.3 Results:

During data taking, the X-ray tube was operated at 50 kV and 80 µA. The detector voltage (sum of the GEM foil voltages) was varied across 895 V, 909 V, 922 V, and 935 V. As the voltage increased, the peak of the clustered charge spectra shifted progressively toward higher ADC values. This behaviour clearly indicates enhanced charge amplification at higher operating voltages for a fixed X-ray energy. The corresponding clustered charge spectra are presented in Figure 6.5.

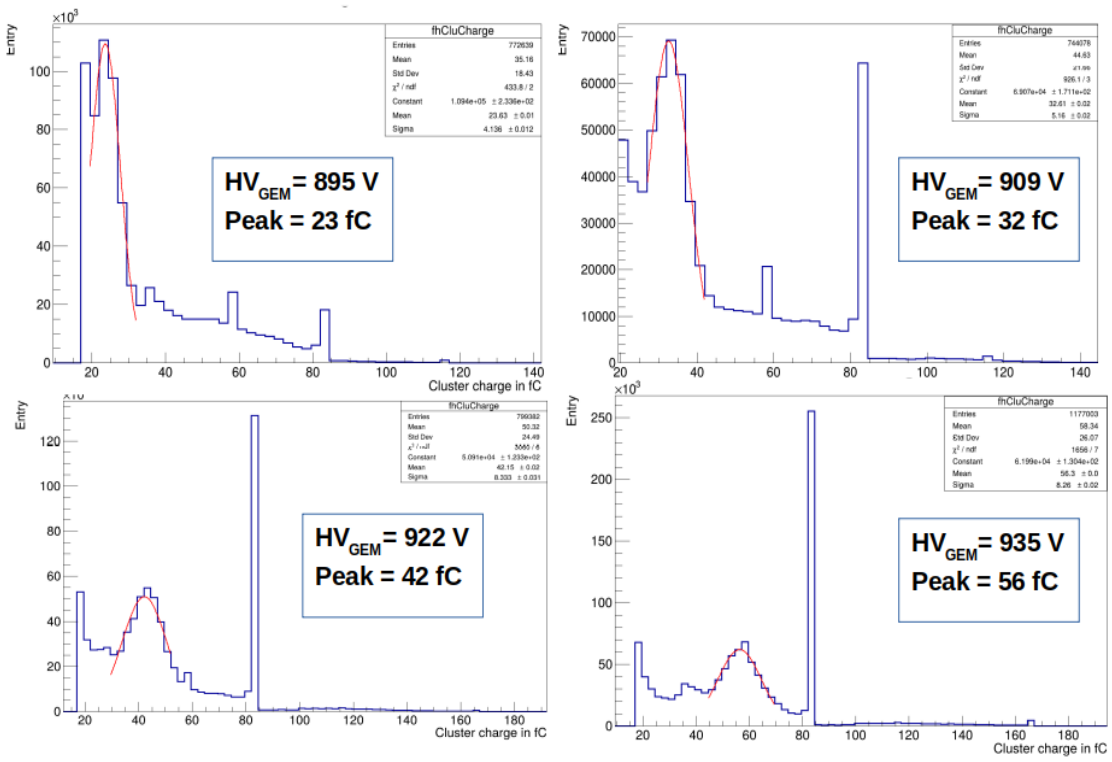

Figure 6.5: Clustered charge spectra with varying GEM voltage.

6.6 Experimental Setup at GSI Detector Lab

A full size prototype of the CBM MuCh first station GEM detector module was tested at the Detector Laboratory at GSI, Darmstadt. The X-ray system at GSI employs a Gold (Au) target and was operated at 50 kV and 80 µA. Owing to the characteristic L shell emission of gold at approximately 10 keV, the resulting spectrum is considerably softer than the 22 keV Ag K emission used at VECC. This softer spectrum enables the study of detector behaviour under different primary ionization conditions within the gas volume.

6.6.1 Test Environment and Detector:

The GSI setup employed a dedicated test box located inside a cleanroom at the Detector Laboratory. The detector under investigation, referred to as the GEM1 module (corresponding

to the first station of the CBM MuCh system), is a large trapezoidal unit mounted on a stable support structure within the enclosure. The X-ray tube was positioned at a distance of approximately 53 cm vertically and 40 cm horizontally from the detector surface, as illustrated in Figure 6.6.

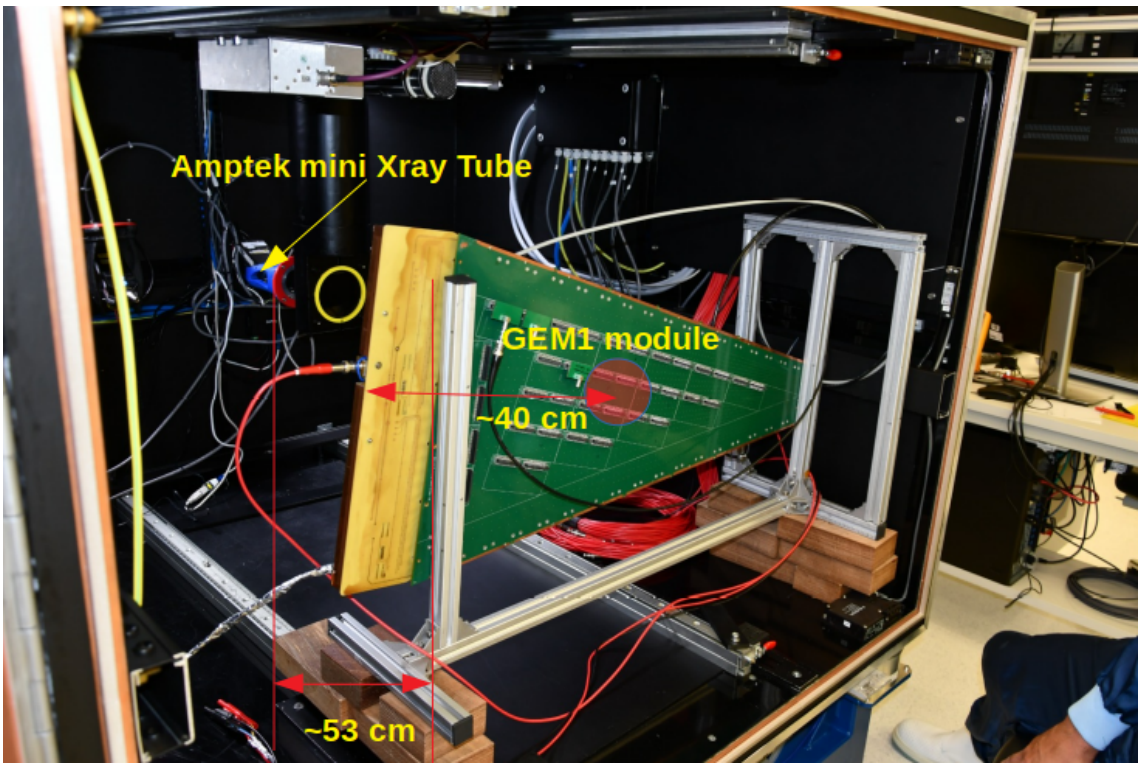

Figure 6.6: Detector setup inside X-ray cabinet at GSI.

6.6.2 Results:

The detector characterization focused on measuring the GEM module branch current as a function of the applied HV under two conditions: with the X-ray source OFF (dark current) and with the X-ray source ON (operating current). The Figure 6.7 shows the branch current of the GEM module in micro Amps (µA) as a function of the applied High Voltage in Volts.

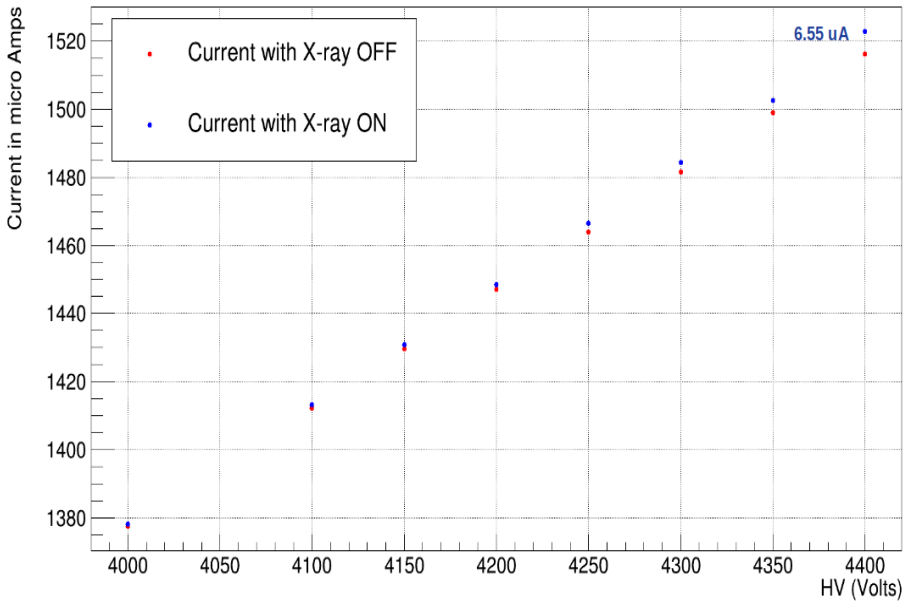

Figure 6.7: Branch Current of GEM1 with X-ray ON and OFF.

The data points show a clear distinction between the two conditions: (i) Current with X-ray OFF (Red Dots): This represents the branch current of the detector resistive chain and (ii) Current with X-ray ON (Blue Dots): This represents the total current, which is the sum of the branch current and the signal current induced by the X-ray flux. The difference between the ON and OFF curves represents the X-ray induced signal current. The magnitude of this difference (6.55 µA at 4400 V) indicates the charge multiplication or gain of the detector.

The anode current of the detector has also been measured using a pico Ammeter as shown in Figure 6.8.

This plot isolates the X-ray induced current, I_{signal} , which is proportional to the gas gain G, assuming a constant primary ionization rate $R_{primary}$:

$I_{signal} = G \,.\, R_{primary}.\ e$

where e is the elementary charge.

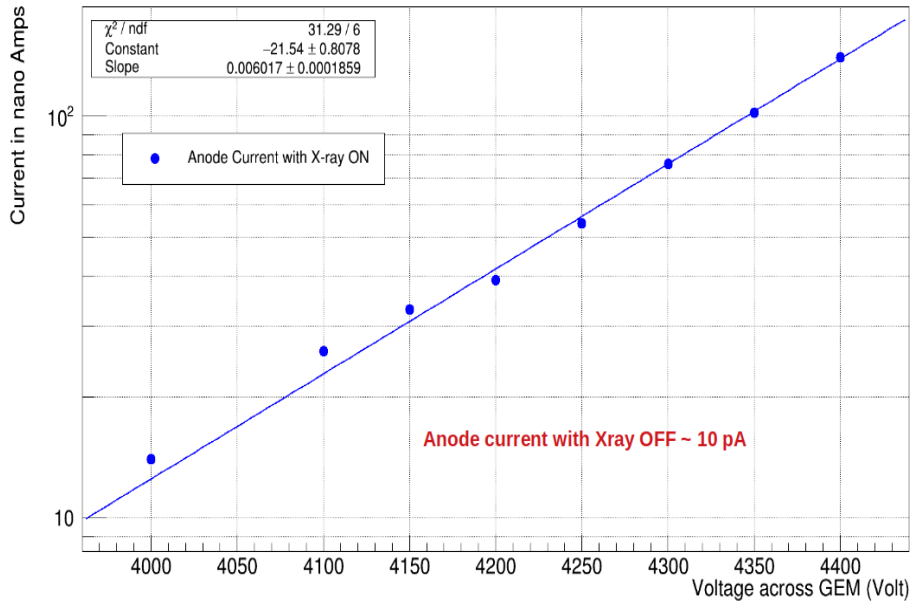

Figure 6.8: Anode Current of GEM1 with X-ray ON.

With X-ray OFF the anode curent is $\sim$ 10 pA, which represents the intrinsic dark current of the detector, which is mainly due to spontaneous processes like electron emission from the cathode or impurities in the gas volume.

Figure 6.8 shows the anode current in nano Amps (nA) on a logarithmic scale against the voltage across the GEM. The raw total dark current of the anode was noted to be extremely low, indicating a very clean detector and robust HV system. Therefore, the measured anode current is predominantly the signal current.

The data points fall close to a straight line on this log plot, confirming the expected exponential increase of the gas gain with the applied voltage. The gain in a gas detector typically follows the formula:

$G \propto \exp(\alpha x)$

where α is the first Townsend coefficient and x is the multiplication length.

A linear fit was applied to the data in the logarithmic regime. The positive slope of the fit confirms the exponential rise of the gain with the applied voltage. The non ideal χ^2/ndf value (5.2 for 6 degrees of freedom) suggests minor deviations from a perfect exponential fit across the entire voltage range, possibly due to minor space charge effects or non uniformity in the multiplication gaps at very high gain. This fit is essential for defining the operational HV point for the CBM-MuCh detector based on the required gas gain.

6.7 Summary and Outlook

6.7.1 Summary of Characterization:

The Triple GEM detector characterization using the Amptek Mini-X2 X-ray source at both VECC and GSI was successfully established. Key findings include:

(i) The Amptek Mini-X2 proved to be a reliable and controllable source for inducing stable ionization in the GEM detectors. Different target materials (Ag at VECC, Au at GSI) allow for flexibility in the ionization energy spectrum, probing different aspects of detector response.

(ii) The Station-1 module demonstrated classic proportional mode behavior, exhibiting an exponentially increasing current (and thus, gas gain) as a function of the applied High Voltage.

(iii) The dark current of the GEM module was measured to be extremely low, confirming the high quality of the detector manufacturing and the cleanliness of the gas system (at the anode).

(iv) The exponential rise of the X-ray induced current was quantified through a log fit, yielding a slope in the tested voltage range.

6.7.2 Outlook:

The initial I-V characterization provides the foundation for setting the operational voltage. Future work must extend these tests to fully characterize the detector performance:

(i) Utilizing the small focal spot of the X-ray source, the detector gain should be mapped across the entire active area to identify and quantify any non uniformities that could impact CBM tracking performance.

(ii) The detector gain must be monitored over extended periods under continuous X-ray irradiation to confirm long term stability and rule out the onset of aging effects.

(iii) The detector should be tested at the maximum flux density achievable with the Mini-X2, simulating the high rate conditions expected in the CBM experiment to confirm its rate capability and investigate space charge effects.

Bibliography

[1] M. Abbas et al, Quality control of mass-produced GEM detectors for the CMS GE1/1 muon upgrade,Nuclear Inst. and Methods in Physics Research, A 1034 (2022) 166716. https://doi.org/10.1016/j.nima.2022.166716

Chapter 7

Summary and Outlook

7.1 Summary

The Compressed Baryonic Matter (CBM) experiment at FAIR is designed to explore the properties of strongly interacting matter at high net baryon density, a region of the QCD phase diagram that remains largely unexplored. Achieving the physics objectives of CBM requires detector systems capable of sustained operation at interaction rates up to 10 MHz in a triggerless, free-streaming data acquisition environment. Within this framework, the Muon Chamber (MuCh) system plays a central role in the measurement of dimuon observables, imposing stringent requirements on detector granularity, rate capability, timing performance, and long-term operational stability.

This thesis presents a comprehensive study on the design, fabrication, characterization, and system level validation of large area triple-GEM detector modules developed for the MuCh detector, with particular emphasis on the second station. A full scale trapezoidal GEM module of approximately one meter length was successfully designed and fabricated at VECC using indigenously developed technologies. To overcome industrial limitations on multilayer PCB size,

a novel joining technique was implemented, achieving mechanical integrity, electrical continuity, and gas tightness with a dead zone limited to approximately 0.2 mm. The effectiveness of this technique was validated through extensive laboratory and beam tests.

Detailed laboratory characterization using a ^{55}Fe X-ray source and cosmic muons established the fundamental performance of the detector. The module demonstrated stable operation with an exponential gain dependence on the applied high voltage, uniform response across the active area within expected limits, and a detection efficiency approaching 98%. The measured time resolution of approximately 18 ns and cluster sizes consistent with pad geometry confirmed the suitability of the detector for high rate tracking applications. Identified noise sources, particularly near the PCB joining region, were successfully mitigated through targeted shielding and grounding improvements, resulting in noise free operation under nominal conditions.

A calibrated gas mixing and distribution system based on mass flow controllers was developed and optimized for large area GEM operation. Systematic studies established the dependence of detector gain on gas flow rate and impurity levels, leading to the adoption of a parallel gas distribution architecture for MuCh. In parallel, a water cooled aluminum support plate was designed to extract the substantial heat generated by the front end electronics. Thermal tests demonstrated stable operation with electronics temperatures maintained well below critical limits, ensuring reliable performance during extended data taking periods.

The performance of the GEM detectors was further validated under realistic high intensity conditions during the mini-CBM beam campaigns at SIS18. The detectors were operated with heavy-ion beams up to interaction rates of the order of 10^7 - 10^8 particles per spill, corresponding to effective hit rates in the range relevant for CBM. Detailed analyses of digi rates, spill structures, and time-slice behaviour demonstrated a linear detector response with increasing beam intensity across different regions of the detector. Correlation studies between GEM1, GEM2, and TOF subsystems showed strong linear relationships, confirming consistent behaviour and common acceptance among the detectors.

Timing correlation analyses between GEM1 and GEM2 established a stable relative time offset with a resolution of approximately 50 ns, which remained constant throughout the run. Spatial correlation studies further confirmed the geometrical alignment of the two GEM stations, demonstrating that particles traversing one detector were consistently observed in the other. Measurements of channel wise and area normalized digi rates showed that the detectors can safely operate at local rates reaching several hundred kHz/cm^2, in agreement with expectations from simulation studies and well within the operational limits of GEM technology.

In addition to prototype characterization, emphasis is being placed on production testing, quality assurance, and planning for series fabrication, which are crucial for the large scale deployment of MuCh GEM detectors. A dedicated X-ray test facility was developed and commissioned at VECC using a commercial Mini X-ray source, enabling systematic irradiation of full size detector modules. Uniformity scans across the active area are ongoing to verify gain homogeneity, identify defective channels, and detect localized inefficiencies arising from GEM foil imperfections or readout issues. These studies will establish acceptance criteria for detector performance prior to installation and will provide a quantitative framework for module qualification.

Overall, the results presented in this thesis demonstrate that the developed large area triple-GEM detectors, together with their associated gas, cooling, readout, and quality assurance frameworks, meet the stringent performance and reliability requirements of the CBM MuCh system. The successful validation of detector response, timing, rate capability, and stability under high intensity beam conditions confirms the readiness of the technology for large scale deployment. The comprehensive production testing and QA strategy established in this work represents a key step toward the series production of MuCh detector modules and their long term operation in the challenging CBM experimental environment.

7.2 Outlook

The work presented in this thesis establishes a solid foundation for the series production and large scale deployment of GEM detectors in the CBM MuCh system. Several important directions naturally follow from this study.

First, the demonstrated fabrication procedures and quality assurance protocols can be directly extended to the mass production of MuCh station-2 modules. The PCB joining technique, GEM foil handling procedures, and assembly workflow developed here provide a validated blueprint for industrial scale manufacturing while maintaining performance uniformity and reliability.

Second, the proposed gas distribution and cooling concepts will be integrated into the final MuCh infrastructure. Long term stability studies under continuous operation, including ageing effects under sustained irradiation, will be essential as the system transitions from prototype testing to full detector installation. Future beam campaigns will allow further refinement of operational parameters, including gain optimization and threshold tuning at the highest interaction rates expected in CBM.

Third, the experience gained during mCBM operation offers valuable feedback for the optimization of the free streaming data acquisition and online reconstruction chain. Improved time alignment, real-time noise suppression, and adaptive masking strategies can be further developed to enhance performance in the full CBM environment, where pile-up and background conditions will be even more demanding.

Finally, once installed in the CBM cave at SIS100, the MuCh detector equipped with GEM technology will enable precision measurements of rare dimuon probes, including low-mass vector mesons and charmonia, in the high μ_B regime. The detector developments and performance validations presented in this thesis therefore represent a critical contribution to the CBM physics program and to the broader field of high-rate gaseous detector technology.

In summary, this thesis demonstrates that large-area triple-GEM detectors are reliable solution for high-rate tracking in the CBM experiment, and it paves the way for their successful deployment in forthcoming FAIR physics runs.